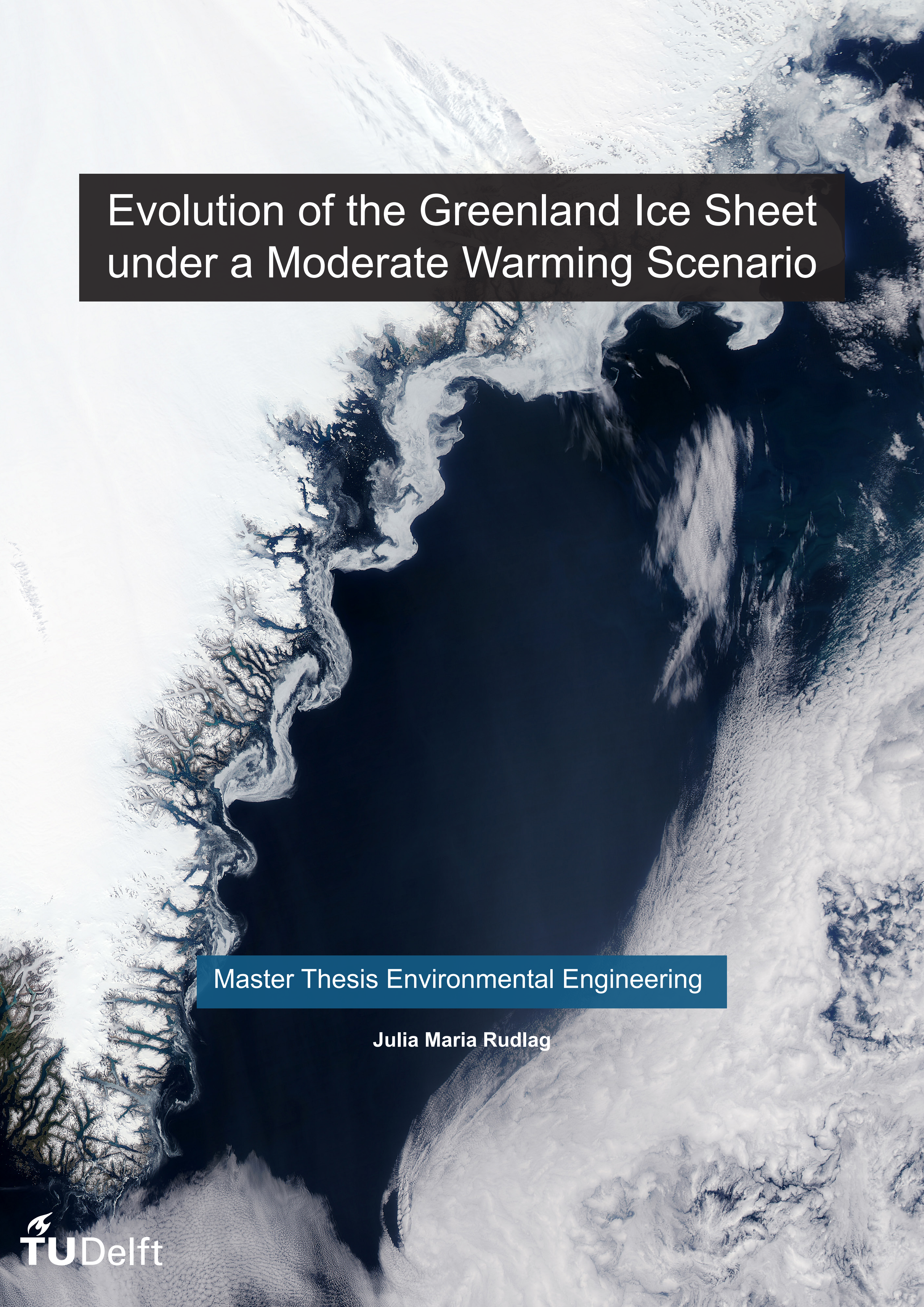

Evolution of the Greenland Ice Sheet under a Moderate Warming Scenario

Master Thesis Environmental Engineering

Julia Maria Rudlag

TU Delft

Evolution of the Greenland Ice Sheet under a Moderate Warming Scenario

by

J.M. Rudlang

Student number: 4530981

In partial fulfilment of the requirements for the degree of

Master of Science
in Environmental Engineering

at the Delft University of Technology,
to be defended publicly on Friday 7^{th} of October, 2022 at 13:00 PM.

Thesis assessment committee:	Dr. M. Vizcaino,	TU Delft, Chair & main supervisor
	Dr. S. Lhermitte,	TU Delft, Committee member
	Dr. M. Hrachowitz,	TU Delft, External committee member

An electronic version of this thesis is available at http://repository.tudelft.nl/.

On the cover: July 16, 2015 - NASA image courtesy Jeff Schmaltz, LANCE/EOSDIS MODIS Rapid Response Team at NASA GSFC. Retrieved from:https://earthobservatory.nasa.gov/images/86322/sea-ice-near-greenland

TU Delft

Abstract

The Greenland ice sheet (GrIS) is an important component of the climate system and is a key contributor to future sea level rise, as it is storing frozen water that would raise sea levels by 7.4 m should it all melt (Bamber et al., 2018). Of particular concern is the amount of global warming we are facing now and in the future, as it is becoming more likely that even if our emissions are significantly reduced, global warming will reach at least 2°C (Arias et al., 2021). Much research concerns the future contribution of the GrIS to sea level rise for high emissions scenarios (upper bound) and low emission scenarios (lower bound), but there are few studies giving the main focus to what is becoming a more likely future, the moderate emissions scenarios. This research aims to quantify the mass loss of the Greenland ice sheet and subsequent contribution to future sea level rise under a moderate CO_2 concentration scenario over a multimillennia timescale. An idealised simulation of 3000 years, where CO_2 concentrations are increased by 1% annually until reaching two times pre-industrial values and then kept constant, is run with the high-resolution Community Earth System Model version 2.1 (CESM2.1) and Community Ice Sheet Model version 2.1 (CISM2.1). The climate, run with CESM2.1, is simulated for 1000 years. After 500 years, it is assumed that the climate is close to equilibrium, and thus one climate year is used for five years of forcing the ice sheet in CISM2.1, resulting in 3000 years of ice sheet simulation. At the end of the simulation, the global mean annual temperature has increased by 5 °C and the temperature over Greenland is 9°C warmer than pre-industrial. The rate of sea level contribution in the first centuries is lower than the observed contemporary mass loss of 0.7 mm yr^{-1} (Shepherd et al., 2020) but increases after year 710 to a rate of 1 mm yr^{-1}. Another increase of mass loss is happening from the year 1380 until the end of the simulation where the rate is 2 mm yr^{-1} and the total contribution to sea level rise is 4.1 m. The limited mass loss in the period between years 71-400 and its increase thereafter is found to relate to temporal strong weakening and posterior recovery of the NAMOC. This study projects that the GrIS is a major contributor to future sea level rise, even in a moderate warming scenario, and that the changing NAMOC has a noteworthy effect on the GrIS mass budget.

Acknowledgements

Dear reader,

This thesis is my final work for obtaining a master's degree in Environmental Engineering. I followed the specialisation of Science, where I really enjoyed learning about the hydrological cycle, meteorology, oceanography, atmospheric science, and last but not least, the cryosphere. It is with passion for climate change and nature that I present this report.

First and foremost, I would like to thank my main supervisor and chair of the assessment committee: Miren Vizcaino. It has been a pleasure working with you and learning from your expertise on Greenland and climate modelling. Thank you for all the guidance, encouragement and feedback. Then, I would like to thank the rest of my assessment committee, Stef Lhermitte and Markus Hrachowitz. Thank you for the solid feedback and enthusiasm for my project. I would also like to thank Filippa Jansen for proofreading key sections and helping me improve my writing style and language. Lastly, a huge thank you to my friends, especially Lauran, Juliette, Jorijn, Nessie, Dyngja and Blossa and my family for all the support and coffee breaks during my studies.

Julia Maria Rudlang
Delft, October 2022

Contents

Abbreviations

AIS	Antarctic Ice Sheet
AGCM	Atmospheric General Circulation Model
AMOC	Atlantic Meridional Overturning Circulation
AR6	Sixth Assessment Report
BMB	Basal Mass Balance
CAM6	Community Atmosphere Model version 6
CESM2	Community Earth System Model version 2
CICE5	Los Alamos National Laboratory sea ice model version 5
CISM2	Community Ice Sheet Model version 2
CLM5	Community Land Model version 5
CMIP6	Coupled Model Intercomparison Project phase 6
EC	Elevation Class
ELA	Equilibrium Line Altitude
E_M	Melt Energy
ESM	Earth System Model
GHF	Ground Heat Flux
GMNST	Global Mean Near-Surface Temperature
GMSL	Global Mean Sea Level
GMSLR	Global Mean Sea Level Rise
GrIS	Greenland Ice Sheet
ID	Ice Discharge
IPCC	Intergovernmental Panel on Climate Change
ISMIP6	Ice Sheet Model Intercomparison Project for CMIP6
JJA	June-July-August
ka	Thousand years ago
LGM	Last Glacial Maximum
LHF	Latent Heat Flux
LIG	Last Interglacial
LW_{net}	Net Longwave Radiation
MB	Mass Balance
MOSART	Model for Scale Adaptive River Transport
NAMOC	North Atlantic Meridional Overturning Circulation
PI	Pre-industrial
RACMO2	Regional Atmospheric Climate Model 2
RCM	Regional Climate Model
POP2	Parallel Ocean Program version 2
ppm	Parts per million
RCP	Representative Concentration Pathway
SEB	Surface Energy Balance
SHF	Sensible Heat Flux
SLE	Sea level equivalent
SLR	Sea level rise
SMB	Surface Mass Balance
SNICAR	Snow, Ice, and Aerosol Radiation model

SSP	Shared Socio-economic Pathway
SW$_{net}$	Net Shortwave Radiation
TOA	Top of the Atmosphere
WE	Water equivalent

List of Figures

List of Tables

1 Introduction

The Greenland Ice Sheet (GrIS) and the Antarctic Ice Sheet (AIS) are the largest and most uncertain contributors to future sea level (Arias et al., 2021). Both the Greenland Ice Sheet and the Antarctic Ice Sheet are at the moment storing frozen water of 7.4 m and 58.3 m sea level equivalent, respectively (Bamber et al., 2018). Even with extensive research, there is still little known or properly understood about the many processes of ice sheet mass loss, and their interaction with the Earth System (Fyke et al., 2018; Goelzer et al., 2017). As such, the GrIS has been identified as a tipping element in the Earth system (Lenton et al., 2008). A tipping element is a large-scale Earth system component that could pass a critical threshold, a tipping point. A tipping point, if crossed, could change the state of the Earth system (Lenton et al., 2008). As global emissions continue to rise, so do concerns for the GrIS reaching a tipping point, where mass loss becomes irreversible and commits us to future sea level rise (SLR).

The Greenland Ice Sheet is already showing sensitivity to climate change by increased mass loss and larger contribution to sea level rise during the recent decades (Arias et al., 2021; Shepherd et al., 2020; van den Broeke et al., 2016). It is thus important to assess simulations of past, present and future ice sheet evolution, in order to create a deeper comprehension of the complexity, significance and evolution of the Earth's ice sheets. Knowledge of internal variability and forced changes in the climate system have improved. This is reflected in the advances in the field of climate modelling, where much work is being done to improve the quantification of uncertainties in future climate projections. The Coupled Model Intercomparison Project 6 (CMIP6, Eyring et al., 2016) and the Ice Sheet Intercomparison Project 6 (ISMIP6, Nowicki et al., 2016) are global efforts to establish "large ensembles" simulations and models (Eyring et al., 2016). The ISMIP6 is the sixth assessment of researching the ice sheets (Nowicki et al., 2016). The CMIP6 and ISMIP6 give a structured way of describing standards of simulations used for climate projections and keeping track of the evolution. CMIP6 scenarios are based on new future pathways called the Shared Socioeconomic Pathways (SSP) (O'Neill et al., 2016). Major developments are happening in the field of Earth system models, especially concerning the ice sheet-climate model coupling. In the past, the ice sheets have been modelled in the climate models as white, passive mountains (Lofverstrom et al., 2020), when in reality the ice sheets are affected by a changing climate and are in turn affecting the climate. To achieve more realistic and robust projections for sea level rise, work is being done to include this crucial coupling in Earth system models. The CESM2-CISM2 (Danabasoglu et al., 2020; Lipscomb et al., 2019) is a novelty, and one of the few global models that include a realistic and interactive SMB calculation with advanced snow and firn physics and downscaling via elevation classes (EC) (Muntjewerf et al., 2021; Sellevold et al., 2019). The simulations used in this thesis run with the CESM2-CISM2 follow the framework for coupled ice sheet-climate model experiments (ISMIP6; Nowicki et al., 2016).

This research aims to gain insight into the processes leading to mass loss of the Greenland Ice Sheet (GrIS) and hence contribute to global mean sea level rise. To this end, an idealised simulation run with the CESM2-CISM2 model is analysed, where CO_2 concentrations are raised by 1% until levels are doubled compared to 1850, hereafter called pre-industrial (PI). A throughout analysis of GrIS under a 4xCO_2 simulation, also with CESM2-CISM2, has been done by Muntjewerf, Petrini, et al. (2020a) and is used as a comparison to the 2xCO_2 simulation. Furthermore, a pre-industrial control simulation, also run with CESM2-CISM2, is used for reference where the climate is continuously forced with pre-industrial conditions for 300 years. In addition, state-of-the-art literature is used to place the 2xCO_2 simulation into a wider context in this introductory section and in the discussion. The atmospheric CO_2 concentration reaches a maximum of 569 ppm, which falls in the neighbourhood of the SSP2-4.5 scenario (Arias et al., 2021; Meinshausen et al., 2020). This places the simulation in more-or-less a moderate warming scenario and the analysis in this thesis provides insight into a future projection of the evolution of the Greenland Ice Sheet.

Most studies on future climate projections concern extreme cases of high emission scenarios (Aschwanden et al., 2019; Huybrechts et al., 2011; Muntjewerf, Sellevold, et al., 2020; Van Breedam et al., 2020) because of the need for an upper bound of projections. There is also much research on less extreme cases that function as a lower bound. This lower bound is in line with the ambitions of managing the world's emissions and reaching the Paris Agreement of less than 1.5$°C$ warming. However, with how the situation is looking today, even in the best-case scenario, the low-emission scenarios such as the SSP1-1.9, the global mean surface temperature is likely to warm just below or slightly more than 2$°C$ (Arias et al., 2021; Gaffney & Rockström, 2021). Therefore, it is very relevant to start investigating and evaluating moderate warming scenarios, in order to give a better quantification and constraint on future changes in the Earth system, and relevant for this research: on the mass loss of the Greenland Ice Sheet and the consequent contribution to sea level rise.

1.1. A brief history of Climate Change on Earth

Paleoclimate evidence and reconstructions of past climate evolution can aid in constraining future estimates of climate change and identifying important players in the system, like sea level and ice sheets (Arias et al., 2021). It also makes it possible to grasp how the climate on Earth is evolving over a longer timescale due to forcings and perturbations of the system (Gaffney & Rockström, 2021). This has enabled scientists to identify specific climate states of the Earth system. Simplified, there are three climate states, which are determined by the global mean surface temperature (relative to PI). The hothouse with temperatures above 4$°C$ and no ice on the poles. The icehouse, where there is ice on the poles, like today. The icehouse can either be in the state of an ice age with temperatures between -5$°C$ and -2$°C$, or in the milder, interglacial state with temperatures between -1$°C$ and 2$°C$. The third state is the snowball, where ice is covering the whole of the planet and temperatures are below -5$°C$ (Gaffney & Rockström, 2021).

Wind back 2.7 million years: the Earth is entering into a relatively stable icehouse state where several ice age cycles are about to begin. The Antarctic ice sheet is formed, followed by the growth of an ice sheet over the North Pole. This is the Pleistocene Epoch, where the Earth bounced back and forth between slightly colder and warmer states. The shift between ice ages and interglacials is linked to the Milankovitch cycle, which describes the coupling between icehouse states and celestial motion. The Milankovitch cycle outline how the temperature changes significantly due to the elliptical orbit of the Earth around the sun (and thus where the sun falls and during what season) and the change in tilting as it orbits (Gaffney & Rockström, 2021; Milankocivh, 1998). Evidence from these interglacial periods is today used in part to constrain the projections of the polar ice-sheet response to global warming (Dutton et al., 2015). Such evidence was found in the 1990s during an expedition to Antarctica where ice core drillings revealed bubbles of air trapped in the ancient ice. This gave an indication of the atmospheric composition of the last eight ice age cycles and their remarkable stability. Although every interglacial period was different and varying, the temperature has not risen more than 2$°C$ above the average temperature of the past 10 millennia (Gaffney & Rockström, 2021). Furthermore, ice core drillings from Greenland reveal repeated, large and abrupt shifts in Northern Hemisphere climate during the last ice age (Barker et al., 2011). Other evidence from the past is sediment cores with preserved pollen records providing information about vegetation during the Last Interglacial (LIG)(Sommers et al., 2021).

Several studies conducted on the Last Interglacial (Barker et al., 2011; Dutton et al., 2015; Fyke et al., 2011; Sommers et al., 2021), which took place 129-116 thousand years ago, concluded that the sea level was about 6-9 m higher than the present day and that an increase of a few degrees in global mean temperature, resulted in several meters of sea level rise. For example, the study by Sommers et al. (2021), where an 8000-year transient simulation of the LIG, approximated the Greenland Ice Sheet to have contributed 3.8 m to global mean sea level rise. Furthermore, the study demonstrated how GrIS evolved over a millennia time scale, substantiating the fact that the ice sheet, once set in motion, takes an immensely long time to find a new equilibrium state (Sommers et al., 2021).

Following the Last Interglacial, the Last Glacial period took place and then followed the Holocene. The Holocene is the very climactic-stable period spanning 12000 years, sometimes called the Goldilocks epoch, due to temperatures not being too warm nor too cold (Gaffney & Rockström, 2021). The global average temperature only went up or down by $1°C$, and levels of CO_2 were more or less at 280 ppm up until the industrial revolution. As the industrial revolution began, it marked the onset of incredible growth and further evolution of humankind. It marked the beginning of the Great Acceleration, as seen in levels of CO_2, ocean acidification, global mean surface temperature and other socio-economic trends such as transportation, international tourism, water use and urban population to mention a few (Gaffney & Rockström, 2021). Although the industrial revolution started in 1850, it is recently agreed that it is around 1950 that the accelerating effects of rapidly increased emissions of greenhouse gases, began to overwhelm Earth's life support system. This is a human-driven trajectory, pushing the once stable Earth system towards a hothouse state (Steffen et al., 2018). Thus, many scholars and scientists are using the term Anthropocene: a new geological epoch, starting from when the stable Holocene conditions were shaken out of balance, sometime between 1850 and 1950. The epoch is yet to be formalised by stratigraphers, but it is adopted by many academic disciplines (Crutzen, 2002; Gaffney & Rockström, 2021; Steffen et al., 2018).

As the ice cores from the 1990s Antarctica expedition proved, the Earth is very sensitive to changes in greenhouse gases. For the last 2.7 million years, the atmospheric CO_2 levels have ranged between 170 parts per million (ppm) during the ice ages and 280 ppm during the warm interglacials. They have not been lower, nor higher. In 2021 we passed CO_2 concentrations of 414 ppm (Lindsay, 2022), an increase by a factor of 1.5 compared to that in 1850. Today, the average temperature is 1.09 degrees higher than PI. Continued at this rate, warming will exceed 1.5 degrees in the early 2030s (Arias et al., 2021). This is alarming considering the effects of today's warming, such as frequent extreme weather, floods and droughts, forest fires, a decline in biodiversity and accelerated GrIS mass loss and sea level rise. Further climate change can be amplified or reduced by positive or negative feedbacks. An example of positive feedbacks is the weakening of the carbon cycle by the thawing of permafrost and dieback of the Amazon and boreal forest. Another example of a positive feedback is the decrease of the Arctic sea ice by a warming climate. This exposes more dark ocean, which then absorbs more heat due to the lower surface albedo, reinforcing the sea ice loss. The ice-albedo feedback is also relevant for the mass loss of GrIS. Thus, the implication of the current changes in the Earth systems' behaviour is that even if the target of the Paris Agreement is met there is a cascade of feedbacks that should not be overlooked, as these feedbacks could irreversibly change the state of the Earth (Steffen et al., 2018).

1.2. Sea Level Change

The global mean sea level (GMSL) varies through volume change by thermal expansion when the oceans warm and the heat content increases, causing a lowering in density and volume expansion (or opposite when it cools). Sea level also changes by the addition or removal of water, such as changes in the cryosphere and land-water storage (Dutton et al., 2015; Fox-Kemper et al., 2021).

The prognosis of the current GMSL is that during the 20^{th} century, the sea level rose faster compared to the last three millennia. Since the Great Acceleration, the global sea level rate has increased with a rate of 2.3 mm yr^{-1} between 1971 and 2018, and as much as 3.7 mm yr^{-1} between 2006 and 2018. And today, the sea level has risen by 0.2 m over the period from 1901 to 2018 (Arias et al., 2021). The partitioning of sea level change over the 20^{th} century is estimated to be about 32% from thermal expansion, 52% from mass loss of glaciers and 29% from GrIS (Fox-Kemper et al., 2021). Although, we have seen in the past that even larger parts of sea level change have been because of the area and volume changes of the GrIS and AIS (Dutton et al., 2015).

The AR6 concluded that until 2050, there is no dependency upon the emission scenario regarding changes in sea level. And relative to the period between 1995-2004 the GMSL is projected to rise between 0.18–0.23 m. Only after 2050, the sea level changes become dependent upon emission scenarios, with a projected sea level rise between 0.38 m for SSP1-1.9 and 0.77 m for SSP5-8.5 by 2100 (Fox-Kemper et al., 2021). Important to note is that these projections do not include the uncertain ice-sheet-related processes, such as the disintegration of marine ice shelves, marine ice sheet and ice cliff instability around Antarctica, nor unprojected changes in surface mass balance and ice loss from GrIS (Fox-Kemper et al., 2021). Beyond 2100, the oceans will continue to warm due to the deep-ocean heat uptake and the mass contribution from GrIS and AIS, causing sea levels to continue to rise for several centuries. Hence, the changes in global warming today and in the future are committing us to sea level rise for a long time. Even if global warming is limited to $2°C$, the GMSL will rise between 2 and 6 m in the coming 2000 years. With a peak warming of $3°C$, the committed sea level rise over 2000 years is projected to be between 4 to 10 m (Fox-Kemper et al., 2021).

1.3. Change in Ocean Circulation

Increased atmospheric and ocean temperature and freshwater influx to the ocean from GrIS not only affect the sea level, but also the Atlantic Meridional Overturning Circulation (AMOC) and more specifically its northern branch, the North Atlantic Meridional Overturning Circulation (NAMOC). The AMOC is the main overturning current system in the Atlantic Ocean which transports warm, salty upper-ocean water northwards, and the deep counter-current transports deep, cold water southwards (Fox-Kemper et al., 2021).

The AMOC is likely to slow down in the coming centuries due to warmer oceans, increased freshwater from GrIS, changes in Arctic sea ice and increased precipitation over northern seas due to a warmer atmosphere (Arias et al., 2021). Compensation for the added heat in the oceans takes the form of a redistributed cooling in the North Atlantic basin (Bryden et al., 2020; Fox-Kemper et al., 2021). The reduction in ocean heat transport is already and will continue to create a so-called “cold spot” in the northern Atlantic, and subsequent slower warming compared to the rest of the Arctic (Chemke et al., 2020; Noël et al., 2022). The AMOC has been monitored since 2004, but this is not long enough to say anything certain about emerging variability and long-term changes and trends. Furthermore, the confidence in model results is low due to model disagreements on quantitative trends such as the magnitude and timing of AMOC decline (Fox-Kemper et al., 2021). However, most models and all CMIP6 models agree that the AMOC will weaken over the 21^{st} century. After 2060 the evolution of the AMOC becomes dependent on the emission scenario, where low-emission scenarios project stabilisation and high-emissions scenarios project further decline (Fox-Kemper et al., 2021; Menary et al., 2020; Weijer et al., 2020).

1.4. Arctic Sea Ice

A warmer atmosphere and warmer oceans will also have significant loss of the Arctic sea ice, which will further have cascading effects for the further ocean and atmosphere warming, as well as for Greenland. Loss of Arctic Sea ice is found to be linear with increasing global mean surface temperature, and thus also to the cumulative anthropogenic CO_2 emissions from observational data and outcomes of the CMIP6 models (Fox-Kemper et al., 2021).

As such, the Arctic sea ice area remains an important indicator of large-scale climate change. This is often assessed as the sea ice extent, defined as the total area of all grid cells with at least 15% sea ice concentration. Satellite observation has revealed that the Arctic sea ice has been reducing every month since 1978. Especially, from August to October, the sea ice area was 25% smaller (2 million km^2) between 2010–2019 compared to 1979-1988 (Fox-Kemper et al., 2021). Further loss of sea ice means that the ocean is warming, as well as the atmosphere around due to the loss of ice and snow on the sea ice surface that otherwise reflect a lot of the shortwave radiation.

It is likely that the Arctic Ocean will become virtually sea ice-free in September when sea ice is at a yearly minimum, before 2050 regardless of emission scenario (SSP) (Fox-Kemper et al., 2021). However, CMIP6 models found that is likely that throughout this century the Arctic Ocean remains sea ice-covered during winter (Fox-Kemper et al., 2021). Investigating temperature thresholds for loss of sea ice projects that 1.5°C to 2°C warming is likely to result in complete loss of sea ice during September in some years. However, global warming of 3°C will see a virtual sea ice-free Arctic Ocean in September in most years (Fox-Kemper et al., 2021). Subsequent, larger global warming will mean even longer ice-free periods in most years.

1.5. Greenland Ice Sheet

Above 60 degrees north lays the northern largest permanent ice- and snow-covered area: The Greenland Ice Sheet, with steep ice margins, a maximum thickness over 3 km, distinct melt and weather patterns, with annual mean temperatures ranging from -30.5 to -3.5°C and a volume of frozen water equal to about 7.4 global mean sea level rise (Bamber et al., 2018; Ettema et al., 2010). There is uncertainty in the GrIS sensitivity to global warming, which causes concerns for the future projections of its evolution, as changes in the ice sheet affect sea level and regional and global climate. Reconstructions of the past, show that the GrIS have both been much larger and smaller than today, and a change in the ice sheet can be triggered by temperature changes of only a few degrees (Gaffney & Rockström, 2021; Steffen et al., 2018). In recent years (2012 to 2017), the mass loss from the Greenland ice sheet has been 239 Gt yr^{-1}, which is about 0.7 mm yr^{-1} of sea level equivalent (SLE) (Shepherd et al., 2020). The increased contemporary mass loss is caused by increased runoff from atmospheric warming and increased ice discharge from ocean warming (Fox-Kemper et al., 2021; van den Broeke et al., 2016)

The GrIS gains mass by precipitation, mainly by accumulation of snow (Fyke et al., 2018). In winter, most precipitation falls along the southeast coast due to mid-latitude transient low-pressure systems moving across the North Atlantic. During summer, more precipitation, compared to during the winter, falls on the western margins and interior of the GrIS (Ettema et al., 2010; Fyke et al., 2018). The varying weather originates from warm air from the equator, the pressure difference between the Icelandic low and Azores high, and the warm ocean currents moving northwards. It is therefore not surprising that changes in the ocean currents, such as the NAMOC, could also influence the GrIS by causing shifts in precipitation patterns and local temperatures. Furthermore, the ice sheet loses mass by surface melt causing surface meltwater runoff, sublimation and direct mass loss to the ocean by iceberg calving or melting (Fyke et al., 2018). The mass balance of the ice sheet can be expressed as:

$$MB = SMB + BMB – ID \tag{1.1}$$

SMB is the Surface Mass Balance, BMB is the Basal Mass Balance and ID is Ice Discharge. ID takes place where the ice sheet meets the ocean and can be influenced by for instance warmer ocean temperatures. The SMB is affected by atmospheric processes such as precipitation, radiation, cloud cover and heat advection (Cuffey & Paterson, 2010). Positive SMB means surface mass gain and negative means surface mass loss. The Equilibrium Line Altitude (ELA) divides the ice sheet into the accumulation area (SMB > 0) and the ablation area (SMB < 0). Warmer temperatures lead to expansion of the ablation area, causing more melt as the ice sheet margin thins and a steeper topographic gradient forms around the ELA enhancing ice flow to the margins. Today the mass loss from BMB is negligible, but the loss from SMB and ID is important. GrIS loses almost as much mass from SMB as from ID. SMB will become the dominant part of mass loss in the coming century, however, ID will continue to be an important source of mass loss, due to large variability in SMB (Choi et al., 2021; Fox-Kemper et al., 2021). In the period between 1992 and 2000, the GrIS lost a total mass of 4890 Gt, which is equal to a 13.5 mm Global Mean Sea Level Rise (GMSLR) (Arias et al., 2021). The mass loss has accelerated in the last decades, with rates of 39 Gt yr^{-1} during 1992-1999, 175 Gt yr^{-1} during 2000-2009 and 243 Gt yr^{-1} during 2010-2019 (Arias et al., 2021). The largest mass loss has taken place on the northwest and southeast part of the ice sheet (Arias et al., 2021).

There is no question that the GrIS will continue to lose mass in the coming centuries and millennia, but how much and how fast will it be affected by future emissions? Up until 2100, GrIS is projected to contribute 0.01 to 0.10 m to GMSL under SSP1-2.6, 0.04 to 0.13 m under SSP2-4.5 and 0.09 to 0.18 m under SSP5-8.5 (Arias et al., 2021). There has recently been made progress in the field of climate modelling, where the coupling between Earth System Models (ESM) and ice sheet models is improved.

Muntjewerf, Sellevold, et al. (2020) project that the mass loss from GrIS with a coupled ice sheet and climate model would increase sea levels by 0.109 m in 2100 with respect to 2015 under SSP5-8.5. An idealised simulation, run with the same model, where CO_2 increases yearly by 1% until $4xCO_2$, projects a similar sea level rise of 1.140 m (Muntjewerf, Petrini, et al., 2020a).

Aschwanden et al. (2019), by using a stand-alone ice sheet model, predicts that following the SSP2.6 the GrIS could contribute to 0.25 m GMSL, while SSP8.5 contributes 1.74 m past 2100. However, AR6 states that there is low confidence in climate projections until and beyond 2300, due to the uncertainties in climate drivers for projecting ice sheet change (Fox-Kemper et al., 2021). This motivates further research on GrIS mass loss beyond 2100, not only for the low and high emissions scenarios but also for the intermediate.

There is an interesting ongoing debate in contemporary literature on the topic of tipping point and threshold for GrIS irreversible mass loss and sea level rise. It is often considered that such a tipping point is reached when the SMB becomes zero or negative (van den Broeke et al., 2016). Moreover, some studies find a temperature threshold while others find that the tipping point is more connected with ice volume loss. Gregory et al. (2020), found no strict temperature threshold for mass loss. Instead, if the ice sheet loses mass equivalent to 3 to 3.5 m sea level rise, it would not regrow to its present state and an equivalent of 2 m sea level rise would be irreversible. This mass threshold might already be reached in 400 years, should warming reach $10°C$ under the SSP8.5 (Aschwanden et al., 2019). In contrast, Robinson et al. (2012) found a threshold of $3.1°C$ ($1.9–5.1°C$) of global temperature rise with respect to PI, which if reached, will lead to complete melting of the ice sheet.

1.5.1. Surface Mass Balance

Changes in the SMB are and are projected to continue to be one of the largest causes of GrIS mass loss (Fox-Kemper et al., 2021). In order to gain a better understanding of how the ice sheet loses mass, it is important to quantify the evolution of the main components of the SMB. The GrIS has a strong topographic gradient at the margins and high spatial climate variability affecting the surface mass loss. The SMB is defined as follows:

$$SMB = Precipitation – Runoff – Sublimation \tag{1.2}$$

Precipitation is defined as the sum of the snowfall and rainfall. However, snowfall contributes to positive SMB, while only rainfall that is refrozen contributes positively. If not, it contributes to surface runoff, which together with the melt are directly lost to the ocean. Therefore, the SMB can be rewritten as snowfall plus refreezing, minus sublimation and melt:

$$SMB = Snowfall + Refreezing – Sublimation – Melt \tag{1.3}$$

Snowfall is the main contributor to mass gain at the surface, and most snow falls in the southeast due to the storm tracks in this region (Ettema et al., 2010; Fyke et al., 2018). The main source of contemporary surface mass loss is surface melt (van den Broeke et al., 2016), which takes place over larger parts of the ice sheet, but especially at low elevations. However, GrIS surface melt is partitioned between runoff, direct loss of mass, and refreezing. Refreezing occurs when melt at the surface percolates down into the snowpack. The main conditions for surface water to refreeze are enough available pore space and temperatures below freezing point. While this barely adds mass to the snowpack, the phase change of the liquid water releases energy and slightly heats the snowpack, which reduces the potential of refreezing (Fyke et al., 2018). In addition, the refreezing capacity of the snowpack is limited because it acts as a sponge, refreezing up meltwater until there is no more pore space available. Furthermore, most of the refreezing is happening around and just above the ELA. This is because below the ELA melt rates are high, so it is little or no pore space in the snow and firn and at lower elevations, the temperature is close to the melting point. Just above the ELA there is still significant surface melt and precipitation, but temperatures are lower and there is more snow with potential pore space (SMB > 0). Today the main contributor to surface mass loss is increased surface melt. Furthermore, sublimation acts as either mass loss or gain, by directly going from solid state to vapour, or from vapour state to solid (also called deposition). At present, sublimation contributes to mass loss.

1.5.2. The SMB-elevation Feedback

The elevation feedback concerning the SMB is considered a positive feedback mechanism. It follows the principle that at higher altitudes the temperature is colder. If the ice sheet melts, elevation is reduced which results in a warmer climate and further melting (Fyke et al., 2018).

1.5.3. Surface Energy Balance

Most of the mass loss, hence surface melt and runoff, takes place in the summer, during the months of June, July and August (JJA) when the Surface Energy Balance (SEB) is positive. The SEB consists of radiative, turbulent and ground heat fluxes. The melt energy (E_M) is the sum of net surface radiation (SW_{net} + LW_{net}), latent and sensible turbulent surface fluxes (SHF and LHF) as well as the ground heat fluxes (GHF) at the interface between snow and atmosphere (Ettema et al., 2010; Fyke et al., 2018). Furthermore, the melt can be constrained or enhanced by variables such as wind speed, humidity, clouds, surface characteristics and snowfall (Cuffey & Paterson, 2010). The formulation of melt energy is:

$$E_M = SW_{net} + LW_{net} + LHF + SHF + GHF \tag{1.4}$$

1.5.4. The Ice-Albedo Feedback

The Ice-Albedo Feedback is also a positive feedback mechanism, which connects the changes in surface reflectivity to changes in the melt. The albedo regulates how much shortwave energy is absorbed by the snow or ice. Fresh snow is highly reflective, with an albedo of approximately 0.8 (Cuffey & Paterson, 2010). When snow and ice are melting, their albedo lowers, causing more absorbance of solar radiation, and enhancing melt. Bare ice has an albedo of 0.6-0.35 (Cuffey & Paterson, 2010), and as the ice melts away, it exposes bare soil or vegetation, with even lower reflectivity, and the albedo feedback continues.

2
Research Objectives

In this study, a simulation run with the state-of-the-art coupled Earth System model CESM2-CISM2 is analysed. The analysis of the $2xCO_2$ simulation is motivated by the research objectives presented in this section. The $2xCO_2$ simulation provides insight into a future projection of the evolution of the Greenland ice sheet due to its long simulation time and focus on the couplings between climate and ice sheet. Simulating ice sheet dynamics within an Earth system model requires accounting for ice sheet-climate interactions and feedbacks. This interaction is necessary when conducting simulations over longer timescales where ice sheets are subjected to mass change so that the assumption of an ice sheet in equilibrium no longer holds. Moreover, when the equilibrium state of the ice sheet is perturbed, it takes several millennia (if not more) to reach a new steady state.

The main research question is as follows:

How does the Greenland Ice Sheet mass budget respond to a doubling of global CO_2 at a multimillennial time scale as simulated by a coupled ice sheet-climate model?

The evolution of the Greenland ice sheet will be investigated considering a moderate warming scenario at a multimillennial time scale. Its sensitivity to a doubling of CO2 concentrations with respect to pre-industrial (the year 1850) is explored by considering its mass balance: where snow accumulation leads to mass gain and refreezing counteracts increased melt. Furthermore, the mass loss of the Greenland ice sheet and the consequential contribution to global mean sea level rise is quantified. This quantification bridges the gap between low-and high-warming scenarios, as the $2xCO_2$ simulation can be considered a moderate warming scenario (Meinshausen et al., 2020). Furthermore, in the past, most GrIS simulations were based on global or regional climate modelling that was used for offline-forcing of higher-resolution ice sheet models projecting the evolution of Greenland. However, recent work has been done to couple ice sheet models to Earth system models, with the goal to gain insight into the coupling of the ice sheet and climate evolution. The CESM2-CISM2 (Danabasoglu et al., 2020; Lipscomb et al., 2019) is a coupled Earth system model that simulates the interaction between a changing climate and the evolution of the GrIS. The model has been applied to the high emission scenarios SSP5-8.5 (Muntjewerf, Sellevold, et al., 2020) and 1% yearly CO_2 increase until concentration levels is $4xCO_2$ compared to PI (Muntjewerf, Petrini, et al., 2020a). In this thesis, I will examine a $2xCO_2$ simulation and compare it with the $4xCO_2$ extreme warming scenario simulation run with the same model and a control simulation where pre-industrial conditions are maintained. I will quantify future GrIS mass loss and explain the processes involved, such as precipitation evolution in a changing climate, melt and refreezing. A changing Arctic climate is also included in the analysis, with a focus on the consequences of decreased Arctic sea ice, and changes in ocean currents. The multimillennial timescale is crucial for the analysis, as the ice sheet responds to climate change over a long periods of time.

Furthermore, to support the main objective of the thesis, three sub-questions are explored:

1.How do Surface Mass Balance and Surface Energy Balance components evolve under a moderate warming scenario?

I will analyse the time series of the surface mass balance and surface energy balance components of the $2xCO_2$ simulation compared to the PI simulation and $4xCO_2$ simulation, to quantify and explain how the components change and how they are influencing each other, and how they ultimately cause mass loss of the ice sheet. Under a moderate warming scenario, how fast is the mass loss? Which components contribute the most to the mass loss? I will evaluate how the components change as a response to global warming, but also considering the eventual elevation and area change of the ice sheet. Particular focus will be given to the changes in precipitation, melt and refreezing, and potential melt tipping point or distinguished acceleration.

2.How do global, Arctic climate and the climate over Greenland influence the GrIS SMB evolution?

In the $2xCO_2$ simulation, the global climate will continue to warm with the constant CO_2 forcing. Observations today and many future projections see the Arctic warming faster than the global climate. Will this higher warming also affect Greenland? Or will Greenland warm slower than the Arctic? Will the loss of sea ice cause higher warming, leading to a complimentary increased acceleration of GrIS surface mass loss?

3.How does NAMOC evolution impact the GrIS SMB?

In all CMIP6 models, the NAMOC is projected to further decline in the future (Fox-Kemper et al., 2021). This is also the case for most of the simulations run with CESM2-CISM2 (Muntjewerf, Petrini, et al., 2020a; Sellevold & Vizcaíno, 2020), where the NAMOC is decreasing as global warming increases. However, in the $2xCO_2$ simulation, the NAMOC is recovering after a few centuries in a weakened state. As this simulation is a moderate warming scenario, does the relative regional cooling, caused by initially reduced NAMOC, have a major impact on the GrIS SMB? Further, as the NAMOC recovers, will the increased amount of heat again transported to the south of Greenland have an additional accelerating effect on the surface mass loss?

3 Methods

3.1. Model Description

The Coupled Community Earth System Model version 2 (CESM2; Danabasoglu et al., 2020) and the Community Ice Sheet Model version 2 (CISM2; Lipscomb et al., 2019) are part of the new major developments of the state-of-the-art Earth System Models (ESM). ESMs include components for land, ocean, atmosphere, sea ice and ice sheet in a few cases (Sellevold et al., 2019; Smith et al., 2010). As climate change is advancing, with an accelerated melting of the largest ice sheets on Earth, there is a need for robust projections of sea level rise. The CISM2 calculates ice velocities, internal temperatures as well as the dynamical evolution of the dynamical ice sheet, by using a higher-order approximation of the Stokes equations (Lipscomb et al., 2019). The three-dimensional thermomechanically coupled ice sheet model of CISM2 is integrated into CESM2 by a bi-directional coupling of the ice sheet model to the land and atmosphere models and with a one-directional coupling to the ocean model. Advanced ice melt rates calculations account for snow compaction as well as the reflection of solar radiation from the surface in the CESM component (van Kampenhout et al., 2017). The meltwater and ice discharge fluxes are accounted for through the ocean model. Furthermore, the CESM2 includes land and atmospheric models, that react to changes in extent, elevation, and roughness of the ice sheet. Evolution of the ice sheet results in reduced surface albedo and changes in sign and magnitude of the sensible and latent heat fluxes, surface roughness, and ice sheet topography. With CESM2–CISM2, these changes are coupled with the ice sheet and climate, improving our understanding of the dynamics between the GrIS and climate, in the past, present and future (Muntjewerf, Petrini, et al., 2020a; Sommers et al., 2021; van Kampenhout et al., 2020). The separate components of the CESM2–CISM2 are discussed below.

Atmosphere model

The Community Atmosphere Model 6 (CAM6; Gettelman et al., 2015; Lin and Rood, 1997) simulates the atmospheric processes and the geometry of the ice sheet is communicated to this model component. The model performs on a horizontal grid with a nominal resolution of 1° with 32 levels in the vertical with the upper boundary at 3.6 hPa (~ 40 km). Improvements have been made since the CAM5 in every atmospheric physics parameterisation, except for radiative transfer. The cloud microphysics is improved so that the cloud biases are reduced over Greenland (Lenaerts et al., 2020; Liu et al., 2015). This further includes the representation of cloud liquid water and longwave forcing. Furthermore, the representation of orographic precipitation, near-surface wind, turbulent heat and moisture fluxes are also improved compared to CAM5 (Lenaerts et al., 2020; Scinocca & McFarlane, 2000; van Kampenhout et al., 2020).

Land model

The Community Land Model Version 5 (CLM5; Lawrence et al., 2019), simulates the land processes, which includes biogeophysical and biochemical processes, as well as snow hydrology. The resolution of the horizontal grid is also 1° (0.90° latitude x 1.25° longitude). The heterogeneity of the landscape on Greenland is represented through different surface types. The uppermost level is the surface type called the land unit, where each grid cell is assessed and fractions in the grid cell are identified as a glacier, lake, wetland, urban, vegetated, or crop surface. Heterogeneity of the state variables within each land unit is accounted for in the next level, the column level, referred to as elevation classes (ECs; Lipscomb et al., 2013), which includes the impact of subgrid-scale variations in topography on the surface mass balance and surface energy balance calculations.

The discretization, in the vertical direction, between soil and snow differs within the model. The soil column has a fixed number of layers, while the snow and firn have variable numbers of layers with a maximum snow depth defined as H_{max} which is equal to 10 m water equivalent (mWE). This maximum depth allows for the development of firn layers sufficiently deep for refreezing and storage of surface meltwater to take place in areas with perennial snow cover (Muntjewerf et al., 2021; van Kampenhout et al., 2017).

The albedo of the snow is calculated with the SNow, Ice, and Aerosol Radiation model (SNICAR), which simulates the spectral albedo of snow in a multilayer approximation, to consider vertically resolved solar absorption, snow grain size evolution, and aerosol impurities in the snow (Flanner & Zender, 2006; Flanner et al., 2007). This improves the simulation of the surface albedo and snow melt (Muntjewerf et al., 2021).

Furthermore, the heat and water fluxes, as well as the phase changes between liquid and solid water, are also accounted for in all vertical layers for each column if the upper boundary condition is set as the overlying atmospheric heat fluxes. The lower boundary is set to net-zero heat flux. The surface runoff is directed to the ocean by the Model for Scale Adaptive River Transport (MOSART; Li et al., 2015). Transport is based on present-day topography gradients and is simulated with time-varying velocities and channel water depths (Muntjewerf et al., 2021).

Ocean model
Ice sheet meltwater and solid ice discharge are passed to the ocean with the Parallel Ocean Program version 2 (POP2; Danabasoglu et al., 2012; Smith et al., 2010) that simulates the ocean processes. The horizontal grid resolution is nominal 1°. The vertical component of the ocean is discretized in 60 levels and the POP2 conserves volume.

Sea-ice model
The Los Alamos National Laboratory Sea ice model version 5 (CICE5; Hunke et al., 2017) is used to represent the sea ice dynamics, by determining the horizontal transport, ridging, and elastic-viscous-plastic rheology. The sea-ice model shares the same grid as the ocean model. The salinity profiles and sea ice temperature are divided into eight layers, in the vertical direction. Furthermore, a three-layer snow model makes sure that the temperature distribution in the snowpack on the sea ice is accounted for (Muntjewerf et al., 2021).

Land-ice model
Further, the ice sheets are simulated by CISM2 (Lipscomb et al., 2019), which is a parallel, three-dimensional thermomechanical ice sheet model solving several approximations of the Stokes equations for incompressible viscous flow. Greenland is simulated with a 4 km rectangular grid founded on a polar stereographic projection. A flotation criterion is used for ice discharge at the margins in most of the Greenland simulations, which directly calves floating ice to the ocean (Muntjewerf et al., 2021).

3.2. Coupling Description

The large difference in resolution between climate and ice sheet models is one of the challenges when coupling models. The coupling between CISM2 and CESM2 is no exception due to the fact that the ice sheet component runs on a 4 km grid and the CLM5 a nominal 1°. The coarser resolution of CLM5 makes it harder to accurately capture the steepest ice sheet margins, which is important as the surface energy and mass budgets of the ice sheet are very dependent on elevation. However, the various ECs used in CLM5 account for subgrid-scale variation in elevation over the glaciated land units by binning the fraction of this unit in each grid based on the topography from the higher resolution ice sheet model. Furthermore, the surface energy fluxes are coupled to the SMB by downscaling atmospheric variables. A uniform lapse rate of –6 K km^{-1} is the grid cell temperature used in CLM5. Together with an assumed vertically uniform relative humidity allows for the EC-specific potential temperature, specific humidity, air density, and surface pressure to be determined. Precipitation is partitioned into rain or snow, based on the elevation-corrected near-surface temperature. If the downscaled surface temperature is below -2$°C$, the precipitation is taken as snow. If the downscaled surface temperature is above 0$°C$, precipitation is assumed to fall as rain. The annual accumulated SMB in each of the glacier land units in every ECs is calculated, and the SMB is remapped from the coarser CLM5 to the higher resolution ice sheet model grid. Since the grid in CLM5 can have fractions of several land units, there is an implementation of dynamic land units as the ice sheet extent changes. For every grid cell in CLM5, the glacier elevation classes are set based on the topography in CISM2. The coupler remaps the ice sheet geometry from CISM2 to CLM5 as it evolves, and further uses the ice sheet extent in CIMS2 to also recompute the fractional glacier coverage. This also allows for a dynamic change from glaciated to vegetated land units with the retreating ice sheet (Muntjewerf et al., 2021).

Over longer periods, the change in geometry of the ice sheet is significant and can influence atmospheric circulation. In CESM2 this is accounted for by updating the topographic boundary conditions, which modifies the CAM6 boundary conditions and will restart files based on ice sheet elevation changes in CISM2.

The coupling between the ice sheet and the ocean is one-directional, thus only information on freshwater flux travels from the ice sheet into the ocean from the marine-terminating glaciers, whereas information on the ocean is not passed to the ice sheet. The surface runoff consists of liquid water at the ice sheet surface and the fluxes are computed in the surface hydrology module of CLM5. The basal melting happens at the base of the ice sheet where it is at a pressure melting point caused by friction and geothermal heat, and this is computed in CISM2 (Muntjewerf et al., 2021).

3.3. Model Evaluation

The simulations used in this study are run with the CESM2-CISM2 and are initialised from a spun-up pre-industrial climate/ice-sheet state (Lofverstrom et al., 2020). In this state, the ice sheet volume is 12% larger than present-day observations with a residual drift of $\sim$ 0.03 mm SLE yr^{-1}. The ice sheet area is also about 15% larger than the present day, due to a more extensive ice sheet simulated in the north.

The spin-up procedure is important as the model and model components should start from an initial stable condition free of residual drift. In order to achieve this, the spin-up should ideally capture the full characteristics of a coupled ice sheet and climate system by for instance including a coupled simulation over the Last Glacial Cycle. However, due to the long simulation time required, this is not feasible. One method to reduce the computational time and cost is to accelerate the ice sheet with respect to the other components. The assumption used is that from year-to-year the changes in area and topography of the ice sheet are small. The approach described by Lofverstrom et al. (2020), models a coupled climate system based on a spin-up by alternating between a fully coupled model configuration and a computationally cheaper configuration. The atmospheric component is replaced by a data model with prescribed boundary conditions. The broader coupled model state does not experience unrealistic drift by ensuring an adequately constrained data atmosphere by periodically re-establishing the atmospheric forcing. The simulated spin-up climate is similar to the pre-industrial control climate which is fully coupled to a simulation with prescribed GrIS. Although the final state of the iterative spin-up procedure presents some biases, they are similar to previous efforts and do not invalidate the procedure. The biases are related to intrinsic CESM2 climate and/or CISM2 ice sheet biases. Overall, this suggests that the iterative method provides a faster and computationally cheaper method for spin-up of complex ESMs (Lofverstrom et al., 2020).

An evaluation of the representation of the GrIS SMB with CESM2 has been done by van Kampenhout et al. (2020), where the GrIS geometry was held fixed. Firstly, the large-scale circulation patterns were evaluated during the late 20th century based on the best-estimate reanalysis data. Secondly, the impact of clouds on the surface energy balance was taken into account by evaluating the CESM2 clouds over

Greenland using observations of cloud water path from remote sensing data. Thirdly, remote sensing data and regional climate models (RCM) output were used to evaluate the surface albedo of the model. And lastly, the mean monthly energy and mass fluxes over GrIS were evaluated using the best-estimate RCM output. The conclusion was that the CESM2 model simulates fairly well the large-scale climate, clouds, surface climate, SEB and SMB. The albedo in the model was biased low, and the summer radiation surplus, compared to the Regional Atmospheric Climate Model 2 (RACMO2), compensates for weaker CESM2 turbulent fluxes. It was also found that the precipitation was overestimated, but GrIS ablation areas in the north and east were underestimated compared to RACMO2. Simulated trends of runoff and SMB was smaller than in RACMO2. Even so, the simulated present-day geometry of the GrIS SMB by the CESM2 is physically realistic.

Muntjewerf et al. (2021) demonstrated the CESM2-CISM2 coupling between two climate states with a focus on the major couplings of SMB, ocean freshwater flux from Greenland, dynamic ice sheet margins, and surface topography updating. The high CO_2 coupled simulation shows an integrated SMB decrease and expansion of the ablation areas. The average ELA raises above 2000 m and the ice sheet margins retreat inland and thins. This causes a steeper topographic gradient between the high interior and the margins, and ice velocities increase. The ocean receives freshwater in the form of ice discharge from ice calving, basal melt and surface runoff. Ice discharge decreases as the marine-terminating glaciers thin and retreat inland. Moreover, the ice discharge simulated for the integrated GrIS and the SE basin is in accepted agreement with observations (Enderlin et al., 2014; Muntjewerf, Petrini, et al., 2020b). There are regions where the ice discharge is overestimated (southwest, northeast and north) and underestimated (northwest and central west). However, this coincides with regions of ice thickness over-and under-estimation. At the moment, the coupled model does not include ice shelves or sub-shelf melt. Furthermore, when the ice sheet retreats inland, areas become deglaciated, exposing bare soil or vegetation. This causes lowered surface albedo which affects the surface energy balance. The changes in ice sheet topography are captured by the atmospheric model and in turn, adjust the atmospheric circulation. A model limitation is the calving parameterisation, which currently calves all floating ice. Thus, marine-terminating glaciers are not realistically simulated.

Further planned model improvements include bi-directional coupling to the ocean as well as the implementation of a dynamic ice sheet-ocean mask and a land-ocean mask that will adjust to dynamic ice shelf extent over the ocean. Other improvements to come are routing of the runoff along the dynamic ice sheet surface gradients, instead of present-day topography. Also, the inclusion of dynamic vegetation will be important for long timescale simulations as vegetation plays a crucial role in the albedo and ecosystem feedback (Muntjewerf et al., 2021).

3.4. Simulations

The 2xCO_2 is an idealised simulation run with CEMS2-CISM2. The CO_2 concentrations are increased by 1% per year until the year 70, where CO_2 concentrations are at 569 ppm, which is a doubling compared to PI. After year 70, the CO_2 concentrations are kept constant throughout the simulation. Although this is an idealised scenario, it is interesting to place the simulation into a wider context, such as the shared socio-economic pathway (SSP) scenarios. A study done by Meinshausen et al. (2020)m, uses the reduced-complexity climate-carbon-cycle model MAGICC7.0 to model the greenhouse gas concentration for all the SSP scenarios, from 2015 to 2500. SSP2-4.5 ends with a CO_2 concentration of 579.2 ppm in 2500. This is close to the 569 ppm CO_2 for the 2xCO_2 simulation, and this would fall into the ”Middle of the road” SSP group. A comparison between the extended SSP scenarios and the CESM2 2xCO_2 simulation is displayed in Figure 3.1.

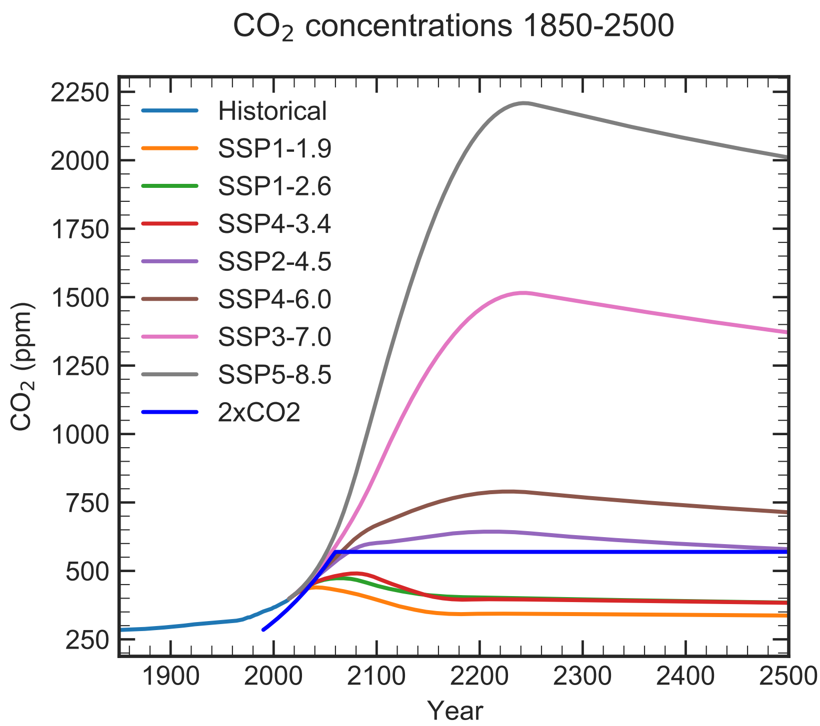

Figure 3.1: Overview of SSP CO_2 concentration scenarios from 1850 to 2500 compared to the CESM2 2xCO_2 simulation. For a better comparison, the 2xCO_2 simulation is plotted with a starting point in the year 1990. Figure recreated from Meinshausen et al., 2020.

In contrast to the SSP scenarios, the CESM 2xCO_2 simulation has a fixed CO_2 concentration once reaching a doubling. This idealisation of the simulation is done to distinguish direct responses of climate and ice sheet from lagged responses and feedbacks, without the effects of aerosol and land use changes, which are taken into account in the SSP scenarios. In many scenario-based simulations, emissions are decreased after some time, in order to mimic future anthropogenic emission cuts, based on social and economic evolution. In these simulations, the CO_2 concentration in the atmosphere will decrease because of the ocean and land sinks that are part of the carbon cycle (Canadell et al., 2021).

The climate component of the model is computationally expensive and is therefore only run for 1000 years. The ice sheet component of the model is run for 3000 years, assuming that after year 500, the climate is not changing too rapidly, and therefore one climate year is used for five years in the ice sheet component. To keep consistency throughout the analysis, the climate components' time axis is stretched to 3000 years when visualising in figures.

Further supporting the analysis of the 2xCO_2 simulation is a pre-industrial control simulation (PI). The control simulation is run for 300 years, also with CESM2-CISM2. The PI simulation reproduces the pre-industrial climate and has a fixed CO_2 concentration of 284.7 ppm. Additionally, a 4xCO_2 simulation following the same setup as the 2xCO_2 simulation is used as an upper bound for the analysis.

4
Results

This section offers an extensive report on the analysis of the Greenland ice sheet under a moderate warming scenario, using a $2xCO_2$ simulation run with CESM2-CISM2. The doubling of atmospheric CO_2 content yields an increased global mean annual temperature of $5°C$, the Arctic (defined as north of 60°N) increased by $11°C$ and Greenland by $9°C$ after 3000 years, with respect to PI. Furthermore, the GrIS contribution to the global mean sea level is 4.1 m. The GrIS contribution to sea level accelerates after year 710 as the NAMOC recovers. Another acceleration takes place after the year 1380 due expansion of ablation areas together with an active ice-albedo feedback and a NAMOC in a new equilibrium state. The main contributor to surface mass loss is melt, where most of the increased melt is partitioned to runoff. At the end of the simulation, melt is about 3.7 times higher than PI. The main contributor to additional melt energy after 3000 years is the net shortwave radiation, contributing to 46% of this additional melt energy, compared to PI. In conclusion, the following results confirm that even under a moderate warming scenario, the GrIS is quite sensitive to climate change as half of the initial mass and area is lost over three millennia.

4.1. Global, Arctic and Greenland Climate Change

The atmospheric CO_2 concentrations in the $2xCO_2$ simulation increases 1% per year, until year 70 when concentrations are two times that of PI levels, after which it is kept constant for the remainder of the simulation. The immediate increase in CO_2 the first 70 years causes radiation imbalance at the top of the atmosphere (Fig.A.1), which triggers an equally rapid increase in global mean near-surface temperature (GMNST) and near-surface temperatures over the Arctic and the Greenland ice sheet. During the first 50 years of the simulation, the global mean temperature increases at a rate of $0.03°C$ yr^{-1}, the Arctic with $0.07°C$ yr^{-1} and Greenland with $0.02°C$ yr^{-1}. The trend analysis is done with a breakpoint detection of the slope and a fitted linear regression (Table A.1). Figure 4.1 shows the near-surface temperature change with respect to the PI simulation. The Arctic is warming the most due to decreasing seasonal terrestrial snow cover and loss of sea ice. The latter exposes the dark ocean surface which in turn absorbs more heat and a positive feedback loop is initiated.

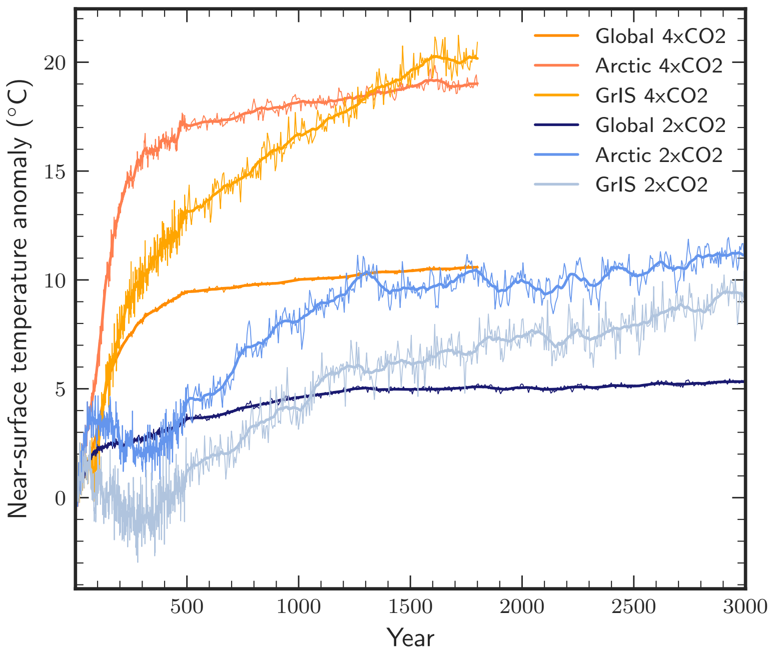

Figure 4.1: Evolution of global, Arctic (north of 60°N) and GrIS annual near-surface temperature with respect to pre-industrial mean ($^{\circ}C$).

After CO_2 stabilisation in the year 70, the global near-surface temperature continues to increase, however at a slower pace of 0.0025$^{\circ}C$ yr^{-1} until the year 1360. Approximately after the year 1360 until the end of the simulation, the rate of global mean temperature increase is 0.0002$^{\circ}C$ yr^{-1}, Arctic is 0.001$^{\circ}C$ yr^{-1} and Greenland is 0.002$^{\circ}C$ yr^{-1}. These are relatively weak warming trends, which could imply that the Earth system is close to a new equilibrium state. This is defined as when the radiation at the top of the atmosphere is equal to zero, and the radiative imbalance at the end of the simulation is 0.5 W m^2. In addition, after 3000 simulation years, the GMNST has increased by 5$^{\circ}C$, the Arctic is 11$^{\circ}C$ warmer and Greenland is 9$^{\circ}C$ warmer compared to the PI simulation (Fig.4.1).

Notably, after year 500, it is assumed that the climate is close to equilibrium, and is only updated in the ice sheet model every five years. Figure 4.1 has thus a stretched time axis in order to better compare with the evolution of the ice sheet. Figure A.2 shows the evolution of the temperature in accordance with the simulated climate years.

Interestingly, the near-surface temperature is decreasing over the Arctic and Greenland region after CO_2 stabilisation, especially over Greenland with a rate of -0.01$^{\circ}C$ yr^{-1} between the years 40 and 300, before warming resumes with a rate of 0.008$^{\circ}C$ yr^{-1}. The Arctic temperature decreases at a rate half of GrIS, -0.005$^{\circ}C$ yr^{-1} during the years 55 to 418, before also increasing with a rate of 0.008$^{\circ}C$ yr^{-1}, until approximately the year 1360. Between 1360 and 3000 there is only a slight warming trend over the Arctic and Greenland (Table A.1) as the Earth system is approaching a new steady state.

The current hypothesis is that the temperature decrease in the Arctic and Greenland region is due to the slowdown of the NAMOC. As the NAMOC slows down, the usual heat transport with the northward ocean currents decreases, providing reduced warming, or a "cooling-effect" around the Greenland region (Fig.A.3). The reduced warming is also visible in the simulated total precipitation pattern, where counter-intuitive to the effect of global warming (warm and moist atmosphere enhancing precipitation), there is a reduction in precipitation around the southern part of Greenland, Iceland and as far as the coast of Scandinavia (Fig.A.4).

Intriguingly, the 4xCO_2 simulation exhibit a slight reduction of about -1$^{\circ}C$ over Greenland and North Atlantic around year 100 with respect to year 70 (Fig.A.2) (Sellevold & Vizcaíno, 2020). However, the slight regional cooling has no effect on the average Arctic or the global temperature. Furthermore, it has no significant effect on the GrIS SMB or Arctic sea ice. This implies that the significant larger global warming effect, compared to the $2xCO_2$ simulation, is stronger than the regional cooling associated with the slowdown of the NAMOC, resulting in a net effect of constant warming.

4.1.1. Arctic Sea Ice

The Arctic becomes seasonally ice-free, defined as sea ice extent below $2x10^6$ km^2, in the middle of the first simulated century, approximately at the same time as the $4xCO_2$ simulation (Fig.4.2). However, in contrast to the high warming simulation, the Arctic does not become year-round sea ice-free in the $2xCO_2$ simulation (Fig.A.5). There is an initial decrease in March sea ice extent, due to the atmospheric CO_2 increase at the beginning of the simulation. However, between CO_2 stabilisation and year 400, sea ice extent increases in both September and March as a response to the regional cooling associated with the slowdown of the NAMOC. The March sea ice extent is even larger than PI levels when NAMOC is at its lowest, around year 410. However, as the NAMOC recovers and warming resume, the sea ice extent decreases. September sea ice extent is completely lost after year 500. The March sea ice extent experiences a decline throughout the simulation as the NAMOC recovers but remains well above $2x10^6$ km^2. The annual integrated Arctic sea ice fraction remains relatively stable with respect to PI, until the recovery of the NAMOC when the fraction is decreasing in most of the Arctic region (Fig.A.6).

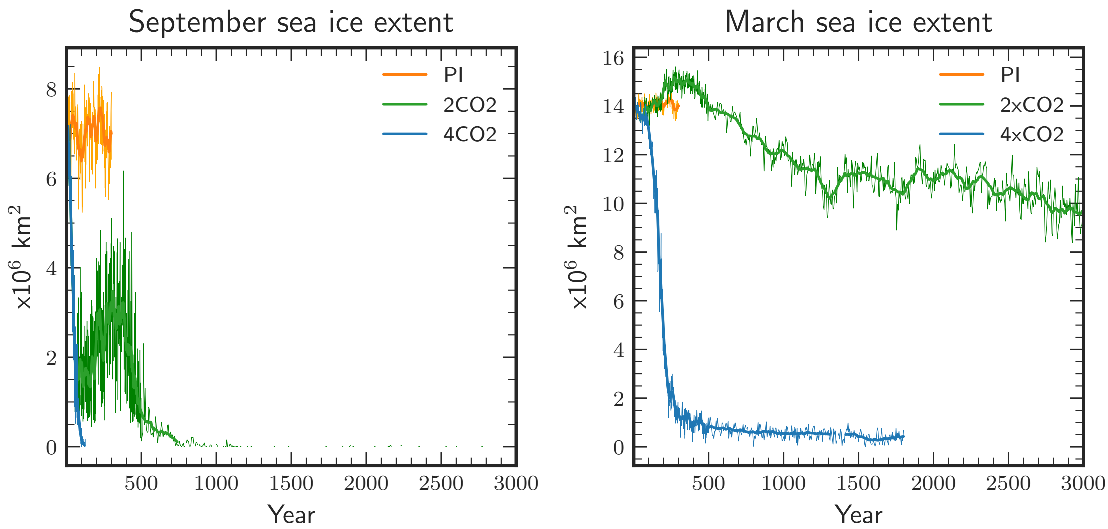

Figure 4.2: Left: September sea ice extent ($x10^6$ km^2). Right: March sea ice extent ($x10^6$ km^2). The sea ice extent is defined as the area north of 60°N where sea ice concentration is greater than 15%.

4.2. Evolution of the NAMOC

The NAMOC weakens substantially during the first 114 years of the simulation, at a rate of -0.13 Sv yr^{-1} both in the $2xCO_2$ and $4xCO_2$ simulation. As seen in Figure4.3, the NAMOC strength is reduced by half during this period, from 24 Sv mean strength during years 1-10, to 12 Sv between years 395-405. After the year 114, the $4xCO_2$ NAMOC evolution continues on a steep decrease, while the $2xCO_2$ simulation decreases less fast, with a rate of -0.02 Sv yr^{-1} until year 410 (Table A.2). The $4xCO_2$ NAMOC strength is at its lowest less than 5 Sv and remains at strengths around 5-6 Sv for the rest of the simulation. This is in contrast to the $2xCO_2$ simulation where the NAMOC recovers after reaching a low point in the period between years 390 and 410 when the strength was only 5 Sv. The strength increases at a rate of 0.018 Sv yr^{-1} between years 410 and 1000. After the year 1000, the NAMOC reaches more or less a new equilibrium state with strengths varying between 17-20 Sv. Although not recovered to PI strength, the NAMOC seems to be relatively stable for the last 2000 years of the simulation. The reduced NAMOC index, compared to PI, means that deep convection does not return to some parts of the Arctic, like the Labrador sea (Fig.A.7).

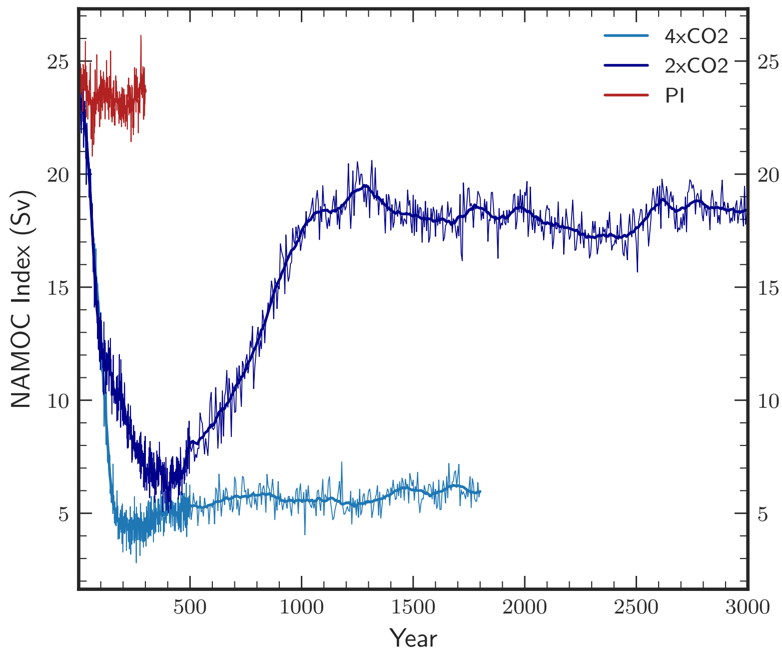

Figure 4.3: Evolution of the NAMOC index. The NAMOC index is defined as the maximum strength of the overturning stream function north of 28°N and below 500 m depth.

4.3. GrIS contribution to GMSLR and Ice Sheet retreat

The GrIS responds rapidly to the CO_2 forcing at the beginning of the simulation, as seen in the slight increase in MB and SMB (Fig.4.4). However, the average surface mass loss between years 1-99 is -3 Gt yr^{-2}, before stabilising between years 100 and 500. The MB decreases by -1.1 Gt yr^{-2}, between years 1-71, and the total mass loss is about -190 Gt yr^{-1}. Between years 71 and 500, the MB is increasing by 0.2 Gt yr^{-2} and has a slight total mass gain of 22 Gt yr^{-1}. After year 500, both MB and SMB are decreasing, MB by -0.5 Gt yr^{-2} and SMB by -0.75 Gt yr^{-2} (Table B.1). The SMB reaches a slower rate after the year 1675, with surface mass loss of -0.1 Gt yr^{-2} until the end of the simulation. The negative MB slows down after year 1900 and decelerates to -0.01 Gt yr^{-2} until the end. Based on the 20-year running mean, the MB is -850 Gt yr^{-1} at the end of the simulation, and SMB is reduced by -1350 Gt yr^{-1}. Ice discharge decreases throughout the simulation, due to thinning of outlet glaciers and their retreat inland. Further, the basal melt changes are small and therefore not considered in this analysis.

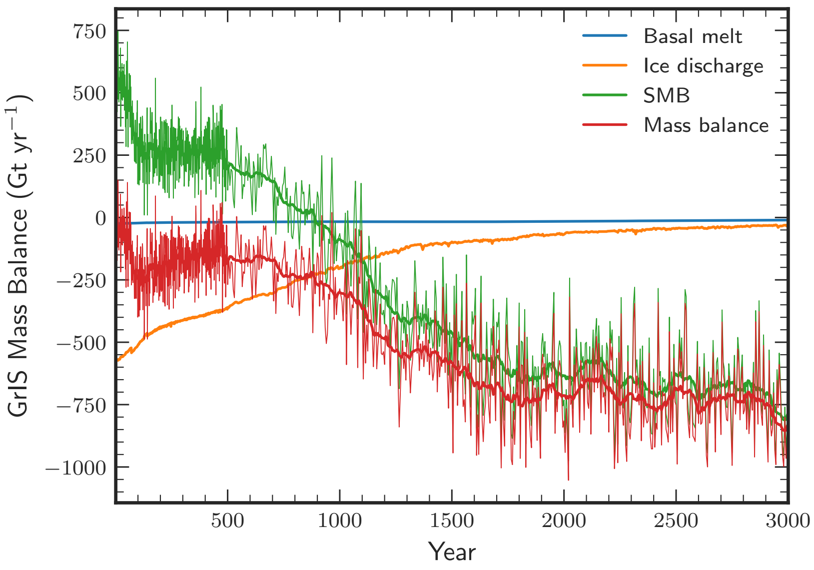

Figure 4.4: Evolution of annual GrIS mass balance (MB) with components (Gt yr^{-1}). The thick lines show the 20-year running mean. Change in mass balance is calculated as: MB = SMB - BMB - ID.

The total GrIS cumulative contribution to global mean sea level rise is 4.1 m after 3000 years (Fig.4.5). The initial rate is 0.47 mm yr^{-1} up until year 710 (Table B.1), and the sea level contribution is 315 mm. Between the years 710 and 1380, the mass loss is significantly increased to 1 mm yr^{-1} and a sea level contribution of 1 m around the year 1380. During the last period of the simulation, between the years 1380-3000, the rate doubles to 2 mm yr^{-1}.

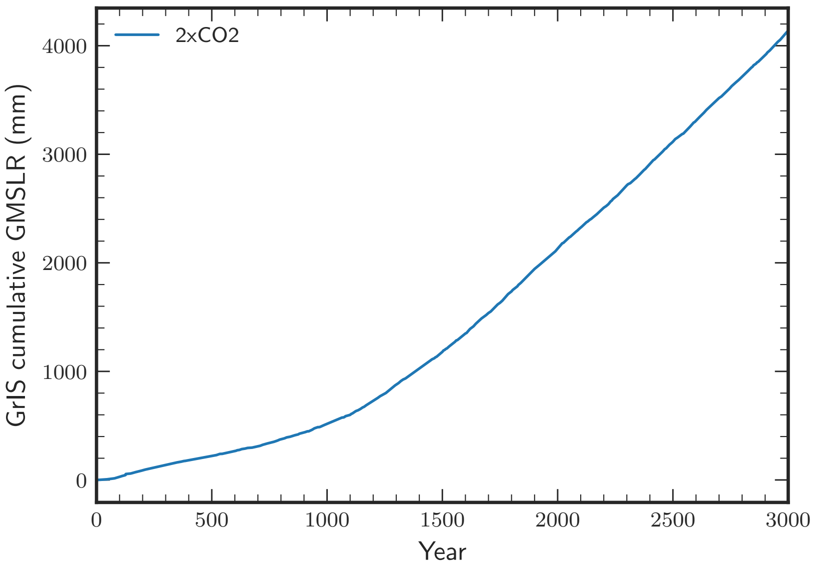

Figure 4.5: Evolution of cumulative GrIS contribution to global mean sea level rise (mm SLE).

During the first 70 years of the simulation, the ice sheet experiences a small positive change in SMB, causing an increase in ice thickness by a few meters over the interior and northern parts, with respect to PI (Fig.B.3, panel showing anomaly between years 60-80). After CO_2 stabilisation, the surface is losing mass along the whole western side, southern and eastern parts of the ice sheet, as well as the interior (Fig.B.2). Although, The maximum surface mass loss is in the western and southern ablation areas. Further, the ice sheets' southern dome disintegrates from the rest of the ice sheet between the years 2525 and 2625 (Fig.B.1), when the ice sheet has decreased by 40% of its pre-industrial area. By the end of the simulation, there is only a small part remaining of the southern dome.

The ablation areas expand throughout the simulation and cause thinning of the ice sheet. The topographic gradient becomes steeper, as the difference between the low-lying ablation areas and the high interior becomes larger (Fig.B.2). As the ice sheet melts, elevation decreases, and the ELA reaches further into the ice sheet. The steeper topography enhances ice flow from the interior to the margins (Fig.B.4). At the end of the simulation, only 50% of the original ice sheet is left, with a 50% ablation area coverage. (Fig.4.6). In comparison, in the 4xCO_2 simulation, the ablation area covers 50% of the ice sheet already at year 210.

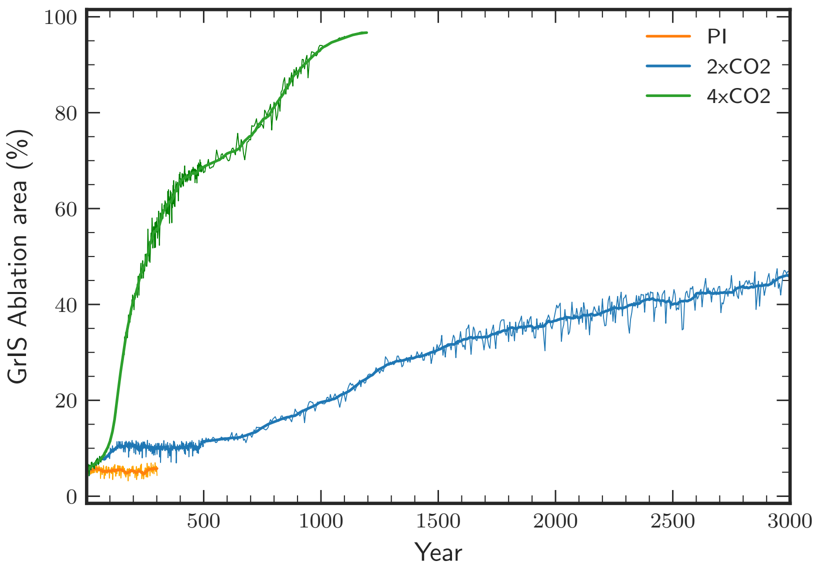

Figure 4.6: Evolution of annual mean GrIS ablation area in % from total ice sheet extent for 2xCO_2, 4xCO_2 and PI. The thick lines show the 20-year running mean.

4.4. Surface Mass Balance

A reduced SMB is considered the largest contributor to the mass loss of GrIS today and in the future (Choi et al., 2021; van den Broeke et al., 2016). There are several contributors to the SMB change (Eq.1.3), such as precipitation, melt and refreezing, runoff and sublimation. The SMB evolution for the 2xCO_2 simulation can be divided into five periods, where the 20-year mean is considered, where the SMB evolution is experiencing a significant acceleration or deceleration. The first period is from year 60 until year 80, which is when the CO_2 concentrations stabilise. The second period is between years 90-110, which shows the ice sheet response just after CO_2 stabilisation and a rapid NAMOC decrease. The third period is from year 390 until year 410 when the NAMOC is at its weakest in the simulation. The fourth period is between the years 1225-1325 when the NAMOC has recovered to a new equilibrium state. And finally, the fifth period from year 2900 until year 3000, which is the end of the simulation.

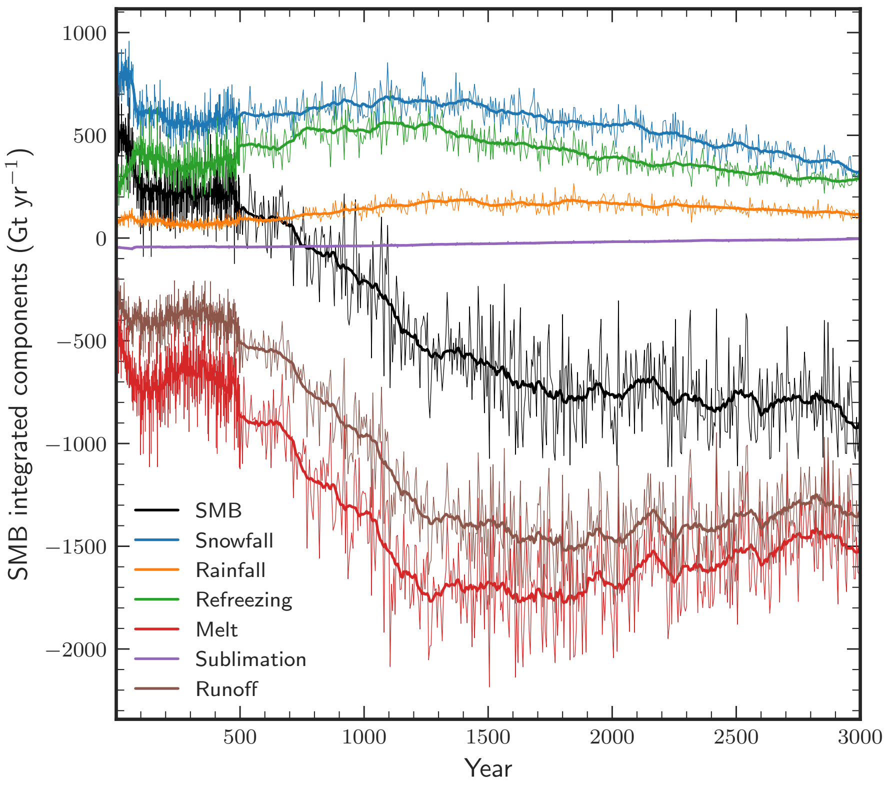

Figure 4.7: Evolution of the annual integrated GrIS SMB components (Gt yr^{-1}). The thick lines show the 20-year running mean.

At CO_2 stabilisation, the annual, integrated GrIS SMB has decreased by almost 200 Gt yr^{-1} (~ 46%) compared to PI simulation (556 Gt yr^{-1}) (Table 4.1). Melt is the main contributor to surface mass loss throughout the simulation (Fig.4.7). At the year 70, the increase in melt causes the runoff to almost double compared to PI simulation. However, the associated mass loss is partially attenuated by refreezing of melt and rainwater into the snowpack. Between the years 60-80, the refreezing capacity is high, with as much as 49% of the melt and parts of the increased rainfall being refrozen into the snowpack. The refreezing capacity is defined as the fraction of refreezing to available meltwater. Between years 60-80, the refreezing capacity is at a maximum, with 50% of the surface water being refrozen. As a consequence, the surface mass loss is relatively stable, with a loss of only 35 Gt yr^{-1} between years 90 and 410 (Fig.4.7). This limited mass loss is caused by a moderate decrease in precipitation and small reductions in melt and runoff. Both are related with reduced warming from a weak state of the NAMOC during this period. However, as the NAMOC strengthens, the SMB experiences an accelerated decrease, due to continuous global warming and recovered heat transport from the NAMOC, causing increased melt, with most of it being partitioned as runoff. In addition, the sublimation is decreasing throughout the simulation (Table 4.1) and is 88% smaller than PI, as more deposition takes place over the expanded ablation areas at the end (Fig.C.5). The SMB turns negative between year 700 and 800, when fitting a linear regression to the absolute data, or between years 720-740 when considering the 20-year running mean. At the end of the simulation, the SMB has decreased to -899 Gt yr^{-1} (~ 60% decrease). The SMB is still exhibiting a negative trend at the end of the simulation, especially visible when considering the change in mm yr^{-1} (Fig.C.1) as decreasing ice sheet area is taken into account.

	PI 1-20	Years 60-80	Years 90-110	Years 390-410	Years 1225-1325	Years 2900-3000
SMB	556 (87)	374 (94)	249 (106)	215 (91)	-574 (140)	-899 (139)
Precipitation	863 (74)	846 (111)	699 (62)	657 (55)	844 76)	454 (42)
Snowfall	790 (68)	725 (98)	617 (59)	582 (44)	662 (65)	336 (34)
Rain	73 (11)	100 (20)	81 (14)	75 (16)	183 (28)	118 (18)
Refreezing	221 (53)	388 (47)	413 (82)	371 (75)	554 (46)	281 (27)
Melt	410 (89)	691 (89)	737 (152)	695 (139)	1757 (146)	1511 (150)
Sublimation	45 (4)	49 (6)	44 (3)	42 (3)	31 (4)	5 (4)
Runoff	262 (48)	403 (64)	405 (79)	399 (74)	1386 (122)	1348 (135)
Rain (%)	8.5	12	11.6	11.4	21.7	26
Refreezing (%)	45.8	49	50.5	48.2	28.6	17

Table 4.1: Overview of annual ice sheet integrated Surface Mass Balance components as absolute mean (standard deviation) between the indicated 20-year periods (Gt yr^{-1}). SMB = Snowfall + Refreezing – Melt – Sublimation. Rain (%) = Rain * 100 / (Snowfall + Rain). Refreezing (%) = Refreezing * 100 / (Rain + Melt).

4.4.1. Precipitation

The fraction of precipitation falling as rain increases throughout the simulation, from 8.5% in PI simulation to 26% at the end of the simulation (Table 4.1). As the atmosphere becomes warmer, it holds more moisture, leading to more precipitation. Snowfall occurs over the whole ice sheet, however more intensely on the south and southeastern margins (Fig.C.2). Rain falls along the west, south and eastern margins of the ice sheet (Fig.C.3). Throughout the simulation, these are the maxima locations of rainfall intensity. However, after year 1000, the net effect of a recovered NAMOC and continuous global warming is increased rainfall, and rainfall falling around the whole margin of the ice sheet. As the ice sheet reduces in extent and elevation is lowered, rainfall is occurring closer to the interior at the end of the simulation.

The annual integrated time series of snow and rainfall (Fig.4.8) shows that the snowfall drops sharply, about -100 Gt yr^{-1} right after CO_2 stabilisation. Rainfall has a smaller drop, only about -20 Gt yr^{-1}. The decrease could have a connection to the slowdown of the NAMOC, causing reduced warming, and consequently reduced precipitation. Especially in snowfall, noticeably on the south and southeastern margin (Fig.C.2). Rainfall remains quite stable during the period of NAMOC weakening (Fig.4.8). As the NAMOC recovers, both snowfall and rainfall increase, snowfall only by 80 Gt yr^{-1} between the years 1225-1325 when compared to years 390-410. Rainfall on the other hand increases by 108 Gt yr^{-1} and the fraction falling as rain has doubled, over the same period compared to years 390-410 (Table 4.1). The total precipitation is at the same level as PI levels during the period 1225-1325. However, by the end of the simulation, total precipitation is reduced to about half of what it was in the PI simulation, which is mostly due to decreased snowfall.

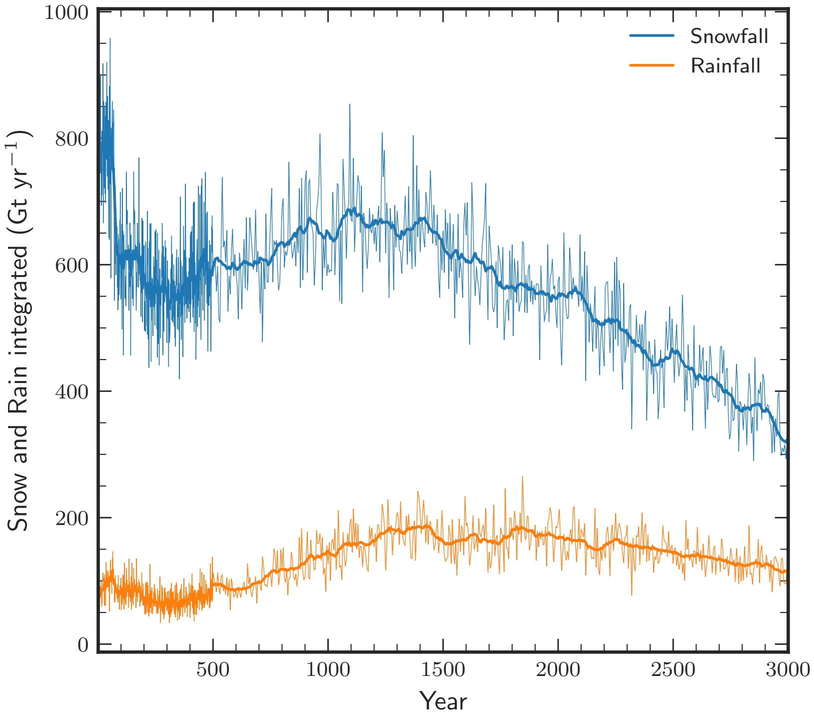

Figure 4.8: Evolution of integrated annual GrIS timeseries of snowfall and rainfall in Gt yr^{-1}. The thick lines show the 20-year running mean.

The decline in the absolute amount of precipitation at the end of the simulation can be attributed to area change. As the GrIS reduces in extent, there is less ice sheet area to receive the precipitation. Figure C.4 takes into account the area change of the ice sheet. The evolution of snow and rainfall is smoother compared to Figure 4.8. Snowfall is relatively stable after the year 1225 until a decrease during the last 100 years of the simulation. This decrease is debatable, as it could either be a continued decrease as the ice sheet area further reduces or it could be variability in the snowfall. Rainfall increases steadily from year 500 onwards and becomes relatively stable at the end of the simulation.

4.4.2. Melt and Refreezing

Melt and rain are the largest contributors to negative SMB change during the whole simulation. Melt dominates runoff, which is the part of the melt and rainfall that is not refrozen into the snowpack, and thus ultimately lost to the ocean. Melt takes place around the whole ice sheet margin, below 2000 m, with the maximum melt on the western side of the ice sheet (Fig.4.9). At the end of the simulation, melt is occurring over the whole, albeit reduced ice sheet and the melt is almost four times higher than in the PI simulation (Table 4.1).

Right after CO_2 stabilisation, there is a small decrease in the melt, seen better reflected in the decrease in the runoff between years 70-100 (Fig.4.7). During this period, snow and rainfall are reduced and the amount of refreezing increases, with a larger refreezing capacity of 50% (compared to 46% at PI) (Table 4.1). The increase of CO_2 up until year 70 and the associated temperature increase, causes higher availability of water to be refrozen by increased surface melt and rainfall. However, the absolute amount of refreezing is relatively stable in the following period from the year 70 until the year 410 when the NAMOC weakens. The amount of refreezing is at a maximum once the NAMOC is recovering, with 554 Gt yr^{-1} being refrozen, in the period between years 1225-1325, which is more than doubled compared to PI values. Although relatively more water is refrozen at this point, the refreezing capacity is decreasing, due to the fact that the snowpack becomes more saturated, with less pore space available for continued storage of surface water. The refreezing capacity can be compared to a sponge taking up water: as it takes up more water, it becomes more saturated until there is no more free pore space. This is also what is happening to the snowpack, especially since amount of snowfall is not keeping up with the increased surface water. At the end of the simulation, the amount of refreezing is 281 Gt yr^{-1}, which is about the same as PI levels, and refreezing capacity is only at 17%. In addition, the refreezing pattern follows the ELA evolution closely (Fig.4.9). This has to do with the fact that the ELA divides the ice sheet into ablation and accumulation area, where liquid surface water (rain and meltwater) decreases with elevation, while snow thickness increases with elevation from this point. Liquid water and pore space are the main two components of refreezing, which proves to be ideal around the equilibrium line altitude. Elevation change is also affecting the melt and the refreezing. As the ice sheet melts, the elevation is lowered, and temperatures increase. Thus, the snowpack will also become warmer as it becomes situated at lower elevations, and will not have a cold enough temperature to accommodate refreezing. In addition, lower elevations and warmer temperatures promote further melting of the ice sheet.

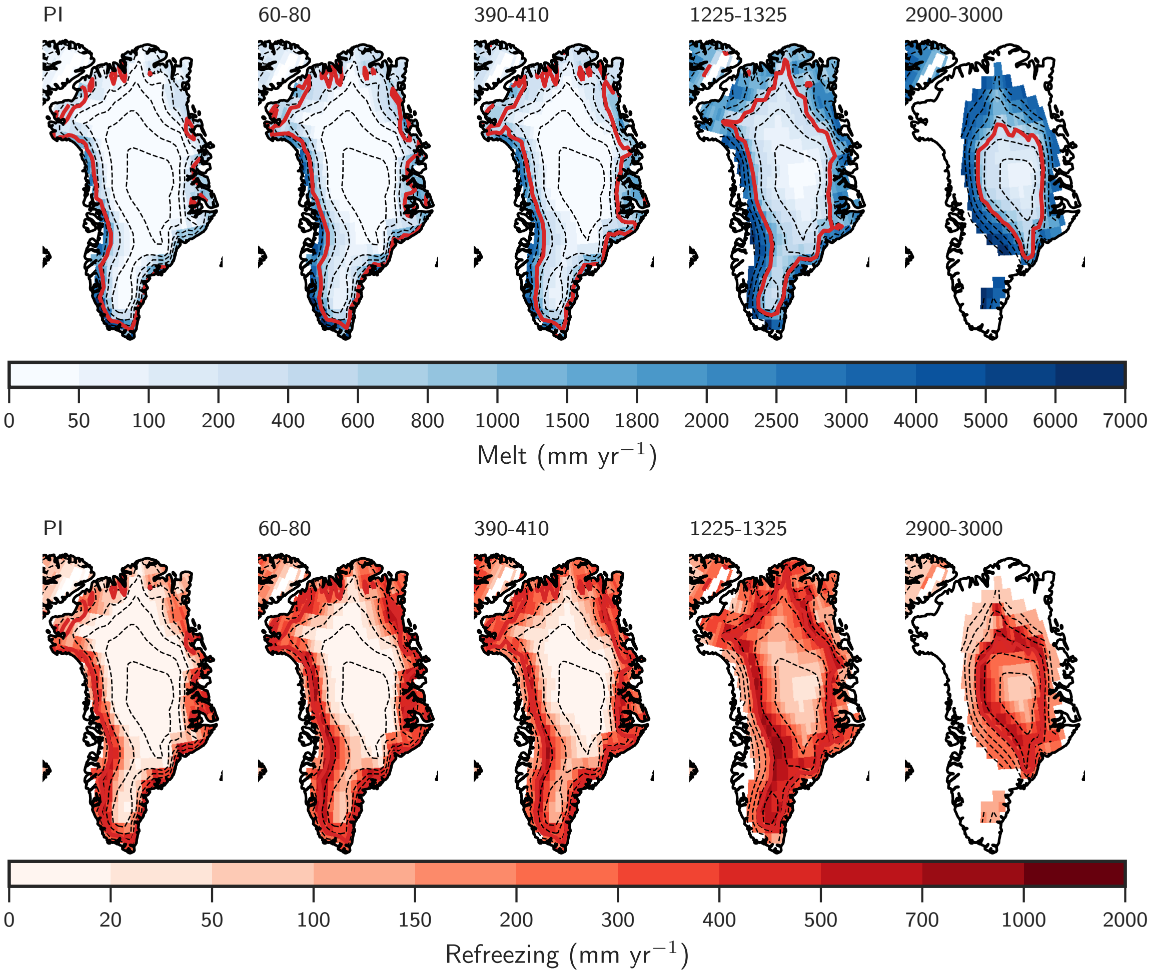

Figure 4.9: Evolution of the absolute annual mean integrated GrIS melt (top panel) and refreezing (bottom panel) (mm yr^{-1}). Contour lines for every 500 m elevation. The red contour line denotes the ELA. The time period is indicated with years on top of the panels.

4.5. Surface Energy Balance

The surface energy balance is interdependent on the surface mass balance, and thus key to explaining processes such as the melt acceleration after year 500, and the following contribution to sea level rise. Melt energy is largest during the summer months of June-July-August (JJA). Therefore, the components in this section are investigated as an average over JJA, integrated over GrIS (Fig.C.6).

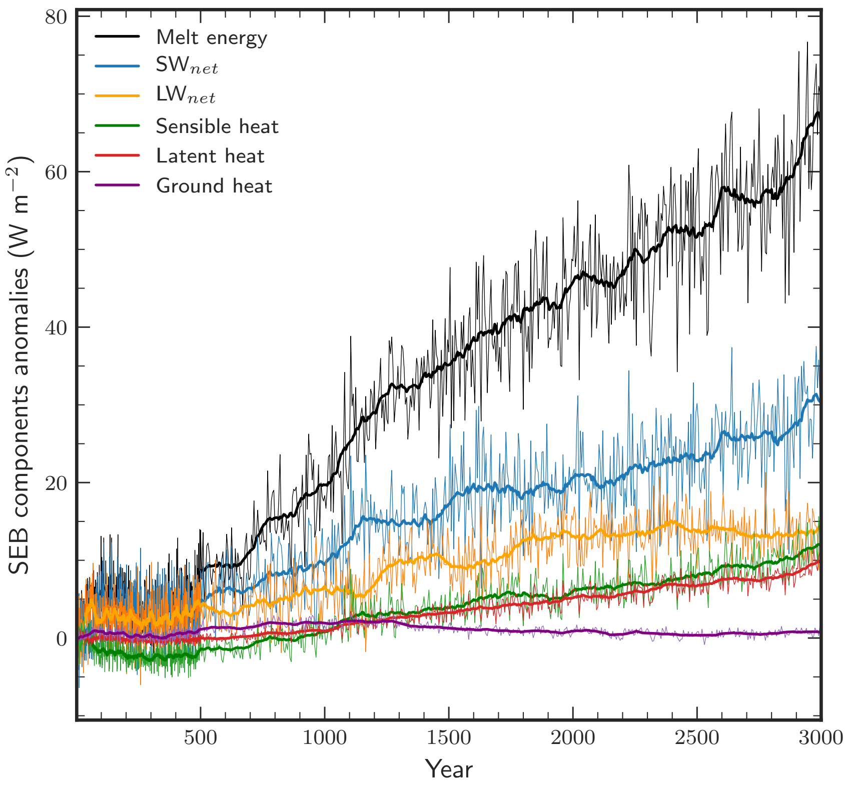

Figure 4.10: June-July-August GrIS integrated surface energy balance anomalies (W m^{-2}) with respect to the pre-industrial mean. The thick lines show the 20-year running mean.

The surface energy balance increase in the 2xCO_2 simulation is caused by radiative and non-radiative fluxes (Eq.1.4). Radiative fluxes are the net shortwave-and longwave-radiation, while the non-radiative fluxes are sensible heat, latent heat and ground heat (Fig.4.10). During the first years of the simulation, the increased amount of CO_2 in the atmosphere causes LW_{in} to increase. As temperature increases, increased water vapour content and more liquid clouds are forming (Fig.C.8). This also causes incoming shortwave radiation to decrease (Fig.C.9). Net longwave radiation is thus the main contributor to the melt energy during the first 70 years of the simulation, contributing 74% to the additional melt energy. Between years 70 and 500, the SW_{net} and LW_{net} compete to be the largest contributor to melt energy. SW_{net} is dominant over longer periods, typically with a contribution around 50% and LW_{net} about 36%. This pattern shows a decadal anti-correlated oscillation between SW_{net} and LW_{net}, that becomes centennial after year 500. This coincides with the increase in liquid-containing clouds (Fig.C.8), and also the evolution of clouds at lower altitudes, known to decrease shortwave radiation (Fig.C.10). Such an oscillation is likely due to regional climate variability.

	PI 1-20	Years 60-80	Years 90-110	Years 390-410	Years 1225-1325	Years 2900-3000
Albedo	0.771 (0.007)	0.759 (0.006)	0.753 (0.009)	0.754 (0.008)	0.690 (0.007)	0.611 (0.012)
T2m	-6.7 (0.8)	-4.7 (0.6)	-4.6 (0.9)	-4.9 (0.7)	-1.3 (0.4)	0.2 (0.4)
Tsurface	-6.4 (0.7)	-5.3 (0.5)	-5.2 (0.8)	-5.4 (0.7)	-2.3 (0.3)	-1.5 (0.3)
SWin	280.9 (4.3)	272.5 (6.1)	275.3 (4.4)	272.4 (5.2)	256.0 (5.4)	225.4 (6.3)
LWin	233.5 (3.9)	246.3 (4.2)	245.1 (3.3)	245.2 (4.0)	264.6 (3.2)	272.5 (3.4)
Melt Energy	12.1 (2.2)	17.5 (1.9)	18 (3.5)	16.8 (3.2)	45 (4)	78.3 (6.1)
SWnet	63.3 (2.4)	64.9 (2.7)	67.4 (3.2)	66.3 (3.0)	78 (3)	93.9 (4.3)
LWnet	-49.0 (2.2)	-45.0 (3.0)	-46.5 (2.3)	-45.4 (2.8)	-39 (2)	-35.2 (2.6)
SHF	6.6 (1.1)	5.7 (1.1)	5.1 (1.6)	4.5 (1.2)	10 (2)	18.2 (2)
LHF	-6.6 (0.4)	-7.0 (0.4)	-6.8 (0.3)	-7.1 (0.4)	-4 (1)	2.5 (1.3)
GHF	-2.1 (0.2)	-1.1 (0.3)	-1.2 (0.5)	-1.5 (0.5)	0.1 (0.4)	-1.2 (0.4)

Table 4.2: Overview of summer averaged (JJA) integrated GrIS Surface energy balance components as absolute mean (standard deviation). Albedo (-), near-surface temperature ($°C$), surface temperature ($°C$), incoming shortwave radiation at the surface, incoming longwave radiation at the surface, and the surface energy balance components (W m^{-2}). Melt energy = net shortwave radiation + net longwave radiation + sensible heat flux + latent heat flux + ground heat flux.

Until year 500, the net shortwave radiation is for the most the main contributor to melt energy, which up until this point only increased by a few W m^{-2}. Thereafter, it truly becomes the largest, increasing from 17 W m^{-2} before year 500 to 78 W m^{-2} at the end of the simulation (Table. 4.2), with a contribution of 46%. Furthermore, sensible (SHF) and latent heat flux (LHF) and ground heat flux (GHF) are significantly increasing after year 410. In the end, the non-radiative fluxes contribute about 10% of the additional melt energy (Fig.4.10). Most of the additional melt energy is used in the ablation areas (Fig.C.7). The melt energy is only fluctuating by 1-2 W m^{-2} per decade until around year 500 (Table. 4.2). Hereafter, melt energy increases in all ablation areas as they expand, and is especially pronounced on the west, southwestern and northern margins.

The increase in net SW after year 500 is due to the ice-albedo feedback which enhances melt and causes expansion of the ablation areas. This leads to more bare ice being exposed earlier in the year. Ice has a lower albedo, typically between 0.65-0.20 depending on ice condition, compared to fresh snow, aged and wet snow, which have an albedo of about 0.85 to 0.60 (Cuffey & Paterson, 2010). Thus, when snow melts, ages, becomes wet or even completely melts away to reveal ice, the albedo is lowered and the surface absorbs more heat from incoming SW, which starts a positive feedback loop where it continues to warm and melt. The summer (JJA), integrated GrIS albedo is decreasing from 0.77 in PI simulation to 0.61 at the end of the simulation (Fig.4.11). During the slowdown of the NAMOC there are small changes in albedo on the southern part of the ice sheet (Fig.C.11). As the ice-albedo feedback commences, the largest albedo decrease is on the western margins, followed by the northern and eastern margins, indicating larger areas of bare ice. At the end of the simulation, the albedo change is less pronounced on the southeastern margins, due to a steep topographic gradient, limiting the expansion of the ablation areas.

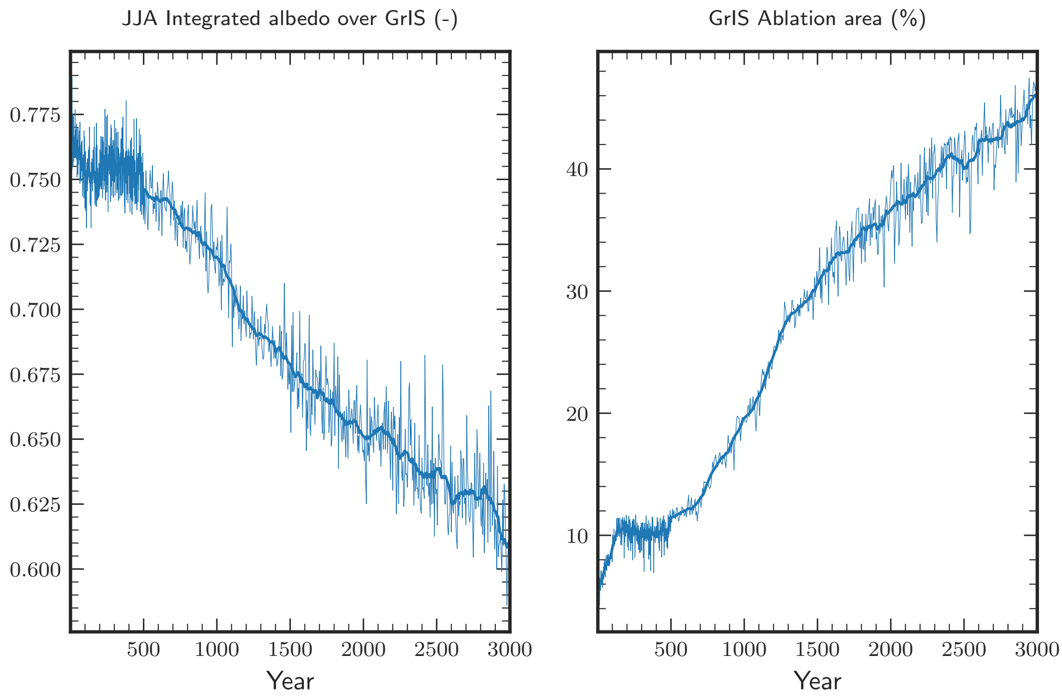

Figure 4.11: Left: Integrated June-July-August albedo (-) over GrIS. Right: Annual integrated GrIS ablation area (%).

The evolution of the sensible and latent heat fluxes concerns the heat and energy exchange between surface and near-atmosphere and can be explained by the evolution of the near-surface and surface temperature change (Fig.C.12). At the start of the simulation, the two temperatures are almost equal and increase at about the same pace. From around year 550, the 2m air temperature is increasing more than the surface temperature, and the difference between them is 1.7$^{\circ}C$ at the end of the simulation. This is due to the fact that the ice sheets' surface temperature cannot increase above the melting point, while the near surface will continue to increase due to global warming. As the near-surface temperature becomes larger than the surface temperature, the temperature inversion between surface and atmosphere becomes stronger, enhancing the turbulent fluxes. The sensible heat flux is heating the surface, as eddies mix the warmer atmosphere, warmer air is brought down to the surface. If the atmosphere is colder, heat is removed from the surface (Cuffey & Paterson, 2010). Further, the latent heat flux concerns the energy in phase changes and is related to the function of the humidity gradient. Heat is received at the surface when atmospheric water vapour condenses. Heat is lost from the surface when moisture evaporates or sublimates (Cuffey & Paterson, 2010).

The JJA GrIS integrated sensible heat flux (Fig.C.13), is positive over the whole ice sheet, except for the southern dome, and some parts of the interior. The positive SHF indicates that there is heat transfer going from the atmosphere to the surface. The SHF pattern remains stable throughout the simulation until the NAMOC has recovered (after year 1000). From this point, the positive SHF increases in intensity around the margins, especially on the western side of the ice sheet. The southern dome remains with negative SHF until the last years of the simulation. While the highest interior is negative throughout the whole simulation.

The latent heat flux is negative over the whole ice sheet in the PI simulation (Fig.C.14), suggesting energy loss from the surface to the atmosphere caused by sublimation. During the summer there is more energy available, and the sublimation takes place at the surface, except for at the margins. This causes the LHF to become more negative, except for at the margins. At the margins, the LHF becomes more positive with more warming. A positive LHF implies that moist air cools as it flows over the cold ice sheet surface, and consequently reaches saturation, leading to condensation and deposition of water vapour. This sign change is only seen in the last years of the simulation. LHF is relatively stable up until the recovery of the NAMOC when positive LHF or mass deposition is occurring around the whole ice sheet margin. Even though the deposition adds mass to the ice sheet, it also adds energy. This increases the melt flux as the mass gain is very small compared to the added energy.

The ground heat flux is the heat transfer between the surface and the sub-surface. With a positive GHF, there is an increase in energy content in the snowpack, and it can be viewed as a pre-condition to melt and mass loss. Ground heat flux is mostly negative over the ice sheet during summer in the PI simulation (Fig.C.15). In the percolation zones, the GHF is positive, which is seen around the ELA. This implies that the energy from latent heat release due to refreezing of meltwater happening in the snowpack is conducted upwards to the surface.

5
Discussion

The existing literature on GrIS evolution is extensive and focuses particularly on the future evolution under high emission scenarios (Aschwanden et al., 2019; Huybrechts et al., 2011; Muntjewerf, Petrini, et al., 2020a; Muntjewerf, Sellevold, et al., 2020; Van Breedam et al., 2020). Some of these projections stem from stand-alone ice sheet models (Aschwanden et al., 2019), and some from coupled ice sheet-climate models with diverse resolutions (Gregory et al., 2020; Huybrechts et al., 2011; Van Breedam et al., 2020). In addition, a few studies focus on recent evolution of GrIS (Ettema et al., 2010; van den Broeke et al., 2016). Furthermore, the CESM2-CISM2 model has previously been used for studies concerning the high forcing scenario 4xCO_2 (Muntjewerf, Petrini, et al., 2020a; Sellevold & Vizcaíno, 2020), for the SSP8.5 scenario (Muntjewerf, Sellevold, et al., 2020), as well as for a simulation on the Last Interglacial period (Sommers et al., 2021).

However, this study is the first to analyse a moderate warming scenario with this high-resolution coupled Earth system model. In this analysis, the 2xCO_2 simulation is considered a moderate warming scenario because it is in the range between the high and low warming scenarios. Considering only CO_2 concentrations, the 2xCO_2 simulation has similar levels as the SSP2-4.5 scenario (Fig.3.1). Although there are differences between the simulation and the scenario, it is justified as comparable because it is in the range between the high and low climate projections. In this section, GrIS contribution to sea level rise as simulated in the CESM2-CISM2 2xCO_2 simulation, and the effect of NAMOC evolution on the SMB will be discussed considering the literature mentioned. An overview can be found in Table A.1.

5.1. GrIS contribution to sea level rise

The largest contributor to mass loss in the 2xCO_2 simulation is the negative SMB change, which decreases by -3 Gt yr^{-2} during the first 100 years of the simulation. Between years 100 and 500 the SMB is more or less stable with only minor fluctuations. From year 500 to 1675 the surface mass loss is -0.75 Gt yr^{-2}. After the year 1675, the SMB further decelerates to -0.1 Gt yr^{-2} until the end of the simulation. After 3000 years, the SMB has decreased by -1200 Gt yr^{-1} compared to PI. Both volume and area are reduced to 50% of the PI simulation. Further, the GrIS contribution to SLR is at a rate of 0.47 mm yr^{-1} during the period between years 1-710 with a cumulative sea level contribution of 315 mm. Between years 710 and 1380, the rate increases significantly, associated with the recovery of the NAMOC, to 1 mm yr^{-1}. The cumulative sea level contribution at the end of this period is 1 m. After the year 1380, the sea level contribution rate doubles to 2 mm yr^{-1} until the end of the simulation. The second significant acceleration is associated with sustained global warming, strong ice-albedo feedback and a NAMOC in a new steady state. After 3000 years, the total GrIS cumulative contribution to the global mean sea level rise is 4.1 m.

To date, several studies have investigated the near-future evolution of the GrIS up until the years 2100 and 2300 (Aschwanden et al., 2019; Edwards et al., 2021; Muntjewerf, Petrini, et al., 2020a; Muntjewerf, Sellevold, et al., 2020), and these are generally also discussed in the sixth IPCC report

(Arias et al., 2021). A large difference between most of these studies and the 2xCO_2 simulation is the fact that they start their simulations with present-day ice sheet and climate, while the 2xCO_2 simulation starts from PI. Aschwanden et al. (2019) used a stand-alone ice sheet model to quantify the contribution to sea level rise from the GrIS over the next millennium by a large ensemble of simulations. By 2100 the projected sea level contribution is between the range of 8-23 mm for the moderate emission scenario RCP4.5. The sea level projections further increase to 350-970 mm by 2300. In comparison, after 100 years, the 2xCO_2 simulation GrIS has contributed about 30 mm SLE, while after 300 years the contribution is 140 mm (Fig.4.5). The lower range of the estimates for RCP4.5 of 350 mm in 2300 occurs around the year 770 in the CESM2 2xCO_2 simulation. Edwards et al. (2021), used statistical emulation of the ice sheet and glacier models from the ISMIP6 (Goelzer et al., 2020), predicting a sea level contribution, relative to 2015, from GrIS of 60 mm (with a range from 10 to 100 mm) by 2100 following SSP2-4.5. In the 2xCO_2 simulation, a 60 mm GMSL contribution is reached in year 149. At this point, the CO_2 concentrations are already stabilised at 560 ppm, while the SSP2-4.5 has a CO_2 concentration of about 600 ppm, and still increasing (Fig.3.1) (Meinshausen et al., 2020). The 2xCO_2 simulation has a higher contribution of mass loss in the first 100 years compared to Aschwanden et al. (2019), however, it is quite similar to Edwards et al. (2021). Although, the 2xCO_2 is losing less mass compared to Aschwanden et al. (2019) estimates by 2300. The GMSL projection of a 4xCO_2 simulation also run with the CESM2-CISM2 (Muntjewerf, Petrini, et al., 2020a), is included as a comparison to the SSP and RCP scenarios, due to the different CO_2 forcing. The CO_2 is increased by 1% until reaching 4xCO_2 in year 140, after which the concentrations are kept fixed, like in the 2xCO_2 simulation. At the simulation year 150 in the 4xCO_2 simulation, the GrIS contribution to SLR is 107 mm. The 2xCO_2 has in year 150 contributed 61 mm to sea level rise. By the end of the 4xCO_2 simulation, after 350 years, the total sea level contribution is 1.14 m, while this level of contribution is only reached for the 2xCO_2 simulation after 1380 years. This illustrates the large differences between a high and moderate warming scenario. In conclusion, the different contributions to GMSL are dependent on both the amplitude and the duration of the warming, which is directly related to the amount of CO_2 in the atmosphere (Charbit et al., 2008).

Study	Model	Simulation Time (Years)	Scenario	GrIS SLR contribution	NAMOC
2xCO_2	Advanced coupled Earth system model CESM2.1-CISM2.1	3000	2xCO_2	4.1 m	Temporarily slowdown Cooling effect
Aschwanden et al. (2019)	Ice sheet model PISM	1000	RCP4.5	1.86-4.17 m	(-)
Charbit et al. (2008)	3D ice sheet model coupled to climate model CLIMBER	18 000	Range of CO_2 emission scenarios CO_2 480-1680 ppm	Low end: 10% to 63% ice volume loss High end: 100% ice volume loss	(-)
Edwards et al. (2021)	Statistical emulation ice sheet models (ISMIP6)	85 (2016-2100)	SSP2-4.5	50 mm	(-)
Gregory et al. (2020)	Ice sheet model (Glimmer) coupled to atmospheric general circulation model (FAMOUS-ice AGCM)	~ 40 000	RCP2.6-RCP8.5	<1.5 - >4 m	(-)
Huybrechts et al. (2011)	Coupled Earth system model LOVECLIM v1	3000	2 and 4 times CO_2	2xCO_2: ~ 3 m 4xCO_2: ~ 8 m	Temporarily slowdown Cooling effect
Muntjewerf, Petrini, et al. (2020a)	Advanced coupled Earth system model CESM2.1-CISM2.1	350	4xCO_2	1.14 m	Collapse
Sommers et al. (2021)	Advanced coupled Earth system model CESM2.1-CISM2.1	8000 years	Last Interglacial	3.8 m	(-)
Van Breedam et al., 2020	Coupled Earth system model LOVECLIM v1.3	10 000	Extended RCP4.5	7.3 m	Temporarily slowdown Cooling effect

Table 5.1: A comparison of contemporary literature and the CESM2 2xCO_2 simulation, concerning GrIS contribution to sea level rise in the future and the effect of NAMOC evolution.

An important feature of the 2xCO_2 simulation is its relatively large length because the GrIS will take several millennia to respond to today's levels of greenhouse gases and settle into a new equilibrium, as prior studies have also noted (Huybrechts et al., 2011; Van Breedam et al., 2020). Huybrechts et al. (2011) used an Earth system model of intermediate complexity for two simulations of 3000 years, where in one simulation the CO_2 concentrations were doubled and one where concentrations were quadrupled, compared to PI. The difference in magnitude and response time between a moderate and high forcing scenario, as found between the CESM2 $2xCO_2$ and $4xCO_2$ simulations, was also seen between the simulations in the study by Huybrechts et al. (2011). The main difference between the $2xCO_2$ conducted in this study and by Huybrechts et al. (2011) is the sea level contribution after 3000 years with respect to the global and Greenland temperature change (compared to PI). At the end of the simulation, Huybrechts et al. (2011) found that the moderate scenario contributes to a sea level rise of about 3 m, while the high scenario contributes 8 m. Thus, the moderate scenario is lower yet relatively similar to the $2xCO_2$ simulation in this study (4.1 m). However, the global and Greenland warming under the moderate scenario was at the end 2 $^\circ C$ and 4 $^\circ C$, respectively. The warming is much higher in this study, with global warming of 5 $^\circ C$ and warming of 9 $^\circ C$ over Greenland. Interestingly, the CESM2 $2xCO_2$ warming is the same as the warming in the high scenario of Huybrechts et al. (2011).

In the following paragraph, the CESM2 $2xCO_2$ simulation will be compared to the study by Sommers et al. (2021). The study investigates the GrIS evolution during the last interglacial (LIG) and is also run with the CESM2-CISM2 model. During the LIG, the Arctic temperatures were warmer than the present day, caused by changes in Earth's orbital configurations, leading to higher insolation anomalies in the Northern Hemisphere. The warmer Arctic temperatures today are caused by anthropogenic emissions. In Sommers et al. (2021) the CO_2 concentration is kept constant at 275 ppm, while during the $2xCO_2$ simulation it is kept constant after reaching 560 ppm. Another main difference is that the LIG simulation starts when the climate is at its warmest, 127 ka (thousand years ago) before it starts to cool after 121 ka. In this study, the global climate warms continuously during the 3000 year period. The GrIS during the LIG lost 3.8 m SLE over a period of 6000 years (127-121 ka), while in the $2xCO_2$ simulation the GrIS lost 4.1 m SLE in 3000 years. In both simulations, the ice sheet loses half of its initial volume. The melt pattern in the LIG simulation is distinctive and the minimum ice sheet extent occurs between 123-121 ka (Fig.5.1). The mass loss is significantly larger in the northern parts during this period compared to the $2xCO_2$ simulation after 3000 years (Fig.C.16). However, the western margin has retreated more in the $2xCO_2$ simulation. The disintegration of the southern dome is seen during the LIG simulation between 123-121 ka (Fig.5.1) and between 2100-3000 in the $2xCO_2$ simulation (Fig.C.16). Although, the remaining $2xCO_2$ southern dome is smaller at the end of the simulation, compared to LIG between 123-121 ka, with the possibility of it completely melting, should the simulation be continued.

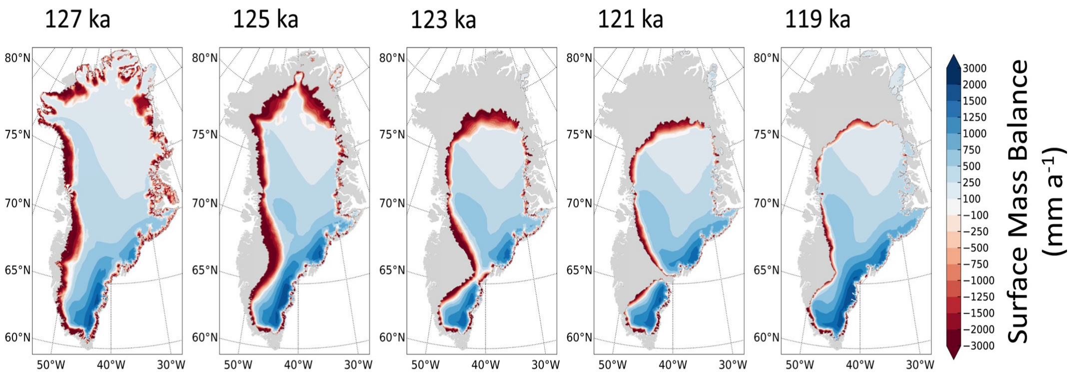

Figure 5.1: Surface mass balance of the Greenland Ice Sheet shown every 2000 years from 127-119 ka. Data are plotted on the Community Ice Sheet Model (CISM2) 4-km grid. The figure and figure caption are from Sommers et al., 2021. The red colours indicate mass loss and the blue colours indicate mass gain.

5.2. NAMOC evolution effect on SMB

In this study, a temporary weakening of the NAMOC causes reduced GrIS mass loss. During the first 114 years of the $2xCO_2$ simulation, the NAMOC decreases with a rate of -0.13 Sv yr^{-1}. The NAMOC strength is around 5 Sv at its lowest between years 390 and 410 (when considering the 20-year running mean). After this, the NAMOC recovers at a rate of 0.02 Sv until reaching a new steady state after the year 1000. The strength does not recover to PI values (24 Sv) but remains between 17 and 20 Sv until the end of the simulation. The slowdown of the NAMOC leads to cooling over the Arctic and Greenland region, which temporarily reduces the surface mass loss. This cooling effect is reported by several studies projecting the evolution of GrIS mass loss (Huybrechts et al., 2011; Muntjewerf, Petrini, et al., 2020a; Muntjewerf, Sellevold, et al., 2020; Van Breedam et al., 2020), and a weakening of the circulation is observed today (Bryden et al., 2020; Chemke et al., 2020) and projected in the future (Drijfhout et al., 2012; Mikolajewicz et al., 2007; Swingedouw et al., 2022). The effect of increased freshwater flux from a melting GrIS on the NAMCO is an ongoing discussion in the field, however, there was a relatively small body of literature found that was concerned with the effect of NAMOC weakening on the GrIS SMB. This question is explored in this section.

There are similarities between the temporarily NAMOC slowdown and reduced GrIS mass loss projected in the 2xCO_2 simulation and the observed deceleration of mass loss from Icelandic glaciers described by Noël et al. (2022). In this study, the slowdown of Icelandic glaciers' mass loss is coinciding with a regional cooling signal in the North Atlantic Ocean. Since Icelandic glaciers are mostly land-terminating, the SMB is the largest contributor to mass loss. Although the GrIS in the 2xCO_2 simulation only becomes land-terminating later in the simulation, the ice discharge contributes to sea level drop (Fig.4.4), and the SMB is the main contributor to mass loss. The Icelandic glacier mass loss increased between 1995-2010 as a response to warmer temperatures. However, after 2011, when the cooling signal emerged, the mass loss was halved compared to the period 1995-2010. This further strengthens the hypothesis of regional cooling due to NAMOC slowdown and consequent surface mass loss decrease between years 71-500 in the 2xCO_2 simulation (Fig.4.4). Interestingly, the study was extended with a simulation that follows the forcing scenario SSP8.5 until 2100 to evaluate if the decreased mass loss persists. Their findings showed that the cooling signal would halt around 2050, causing background warming to prevail. They further identified three stages of glacier mass loss, similar to the 2xCO_2 simulation. The first stage saw mass loss of the glaciers due to warming between the late 90s and 2010. In the second stage, after 2011, the emerging cooling signal caused reduced mass loss. The projected reduced mass loss will continue up until late 2040, and after this, the third stage begins where mass loss will resume as the warming signal again dominates.

The NAMOC evolution effect on GrIS SMB in the CESM2 2xCO_2 simulation is in line with other modelling studies projecting future GrIS mass loss. Huybrechts et al. (2011) reported a small weakening in the warming over Greenland in their 4xCO_2 simulation. The weakening occurred after a freshwater peak from GrIS, leading to a reduction of 25% of the AMOC (Atlantic meridional overturning circulation). Although they make a connection between reduced warming and weakening AMOC, it is still curious that they did not find a cooling effect in their 2xCO_2 simulation, nor reported any weakening of the AMOC during this simulation. In the 2xCO_2 simulation run with the CESM2-CISM2, there is an obvious connection between the reduced warming over both the Arctic and Greenland (Fig.4.1), weakening of the NAMOC (Fig.C.7) and decreasing surface mass loss. The net effect of global warming and NAMOC evolution is cooling between years 60-410 (Fig.A.3). This is not so apparent in the CESM2 4xCO_2 simulation, in contrast to Huybrechts et al. (2011), as the net effect of NAMOC and global warming, is always dominated by global warming, causing consistent GrIS mass loss.

In contrast to the study by Huybrechts et al. (2011), Mikolajewicz et al. (2007) simulated various emission scenarios with an Earth system model and found that the Atlantic Overturning Circulation collapsed in the high emission scenario, temporarily weakened in the low emission scenario and the moderate scenario brought the system close to its bifurcation point, with three out of five runs leading to a collapse of the NAMOC. The temporary weakening or collapse showed to cause cooling over the North Atlantic region. The collapse of the NAMOC in the high emissions scenario caused a cooling of 5$°C$ on the southeast coast of Greenland, with respect to 1751. The overall cooling over Greenland in the CESM2 2xCO_2 simulation is 5$°C$ during the slowdown of the NAMOC, compared to the peak warming in year 70. In their simulations, Mikolajewicz et al. (2007) and Van Breedam et al. (2020) found regional cooling and melt and precipitation reduction as effects of NAMOC slowdown. Interestingly, the cooling effect was lower for the low emission scenarios, where the NAMOC only weakened temporarily. For the moderate and high emission scenarios, the NAMOC weakening was more severe or ended in total collapse. This led to a stronger cooling effect, which in turn showed to have a larger effect on the Greenland SMB. This suggests that larger global warming causes a stronger weakening of NAMOC, which has a larger effect on the GrIS SMB. However, Drijfhout et al. (2012) suggested that the sensitivity of the AMOC for global mean temperature change becomes weaker in a warmer climate, which is more consistent with the CESM2 2xCO_2 and 4xCO_2 simulation. Where the temporarily reduced ocean heat transport causes a net effect of cooling over Greenland between years 60-410 in the 2xCO_2 simulation (Fig.A.3), while in the 4xCO_2 simulation the global warming signal is always stronger.

6
Conclusions

The novelty of this research derives from the analysis of a 2xCO_2 concentration simulation run with an advanced Earth system model (ESM), with the crucial coupling of ice sheet-climate. This coupling is important because just as a change in climate modifies the ice sheet, the climate is modified by changes of the ice sheet. Furthermore, the analysis of this moderate, multimillennial, warming simulation bridges the gap between extensively researched low-and high-emission scenarios, as the world seems likely to approach a "middle-of-the-road" future climate scenario. The idealised 2xCO_2 simulation, run with the advanced ESM model CESM2-CISM2, is compared to a 4xCO_2 and a pre-industrial control simulation run with the same model to support the study. The analysis gives insight into the evolution of the Greenland ice sheet over a period of 3000 years. Analyses spanning such a long timescale are important because the ice sheet plays a significant part in a changing Earth System in the long term due to its slow response time. In this section, conclusions to the research questions are presented.

There are five main time periods investigated in this analysis. The first period is years 60-80, which is around the stabilisation of the CO_2 forcing. The second period is between years 90-110, which captures the changes in ice sheet components just after CO_2 stabilisation and during the rapid NAMOC decrease. The third period is between years 90-410 when the NAMOC is at its weakest in the simulation. The fourth period is between the years 1225-1325 when the NAMOC has recovered to a new equilibrium state. And finally, the fifth period is between the years 2900-3000, which is the end of the simulation.

How does the Greenland Ice Sheet mass budget respond to a doubling of global CO_2 at a multimillennial timescale as simulated by a coupled ice sheet-climate model?

The Greenland ice sheet is losing about half of its mass and volume over the span of 3000 years, compared to pre-industrial (PI) values, due to global warming and other processes caused by a warming Earth system such as a change in the NAMOC, local weather and atmosphere patterns and loss of sea ice.

The overall mass budget of GrIS shows an initial acceleration of mass loss, associated with the CO_2 forcing, of -1.1 Gt yr^{-2}, resulting in 190 Gt yr^{-1} being lost during years 1-71, compared to PI. Between CO_2 stabilisation and year 500, the mass loss decelerates and even changes signs to become mass gain of 0.2 Gt yr^{-2}. On the other hand, the surface mass loss accelerates by -3 Gt yr^{-2} during the first 100 years of the simulation, before becoming quasi-stable until just after year 410. Furthermore, between years 1 and 71, the refreezing has increased by almost 170 Gt yr^{-1} (with a refreezing capacity of ~ 50%) and the amount of melt has almost doubled compared to PI. Also, melt and refreezing is more or less in a stable state during the period between years 71-410. This is associated with a weakened NAMOC and a regional near-surface temperature decrease with respect to year 70 of the simulation. The mass loss accelerates after year 500, by -0.5 Gt yr^{-2}. This is in connection with a strengthening of the NAMOC after year 410, continuous global warming, ice-albedo feedback and elevation-melt feedback. Although summer (JJA) integrated albedo is reduced from 0.77 to about 0.6, it is enough to set off the ice-albedo feedback. This positive feedback enhances ablation area expansion, which constitutes 50% of the ice sheet at the end of the simulation. The main contributor to the negative change in the mass budget is the surface mass balance (SMB). At the end of the simulation, the GrIS contributed almost 4.1 m to the global mean sea level rise.

1.How do Surface Mass Balance and Surface Energy Balance components evolve under a moderate warming scenario?

The SMB and SEB components have initial responses to the rapid increase in CO_2 concentrations at the start of the simulation, before experiencing a serious acceleration in their responses after 500 years until the end of the simulation.

The SMB first becomes negative in year 730 when considering the 20-year running mean, or somewhere between years 700 and 800 if considering a linear fit to the absolute data. An SMB = 0 or negative is often considered a tipping point for irreversible mass loss (van den Broeke et al., 2016). The largest contributor to surface mass loss is melt, which increases by a factor of 3.7 at the end of the simulation compared to PI. Melt dominates the runoff, which is five times higher at the end of the simulation, with respect to PI. Refreezing capacity is peaking at 50% between years 90 and 110, thereafter declining until only 17% at the end of the simulation. Just after CO_2 stabilisation, the snowfall declines rapidly as the CO_2 forcing stabilises. Snowfall does not recover to pre-industrial levels but has a slight increase after year 400 until the end of the simulation. Furthermore, rainfall more than doubles at the end of the simulation compared to PI, with 26% of total precipitation falling as rain (~9% at PI).

Both global warming and the changes in NAMOC affect the precipitation over GrIS. Precipitation decreases during the weakening of the NAMOC, particularly in the south. While it is expected that global precipitation increases with atmospheric warming, the decline in NAMOC has a regional cooling effect, reducing precipitation over GrIS. Snowfall is mostly affected by the NAMOC slowdown between years 70-400, as rainfall remains stable during this period. Between years 1225-1325, the NAMOC reaches a new equilibrium, and both snow and rainfall increase, leading to total precipitation close to PI. However, by the end of the simulation, precipitation is only half of what it was in the PI simulation, which is mostly due to the decreased snowfall and ice sheet extent.

Melt is increasing during the first century of the simulation, with the amount of melt being almost doubled compared to PI values. Then follows a relatively stable period during NAMOC slowdown, before a significant melt increase after year 500, resulting in melt values 3.7 times higher at the end of the simulation compared to PI. Most of the melt originates from the ablation areas, and acceleration in the melt can be attributed to the increase in SW_{net} and albedo decline, LW_{net} and turbulent heat fluxes. Most of the surface melt becomes runoff, which is directly lost to the ocean and thus gives an indication of how much mass is lost from the ice sheet. At the end of the simulation, runoff is five times higher than PI.

Melt that is not partitioned as runoff, is refrozen into the snowpack, under the conditions that there is enough pore space available and that the temperature of the snowpack is at freezing point. During the simulation, the absolute amount of refreezing increases, and has doubled by the end of the simulation compared to PI. This is due to the increase in rain and melt, which provides more liquid water at the surface to be potentially refrozen. The refreezing capacity is defined in this study as the fraction of refrozen water to available water at the surface (the sum of melt and rain). Refreezing capacity goes from 46% in the PI simulation to 17% at the end of the 2xCO_2 simulation. The refreezing capacity is not yet zero but is decreasing because the snowpack becomes more saturated over time as more liquid water is refrozen. Especially as the ablation area expands causing yearly exposure of bare ice, with lower albedo leading to more heat uptake and further melting of the ice sheet. The decline in refreezing capacity results in increased melt and runoff since less surface water can be refrozen and stored in the snowpack.

The Surface Energy Balance is important for explaining the melt evolution, and in this study, the SEB components' progression during June-July-August (JJA) is analysed. The increase in the SEB components is less dramatic compared to the 4xCO_2 simulation.

During the first 70 years of the simulation, when CO_2 is forced, incoming shortwave radiation is reduced as more liquid-containing clouds are forming. The net longwave radiation is therefore the main contributor during this period. However, a pattern of anti-correlated oscillation between net longwave and shortwave is emerging after year 70 and continues on a decadal times scale up until the year 500, when it occurs on a centennial timescale. During the period between years 70 and 500, SW_{net} and LW_{net} alternates begin the main contributor to additional melt energy, with relative percentages of about 50% and 36%, respectively. The anti-correlated oscillation pattern coincides with the evolution of clouds at low altitudes, which are known for decreasing shortwave radiation. After year 500, SW_{net} becomes the main contributor to melt energy, increasing from 17 W m^2 before year 500 to 78 W m^2 at the end of the simulation. At this point, SW_{net} contributes 46% of the additional melt energy. In addition, the ice-albedo feedback is the main driver behind the increase in SW_{net} after year 500. The JJA albedo decreases from 0.77 at PI to 0.6 at the end of the simulation. This causes ablation area expansion from 10% around year 500 to 50% of the total ice sheet extent at the end.

The non-radiative fluxes are also contributing to the additional melt energy, not as much as SW_{net} and LW_{net}, but to about 10% at the end of the simulation. The increase in the non-radiative fluxes is driven by the temperature difference between the surface and the 2m air temperature. The difference becomes relatively large in the later stages of the simulation, as much as 1.7 $°C$. Although it might seem like a small contribution, the effect that the processes of heat exchange between surface and atmosphere and surface and subsurface should not be disregarded.

2. How do global, Arctic climate and the climate over Greenland influence the GrIS SMB evolution?

The responses of the global, Arctic climate and local climate over Greenland differ from one another and thus have different influences on the GrIS SMB. The global climate is continuously warming at an initial rate of 0.03 $°C$ yr^{-1} between years 1 and 70, followed by a slower warming rate until the end of the simulation. The climate over Greenland and the Arctic are initially warming before the near-surface temperatures decrease between years 70 and 418 at rates of -0.01 and -0.005 $°C$ yr^{-1} respectively. This remarkable cooling is followed by an increase in temperatures from year 410 until the end of the simulation. This leads to, at the end of the simulation of a global mean surface temperature increase of 5 $°C$, an Arctic temperature increase of 11 $°C$ and a temperature increase over GrIS of 9 $°C$ compared to PI.

The precipitation pattern over the Arctic becomes drier between years 70 and 410, as the NAMOC weakens, with respect to PI. As a consequence, a negative precipitation change is observed between years 60-410 (with respect to PI) around the southern parts of Greenland, Iceland, the region between Iceland and the UK, as well as the majority of the coast of Norway. Once the NAMOC recovers, the whole Arctic experiences an increase in precipitation, compared to PI, except for the southern tip of Greenland. The largest precipitation increase is found over the interior of Greenland.

The evolution of the fraction of sea ice is also important for the regional climate, as the sea ice reflects shortwave energy and insulates the ocean from the atmosphere. When the sea ice melts, the ocean absorbs the shortwave radiation and warms. The Arctic becomes seasonally ice-free around years 50-70. Interestingly, after becoming seasonally sea-ice free, both the March and September sea ice extent is experiencing regrowth during the slowdown of the NAMOC. However, September sea ice is completely lost after the year 500 as warming resumes due to NAMOC recovery. Nevertheless, the Arctic does not become year-round sea ice-free during this moderate warming simulation.

3. How does NAMOC evolution impact the GrIS SMB?

In this study, the changes in NAMOC have shown to have significant consequences for the GrIS SMB in the $2xCO_2$ simulation. As the simulation reaches CO_2 stabilisation in year 70, the NAMOC is weakening at a rate of -0.13 Sv yr^{-1}. The NAMOC is at a low point between year 390 and 410, with a strength of only 5 Sv. After year 410, the NAMOC is increasing in strength by 0.018 Sv yr^{-1} until reaching a new equilibrium after the year 1000, with a strength varying between 17-20 Sv. The weakening of the

NAMOC causes a cooling effect (drying) over Greenland, causing a decrease in precipitation, especially in the south of Greenland. It also causes expansion of the fraction of sea ice east of Greenland towards Iceland and north of Scandinavia. This evolution goes against the expected pattern of more precipitation and more sea ice melt due to global warming. During the period of temporary NAMOC weakening, the SMB, melt, refreezing and runoff are all more or less stable due to the cooling effect. This reduces precipitation and lowers the near-surface temperature over the Arctic and Greenland.

Most of the simulations run with the CESM2-CISM2 project a significant decline of the NAMOC, both in the idealised 1% simulations and in the SSP-simulations only run with CESM2 (Muntjewerf, Petrini, et al., 2020b). Furthermore, most models participating in the CMIP6 also project a reduction in the NAMOC, and the sixth assessment report from the IPCC states that the NAMOC will decline, however it is more uncertain if it will fully collapse before 2100. In conclusion, the NAMOC will decline in the future, but how fast and how much will depend on several processes, for instance, temperature change, freshwater influx or other regional weather or climatic changes. This study shows that in the 2xCO_2 simulation, the changes in NAMOC have large effects on the GrIS mass budget and the Arctic sea ice.

In conclusion, the GrIS is projected to lose 4.1 m of SLE over 3000 years under CO_2 doubling. Studying the interaction between the ice sheet and a temporary weakening of the NAMOC, displays a dampening effect on the GrIS mass loss. This study has shown the important interactions between the processes in the ice sheet mass balance, such as increased melt, precipitation decrease, lowering of elevation, area reduction and the ice-albedo feedback. The CESM2-CISM2 model used in this study includes the coupling of ice sheet-climate. This coupling is crucial, because taking into account that these parts interact with the climate provides a more realistic representation of our complex Earth system and a more comprehensive overview of the climate change situation and future projections of an increasingly fast-changing climate.

Working across disciplines such as climate science, glaciology, oceanography, anthropology, economy and ecology, and expanding our research on the interrelatedness of processes affecting climate change, we make it possible to come up with more solutions to mitigate climate change, and this gives us hope.

7 Recommendations

The analysis of the $2xCO_2$ simulation run with the coupled Earth system model CESM2 coupled to the ice sheet model CISM2 resulted in the following recommendations:

- **Incorporate the bi-directional coupling between ocean and ice sheet** to realistically simulate the ocean warming effect on marine-terminating outlet glaciers. As the ocean warms, it heats the marine-terminating glaciers, providing additional melt energy. This could lead to a faster retreat of the glaciers and increased freshwater influx to the ocean. Current observations reveal that GrIS ice discharge is increasing as a response to a warmer ocean, compared to PI (Fox-Kemper et al., 2021; van den Broeke et al., 2016). Currently, the ocean forcing is prescribed/parameterised in ice sheet-only models (Aschwanden et al., 2019; Goelzer et al., 2020).

- **Analyse the scenario SSP2-4.5 run with CESM2.1-CISM2.1** in order to investigate the ice sheet response to different CO_2 forcings. Since the SSP2-4.5 scenario does not have a constant forcing of CO_2, it would be interesting to see if it affects the magnitude and timing of the GrIS surface mass balance change.

- **Continue the $2xCO_2$ simulation** to further investigate if the ice sheet reaches a new equilibrium with a reduced ice sheet or if it completely melts. After 3000 years, the ice sheet is still losing mass and is not showing any acceleration or deceleration in the mass loss. This could indicate that the ice sheet will be completely lost within another 2000-3000 years. However, there could also be a stabilisation of the ice sheet within another 1000 years that could possibly see the ice sheet regrow.

- **Investigate the NAMOC decline effect on ocean currents and Antarctica**. Some literature (Barker et al., 2011; Broecker, 1998; Stocker, 1998; Stocker & Johnsen, 2003; Van Breedam et al., 2020) has suggested that weakening in NAMOC can result in warmer waters transported to Antarctica, running the risk of accelerating ice shelves and sea ice melt.

Bibliography

Arias, P., Bellouin, N., Coppola, E., Jones, R., Krinner, G., Marotzke, J., Naik, V., Palmer, M., Plattner, G.-K., Rogelj, J., Rojas, M., Sillmann, J., Storelvmo, T., Thorne, P., Trewin, B., Rao, K. A., Adhikary, B., Allan, R., Armour, K., … Zickfeld, K. (2021). Technical Summary. In V. Masson-Delmotte, P. Zhai, A. Pirani, S. Connors, C. Péan, S. Berger, N. Caud, Y. Chen, L. Goldfarb, M. Gomis, M. Huang, K. Leitzell, E. Lonnoy, J. Matthews, T. Maycock, T. Waterfield, O. Yelekçi, R. Yu, & B. Zhou (Eds.), *Climate change 2021: The physical science basis. contribution of working group i to the sixth assessment report of the intergovernmental panel on climate change* (pp. 33–144). Cambridge University Press. https://doi.org/10.1017/9781009157896.002

Aschwanden, A., Fahnestock, M. A., Truffer, M., Brinkerhoff, D. J., Hock, R., Khroulev, C., Mottram, R., & Khan, S. A. (2019). Contribution of the Greenland Ice Sheet to sea level over the next millennium. *Science Advances*, *5*(6), eaav9396. https://doi.org/10.1126/sciadv.aav9396

Bamber, J. L., Westaway, R. M., Marzeion, B., & Wouters, B. (2018). The land ice contribution to sea level during the satellite era. *Environmental Research Letters*, *13*(6), 063008. https://doi.org/10.1088/1748-9326/aac2f0

Barker, S., Knorr, G., Edwards, L., Parrenin, F., Putnam, A. E., Skinner, L. C., Wolff, E., & Ziegler, M. (2011). 800,000 years of abrupt climate variability. *Science*, *334*(347). https://doi.org/10.1126/science.1203580

Broecker, W. S. (1998). Paleocean circulation during the Last Deglaciation: A bipolar seesaw? *Paleoceanography*, *13*(2), 119–121. https://doi.org/https://doi.org/10.1029/97PA03707

Bryden, H. L., Johns, W. E., King, B. A., McCarthy, G., McDonagh, E. L., Moat, B. I., & Smeed, D. A. (2020). Reduction in Ocean Heat Transport at 26 °N since 2008 Cools the Eastern Subpolar Gyre of the North Atlantic Ocean. *Journal of Climate*, *33*(5), 1677–1689. https://doi.org/10.1175/JCLI-D-19-0323.1

Canadell, J. . G. ., Monteiro, P., Costa, M., Cotrim da Cunha, L., Cox, P., Eliseev, A., Henson, S., Ishii, M., Jaccard, S., Koven, C., Lohila, A., Patra, P., Piao, S., Rogelj, J., Syampungani, S., Zaehle, S., & Zickfeld, K. (2021). 2021: Global carbon and other biogeochemical cycles and feedbacks. In V. Masson-Delmotte, P. Zhai, A. Pirani, S. Connors, C. Péan, S. Berger, N. Caud, Y. Chen, L. Goldfarb, M. Gomis, M. Huang, K. Leitzell, E. Lonnoy, J. Matthews, T. Maycock, T. Waterfield, O. Yelekçi, R. Yu, & B. Zhou (Eds.), *In climate change 2021: The physical science basis. contribution of working group i to the sixth assessment report of the intergovernmental panel on climate change* (pp. 673–816). Cambridge University Press. https://doi.org/10.1017/9781009157896.007

Charbit, S., Paillard, D., & Ramstein, G. (2008). Amount of co2 emissions irreversibly leading to the total melting of greenland. *Geophysical Research Letters*, *35*(12).

Chemke, R., Zanna, L., & Polvani, L. M. (2020). Identifying a human signal in the North Atlantic warming hole. *GNature Communications*, *11*(1540). https://doi.org/10.1038/s41467-020-15285-x

Choi, Y., Morlighem, M., Rignot, E., & Wood, M. (2021). Ice dynamics will remain a primary driver of greenland ice sheet mass loss over the next century. *Communications Earth & Environment*, *2*. https://doi.org/10.1038/s43247-021-00092-z

Crutzen, P. J. (2002). Geology of mankind. *Nature*, *415*(23). https://doi.org/10.1038/415023a

Cuffey, K. M., & Paterson, W. S. B. (2010). Mass balance processes: 2. surface ablation and energy budget [DOI: 10.1016/B978-0-12-369461-4.00005-3]. *The physics of glaciers*. Elsevier.

Danabasoglu, G., Bates, S. C., Briegleb, B. P., Jayne, S. R., Jochum, M., Large, W. G., Peacock, S., & Yeager, S. G. (2012). The ccsm4 ocean component. *Journal of Climate*, *25*(5), 1361–1389. https://doi.org/10.1175/JCLI-D-11-00091.1

Danabasoglu, G., Lamarque, J.-F., Bacmeister, J., Bailey, D. A., DuVivier, A. K., Edwards, J., Emmons, L. K., Fasullo, J., Garcia, R., Gettelman, A., Hannay, C., Holland, M. M., Large, W. G., Lauritzen, P. H., Lawrence, D. M., Lenaerts, J. T. M., Lindsay, K., Lipscomb, W. H., Mills, M. J., … Strand, W. G. (2020). The Community Earth System Model Version 2 (CESM2). *Journal of Advances in Modeling Earth Systems*, *12*(2), e2019MS001916. https://doi.org/https://doi.org/10.1029/

2019MS001916
e2019MS001916 2019MS001916

Drijfhout, S., van Oldenborgh, G. J., & Cimatoribus, A. (2012). Is a Decline of AMOC Causing the Warming Hole above the North Atlantic in Observed and Modeled Warming Patterns? *Journal of Climate*, *25*(24), 8373–8379. https://doi.org/10.1175/JCLI-D-12-00490.1

Dutton, A., Carlson, A., Long, A., Milne, G., Clark, P., DeConto, R., Horton, B., Rahmstorf, S., & Raymo, M. (2015). Sea-level rise due to polar ice-sheet mass loss during past warm periods. *Science.*, *349*(6244), aaa4019. http://dro.dur.ac.uk/18054/

Edwards, T. L., Nowicki, S., Marzeion, B., Hock, R., Goelzer, H., Seroussi, H., Jourdain, N. C., Slater, D. A., Turner, F. E., Smith, C. J., McKenna, C. M., Simon, E., Abe-Ouchi, A., Gregory, J. M., Larour, E., Lipscomb, W. H., Payne, A. J., Shepherd, A., Agosta, C., … Zwinger, T. (2021). Projected land ice contributions to twenty-first-century sea level rise. *Nature*, *593*, 74–82. https://doi.org/https://doi.org/10.1038/s41586-021-03302-y

Enderlin, E. M., Howat, I. M., Jeong, S., Noh, M.-J., van Angelen, J. H., & van den Broeke, M. R. (2014). An improved mass budget for the Greenland ice sheet. *Geophysical Research Letters*, *41*(3), 866–872. https://doi.org/https://doi.org/10.1002/2013GL059010

Ettema, J., van der Broeke, M. R., van Meijgaard, E., & van de Berg, W. J. (2010). Climate of the greenland ice sheet using a high-resolution climate model – part 2: Near-surface climate and energy balance [doi: https://doi.org/10.5194/tc-4-529-2010]. *The Cryosphere*, *4*, 529–544.

Eyring, V., Bony, S., Meehl, G. A., Senior, C. A., Stevens, B., Stouffer, R. J., & Taylor, K. E. (2016). Overview of the coupled model intercomparison project phase 6 (cmip6) experimental design and organization. *Geoscientific Model Development*, *9*(5), 1937–1958. https://doi.org/10.5194/gmd-9-1937-2016

Flanner, M. G., & Zender, C. S. (2006). Linking snowpack microphysics and albedo evolution. *Journal of Geophysical Research Atmospheres*, *111*(12). https://doi.org/10.1029/2005JD006834

Flanner, M. G., Zender, C. S., Randerson, J. T., & Rasch, P. J. (2007). Present-day climate forcing and response from black carbon in snow. *Journal of Geophysical Research Atmospheres*, *112*(11). https://doi.org/10.1029/2006JD008003

Fox-Kemper, B., Hewitt, H. T., Xiao, C., Aðalgeirsdóttir, G., Drijfhout, S. S., Edwards, T. L., Golledge, N. R., Hemer, M., Kopp, R. E., Krinner, G., Mix, A., Notz, D., Nowicki, S., Nurhati, I., Ruiz, L., Sallée, J. .-., Slangen, A. B. A., & Yu, Y. (2021). Ocean, cryosphere and sea level change. in. In V. Masson-Delmotte, P. Zhai, A. Pirani, S. Connors, C. Péan, S. Berger, N. Caud, Y. Chen, L. Goldfarb, M. Gomis, M. Huang, K. Leitzell, E. Lonnoy, J. Matthews, T. Maycock, T. Waterfield, O. Yelekçi, R. Yu, & B. Zhou (Eds.), *Climate change 2021: The physical science basis. contribution of working group i to the sixth assessment report of the intergovernmental panel on climate change* (pp. 1211–1362). Cambridge University Press. https://doi.org/10.1017/9781009157896.011

Fyke, J. G., Sergienko, O., Löfverström, M., Price, S., & Lenaerts, J. T. M. (2018). An Overview of Interactions and Feedbacks Between Ice Sheets and the Earth System. *Reviews of Geophysics*, *56*(2), 361–408. https://doi.org/10.1029/2018RG000600

Fyke, J. G., Weaver, A. J., Pollard, D., Eby, M., Carter, L., & Mackintosh, A. (2011). A new coupled ice sheet/climate model: description and sensitivity to model physics under Eemian, Last Glacial Maximum, late Holocene and modern climate conditions. *Geoscientific Model Development*, *4*(1), 117–136. https://doi.org/10.5194/gmd-4-117-2011

Gaffney, O., & Rockström, J. (2021). *Breaking boundaries the science of our planet* (First). Dorling Kindersley Ltd.

Gettelman, A., Morrison, H., Santos, S., Bogenschutz, P., & Caldwell, P. M. (2015). Advanced two-moment bulk microphysics for global models. part ii: Global model solutions and aerosol-cloud interactions. *Journal of Climate*, *28*(3), 1288–1307. https://doi.org/10.1175/JCLI-D-14-00103.1

Goelzer, H., Nowicki, S., Payne, A., Larour, E., Seroussi, H., Lipscomb, W., Gregory, J., Abe-Ouchi, A., Shepherd, A., Simon, E., Agosta, C., Alexander, P., Aschwanden, A., Barthel, A., Calov, R., Chambers, C., Choi, Y., Cuzzone, J., Dumas, C., … van den Broeke, M. (2020). The future sea-level contribution of the Greenland ice sheet: a multi-model ensemble study of ISMIP6. *The Cryosphere*. https://doi.org/10.5194/tc-2019-319

Goelzer, H., Robinson, A., Seroussi, H., & van de Wal, R. S. . W. . (2017). Recent Progress in Greenland Ice Sheet Modelling. *Current Climate Change Reports volume*, (3), 291–302. https://doi.org/10.1007/s40641-017-0073-y

Gregory, J. M., George, S. E., & Smith, R. S. (2020). Large and irreversible future decline of the Greenland ice sheet. *The Cryosphere*, *14*(12), 4299–4322. https://doi.org/10.5194/tc-14-4299-2020

Hunke, E., Lipscomb, W., Jones, P., Turner, A., Jeffery, N., & Elliott, S. (2017). Cice, the los alamos sea ice model, version 00. https://www.osti.gov//servlets/purl/1364126

Huybrechts, P., Goelzer, H., Janssens, I., Driesschaert, E., Fichefet, T., Goosse, H., & Loutre, M.-F. (2011). Response of the greenland and antarctic ice sheets to multi-millennial greenhouse warming in the earth system model of intermediate complexity loveclim. *Surveys in Geophysics*, *32*(4), 397–416.

Lawrence, D. M., Fisher, R. A., Koven, C. D., Oleson, K. W., Swenson, c. C., Bonan, c., Collier, c., Ghimire, c., van Kampenhout, L., Kennedy, D., Kluzek, E., Lawrence, P. J., Li, F., Li, H., Lombardozzi, D., Riley, W. J., Sacks, W. J., Shi, M., Vertenstein, M., … Zeng, X. (2019). The community land model version 5: Description of new features, benchmarking, and impact of forcing uncertainty. *Journal of Advances in Modeling Earth Systems*, *11*(12), 4245–4287. https://doi.org/10.1029/2018MS001583

Lenaerts, J. T. M., Gettelman, A., Van Tricht, K., van Kampenhout, L., & Miller, N. B. (2020). Impact of cloud physics on the greenland ice sheet near-surface climate: A study with the community atmosphere model. *Journal of Geophysical Research: Atmospheres*, *125*(7). https://doi.org/10.1029/2019JD031470

Lenton, T. M., Held, H., Kriegler, E., Hall, J. W., Lucht, W., Rahmstorf, S., & Schellnhuber, H. J. (2008). Tipping elements in the earth's climate system. *Proceedings of the National Academy of Sciences*, *105*(6), 1786–1793. https://doi.org/10.1073/pnas.0705414105

Li, H. .-., Leung, L. R., Getirana, A., Huang, M., Wu, H., Xu, Y., Guo, J., & Voisin, N. (2015). Evaluating global streamflow simulations by a physically based routing model coupled with the community land model. *Journal of Hydrometeorology*, *16*(2), 948–971. https://doi.org/10.1175/JHM-D-14-0079.1

Lin, S. .-., & Rood, R. B. (1997). An explicit flux-form semi-lagrangian shallow-water model on the sphere. *Quarterly Journal of the Royal Meteorological Society*, *123*(544), 2477–2498. https://doi.org/10.1002/qj.49712354416

Lindsay, R. (2022). Climate change: Atmospheric carbon dioxide. https://www.climate.gov/news-features/understanding-climate/climate-change-atmospheric-carbon-dioxide

Lipscomb, W. H., Fyke, J. G., Vizcaíno, M., Sacks, W. J., Wolfe, J., Vertenstein, M., Craig, A., Kluzek, E., & Lawrence, D. M. (2013). Implementation and initial evaluation of the glimmer community ice sheet model in the community earth system model. *Journal of Climate*, *26*(19), 7352–7371. https://doi.org/10.1175/JCLI-D-12-00557.1

Lipscomb, W. H., Price, S. F., Hoffman, M. J., Leguy, G. R., Bennett, A. R., Bradley, S. L., Evans, K. J., Fyke, J. G., Kennedy, J. H., Perego, M., Ranken, D. M., Sacks, W. J., Salinger, A. G., Vargo, L. J., & Worley, P. H. (2019). Description and evaluation of the community ice sheet model (cism) v2.1. *Geoscientific Model Development*, *12*(1), 387–424. https://doi.org/10.5194/gmd-12-387-2019

Liu, X., Ma, P. .-., Wang, H., Tilmes, S., Singh, B., & Easter, R. C. (2015). Description and evaluation of a new 4-mode version of modal aerosol module (mam4) within version 5.3 of the community atmosphere model. *Geoscientific Model Development Discussions, 8*(9), 8341–8386. https://doi.org/10.5194/gmdd-8-8341-2015

Lofverstrom, M., Fyke, J. G., Thayer-Calder, K., Muntjewerf, L., Vizcaino, M., Sacks, W. J., Lipscomb, W. H., Otto-Bliesner, B. L., & Bradley, S. L. (2020). An Efficient Ice Sheet/Earth System Model Spin-up Procedure for CESM2-CISM2: Description, Evaluation, and Broader Applicability. *Journal of Advances in Modeling Earth Systems*, *12*(8), e2019MS001984. https://doi.org/https://doi.org/10.1029/2019MS001984
e2019MS001984 10.1029/2019MS001984

Meinshausen, M., Nicholls, Z. R. J., Lewis, J., Gidden, M. J., Vogel, E., Freund, M., Beyerle, U., Gessner, C., Nauels, A., Bauer, N., Canadell, J. G., Daniel, J. S., John, A., Krummel, P. B., Luderer, G., Meinshausen, N., Montzka, S. A., Rayner, P. J., Reimann, S., … Wang, R. H. J. (2020). The shared socio-economic pathway (SSP) greenhouse gas concentrations and their extensions to 2500. *Geoscientific Model Development*, *13*(8), 3571–3605. https://doi.org/10.5194/gmd-13-3571-2020

Menary, M. B., Robson, J., Allan, R. P., Booth, B. B. B., Cassou, C., Gastineau, G., Gregory, J., Hodson, D., Jones, C., Mignot, J., Ringer, M., Sutton, R., Wilcox, L., & Zhang, R. (2020). Aerosol-Forced AMOC Changes in CMIP6 Historical Simulations. *Geophysical Research Letters*, *47*(14), e2020GL088166. https://doi.org/https://doi.org/10.1029/2020GL088166 e2020GL088166 2020GL088166

Mikolajewicz, U., Gröger, M., Maier-Reimer, E., Schurgers, G., Vizcaíno, M., & Winguth, A. M. E. (2007). Long-term effects of anthropogenic CO2 emissions simulated with a complex earth system model. *Clim Dyn*, *28*, 599–633. https://doi.org/10.1007/s00382-006-0204-y

Milankocivh, M. (1998). *Canon of insolation and the ice-age problem*. Agency for Textbooks.

Muntjewerf, L., Petrini, M., Vizcaíno, M., da Silva, C., Sellevold, R., Scherrenberg, M., Thayer-Calder, K., Bradley, S., Lenaerts, J., Lipscomb, W., & Lofverstrom, M. (2020a). Greenland ice sheet contribution to 21 st century sea level rise as simulated by the coupled cesm2.1-cism2.1. *Geophysical Research Letters*, *47*, e2019GL086836. https://doi.org/10.1029/2019GL086836

Muntjewerf, L., Petrini, M., Vizcaíno, M., da Silva, C., Sellevold, R., Scherrenberg, M., Thayer-Calder, K., Bradley, S., Lenaerts, J., Lipscomb, W., & Lofverstrom, M. (2020b). Supporting information for ”greenland ice sheet contribution to 21st century sea level rise as simulated by the coupled cesm2.1-cism2.1”. *Geophysical Research Letters*, *47*, e2019GL086836. https://doi.org/10.1029/2019GL086836

Muntjewerf, L., Sacks, W., Lofverstrom, M., Fyke, J., Lipscomb, W., da Silva, C., Vizcaíno, M., Thayer-Calder, K., Lenaerts, J., & Sellevold, R. (2021). Description and demonstration of the coupled community earth system model v2 - community ice sheet model v2 (cesm2-cism2). *Journal of Advances in Modeling Earth Systems*, *13*. https://doi.org/10.1029/2020MS002356

Muntjewerf, L., Sellevold, R., Vizcaíno, M., da Silva, C., Petrini, M., Thayer-Calder, K., Scherrenberg, M., Bradley, S., Fyke, J., Lipscomb, W., Lofverstrom, M., & Sacks, W. (2020). Accelerated greenland ice sheet mass loss under high greenhouse gas forcing as simulated by the coupled cesm2.1-cism2.1. *Journal of Advances in Modeling Earth Systems*, *12*. https://doi.org/10.1029/2019MS002031

Noël, B., Aðalgeirsdóttir, G., Pálsson, F., Wouters, B., Lhermitte, S., Haacker, J. M., & van den Broeke, M. R. (2022). North atlantic cooling is slowing down mass loss of icelandic glaciers [https://doi.org/10.1029/2021GL095697]. *Geophysical Research Letters*, *49*.

Nowicki, S. M. J., Payne, A., Larour, E., Seroussi, H., Goelzer, H., Lipscomb, W., Gregory, J., Abe-Ouchi, A., & Shepherd, A. (2016). Ice Sheet Model Intercomparison Project (ISMIP6) contribution to CMIP6. *Geoscientific Model Development*, *9*(12), 4521–4545. https://doi.org/10.5194/gmd-9-4521-2016

O’Neill, B. C., Tebaldi, C., van Vuuren, D. P., Eyring, V., Friedlingstein, P., Hurtt, G., Knutti, R., Kriegler, E., Lamarque, J.-F., Lowe, J., Meehl, G. A., Moss, R., Riahi, K., & Sanderson, B. M. (2016). The Scenario Model Intercomparison Project (ScenarioMIP) for CMIP6. *Geoscientific Model Development*, *9*(9), 3461–3482. https://doi.org/10.5194/gmd-9-3461-2016

Robinson, A., Calov, R., & Ganopolski, A. (2012). Multistability and critical thresholds of the Greenland ice sheet. *Nature Climate Change*, *2*, 429–432. https://doi.org/10.1038/nclimate1449

Scinocca, J. F., & McFarlane, N. A. (2000). The parametrization of drag induced by stratified flow over anisotropic orography. *Quarterly Journal of the Royal Meteorological Society*, *126*(568), 2353–2393. https://doi.org/10.1002/qj.49712656802

Sellevold, R., van Kampenhout, L., Lenaerts, J., Noël, B., Lipscomb, W., & Vizcaíno, M. (2019). Surface mass balance downscaling through elevation classes in an earth system model: Application to the greenland ice sheet. *The Cryosphere*, *13*, 3193–3208. https://doi.org/10.5194/tc-13-3193-2019

Sellevold, R., & Vizcaíno, M. (2020). Global Warming Threshold and Mechanisms for Accelerated Greenland Ice Sheet Surface Mass Loss. *Journal of Advances in Modeling Earth Systems*, *12*(9), e2019MS002029. https://doi.org/10.1029/2019MS002029

Shepherd, A., Ivins, E., Rignot, E., Smith, B., Van den Broeke, M., Velicogna, I., Whitehouse, P., Briggs, K., Joughin, I., Krinner, G., Nowicki, S., Payne, T., Scambos, T., Schlegel, N., Geruo, A., Agosta, C., Ahlstrøm, A., Babonis, G., Barletta, V. R., … Wuite, J. (2020). Mass balance of the Greenland Ice Sheet from 1992 to 2018. *Nature*, *579*, 233–239. https://doi.org/10.1038/s41586-019-1855-2

Smith, R., Jones, P., Briegleb, B., Bryan, F., Danabasoglu, G., & Dennis, J. (2010). The parallel ocean program (pop) reference manual ocean component of the community climate system model (ccsm) [LAUR-10-01853]. *LANL, Tech. Report*.

Sommers, A. N., Otto-Bliesner, B. L., Lipscomb, W. H., Lofverstrom, M., Shafer, S. L., Bartlein, P. J., Brady, E. C., Kluzek, E., Leguy, G., Thayer-Calder, K., & Tomas, R. A. (2021). Retreat and regrowth of the greenland ice sheet during the last interglacial as simulated by the cesm2-cism2 coupled climate–ice sheet model. *Paleoceanography and Paleoclimatology, 36*. https://doi.org/https://doi.org/10.1029/2021PA004272

Steffen, W., Rockström, J., Richardson, K., Lenton, T. M., Folke, C., Liverman, D., Summerhayes, C. P., Barnosky, A. D., Cornell, S. E., Crucifix, M., Donges, J. F., Fetzer, I., Lade, S. J., Scheffer, M., Winkelmann, R., & Schellnhuber, H. J. (2018). Trajectories of the earth system in the anthropocene. *Proceedings of the National Academy of Sciences*, *115*(33), 8252–8259.

Stocker, T. F. (1998). The Seesaw Effect. *Science*, *282*(5386), 61–62. https://doi.org/10.1126/science.282.5386.61

Stocker, T. F., & Johnsen, S. J. (2003). A minimum thermodynamic model for the bipolar seesaw. *Paleoceanography*, *18*(4). https://doi.org/https://doi.org/10.1029/2003PA000920

Swingedouw, D., Houssais, M. .-., Herbaut, C., Blaizot, A. .-., Devilliers, M., & Deshayes, J. (2022). Amoc recent and future trends: A crucial role for oceanic resolution and greenland melting? *Frontiers in Climate*, *4*. https://doi.org/10.3389/fclim.2022.838310

Van Breedam, J., Goelzer, H., & Huybrechts, P. (2020). Semi-equilibrated global sea-level change projections for the next 10\,000 years. *Earth System Dynamics*, *11*(4), 953–976. https://doi.org/10.5194/esd-11-953-2020

van den Broeke, M. R., Enderlin, E. M., Howat, I. M., Kuipers Munneke, P., Noël, B. P. Y., van de Berg, W. J., van Meijgaard, E., & Wouters, B. (2016). On the recent contribution of the Greenland ice sheet to sea level change. *The Cryosphere*, *10*(5), 1933–1946. https://doi.org/10.5194/tc-10-1933-2016

van Kampenhout, L., Lenaerts, J. T. M., Lipscomb, W. H., Lhermitte, S., Noël, B., Vizcaíno, M., Sacks, W. J., & van den Broeke, M. R. (2020). Present-Day Greenland Ice Sheet Climate and Surface Mass Balance in CESM2. *Journal of Geophysical Research: Earth Surface*, *125*(2), e2019JF005318. https://doi.org/https://doi.org/10.1029/2019JF005318
e2019JF005318 10.1029/2019JF005318

van Kampenhout, L., Lenaerts, J. T. M., Lipscomb, W. H., Sacks, W. J., Lawrence, D. M., Slater, A. G., & van den Broeke, M. R. (2017). Improving the Representation of Polar Snow and Firn in the Community Earth System Model. *Journal of Advances in Modeling Earth Systems*, *9*(7), 2583–2600. https://doi.org/https://doi.org/10.1002/2017MS000988

Weijer, W., Cheng, W., Garuba, O. A., Hu, A., & Nadiga, B. T. (2020). CMIP6 Models Predict Significant 21st Century Decline of the Atlantic Meridional Overturning Circulation. *Geophysical Research Letters*, *47*(12), e2019GL086075. https://doi.org/https://doi.org/10.1029/2019GL086075
e2019GL086075 10.1029/2019GL086075

A

Climate Change

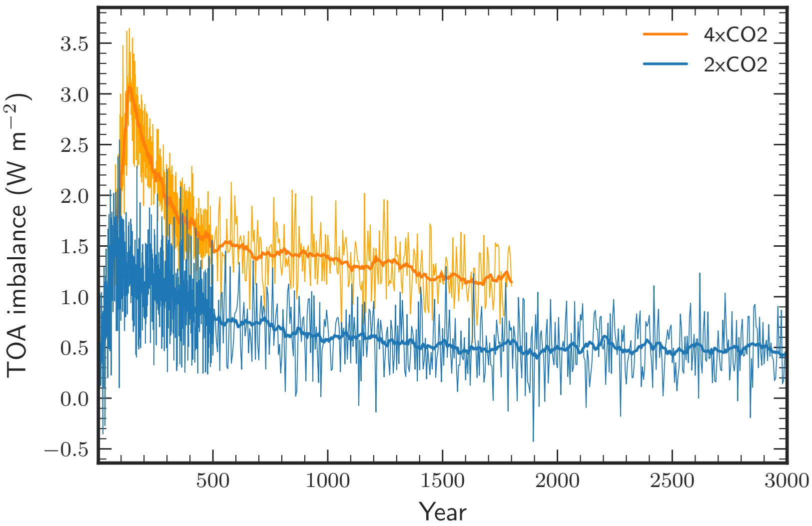

Figure A.1: Evolution of the Top of the Atmosphere Imbalance (W m^{-2}).

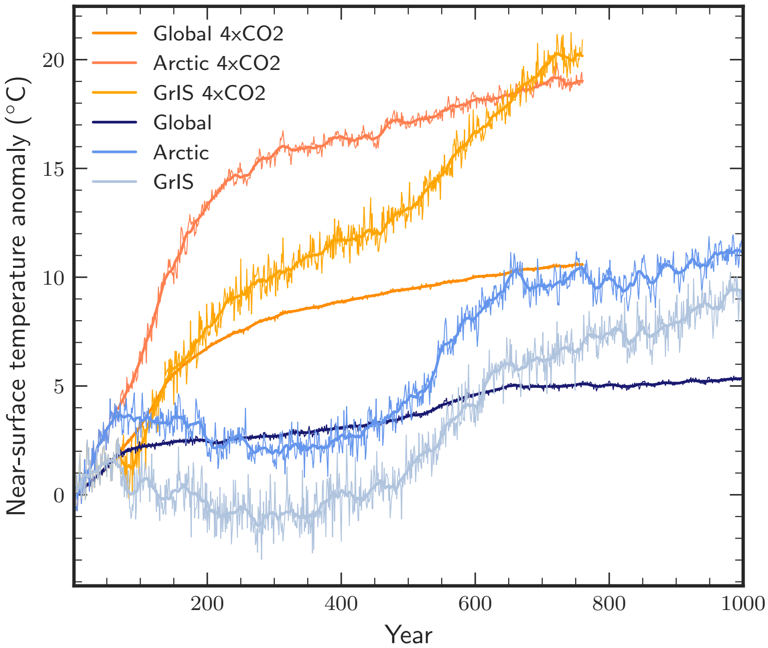

Figure A.2: Evolution of global, Arctic (region north of 60° N) and GrIS annual near-surface temperature anomaly with respect to pre-industrial mean (°C).

Component	Years	Trend	Years	Trend	Years	Trend	Years	Trend
Global	1-55	0.03 (0.001)	55-418	0.003 (0.000)	418-1360	0.002 (0.000)	1360-3000	0.0002 (0.000)
Arctic	1-55	0.070 (0.004)	55-418	-0.005 (0.000)	418-1360	0.008 (0.00)	1360-3000	0.001 (0.000)
Greenland	1-40	0.022 (0.010)	40-300	-0.010 (0.001)	300-1275	0.008 (0.001)	1275-3000	0.002 (0.000)

Table A.1: Trends of near-surface temperature anomaly (°C yr^{-1}) from a breakpoint analysis and linear regression. The standard error of the estimated slope is reported in the brackets ().

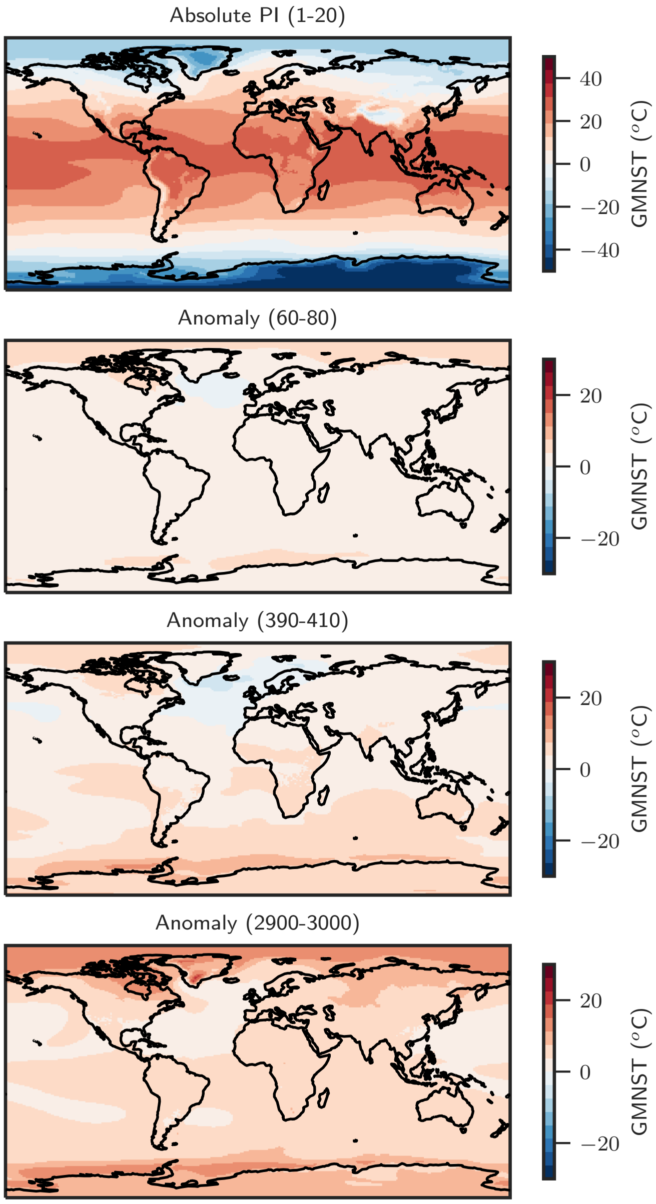

Figure A.3: Evolution of the annual global mean near-surface temperature anomaly ($^{\circ}C$) with respect to pre-industrial. The years indicate the mean considered. The topmost figure is the absolute GMNST for the mean of the pre-industrial.

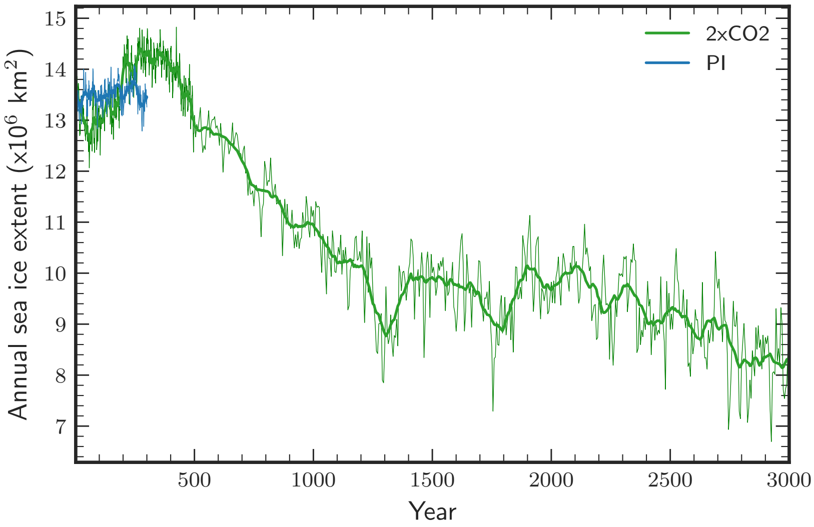

Figure A.5: Evolution of the annual sea ice extent ($x10^6$ km^2) The sea ice extent is defined as the area north of 60°N where sea ice concentration is greater than 15%.

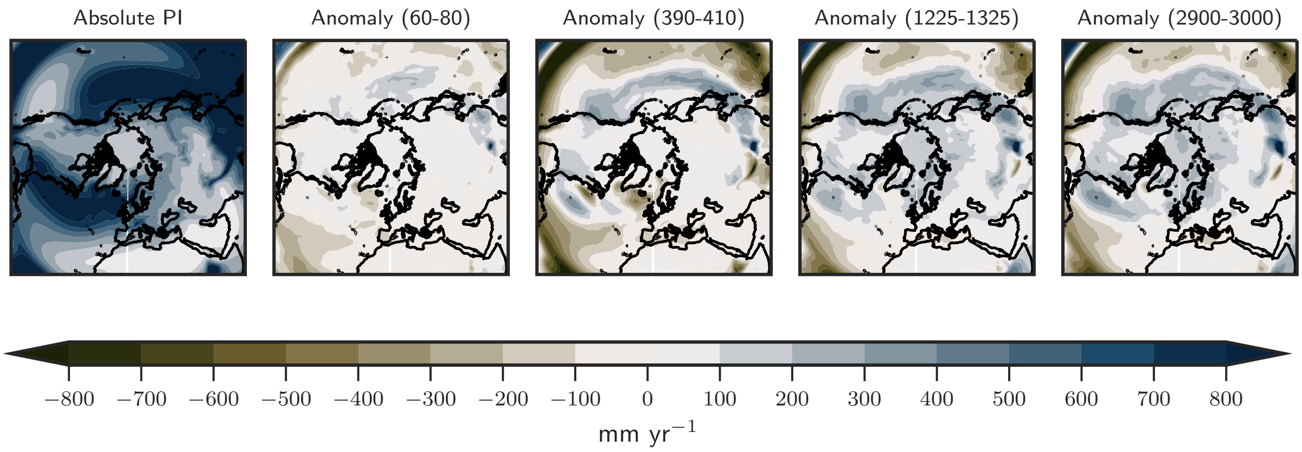

Figure A.4: Evolution of total precipitation anomaly (mm yr^{-1}) with respect to pre-industrial. The years in brackets indicate the mean considered. The leftmost figure is the absolute total precipitation for the pre-industrial mean.

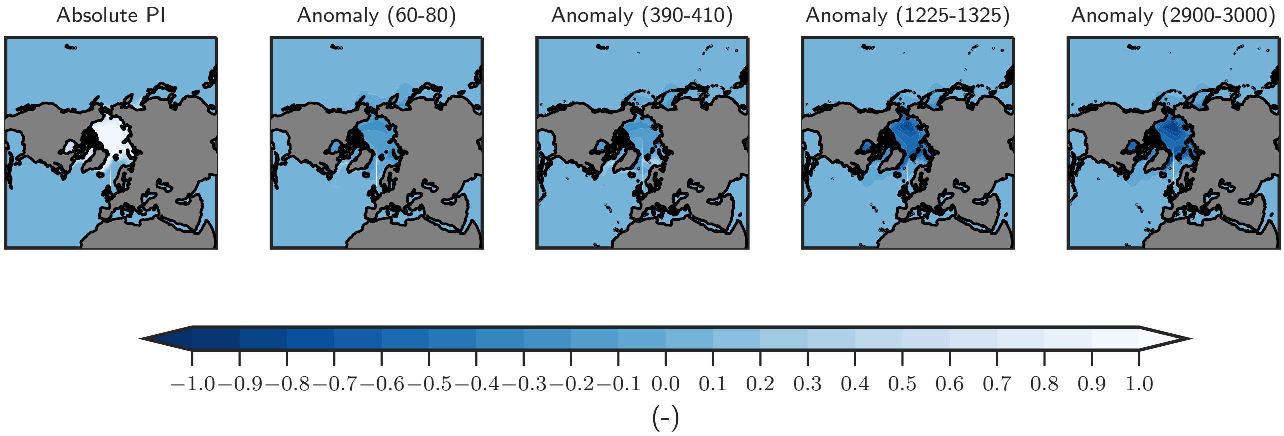

Figure A.6: Evolution of total sea ice fraction anomaly (-) with respect to pre-industrial. The years in brackets indicate the mean considered. The leftmost figure is the absolute sea ice fraction for the pre-industrial mean.

Component	Years	Trend	Years	Trend	Years	Trend	Years	Trend
NAMOC	1-114	-0.126 (0.003)	114-410	-0.020 (0.001)	410-960	0.018 (0.000)	960-3000	0.000 (0.000)

Table A.2: Trends of North Atlantic Meridional Overturning Circulation (NAMOC) strength (Sv yr^{-1}) from a breakpoint analysis and linear regression. The standard error of the estimated slope is reported in the brackets ().

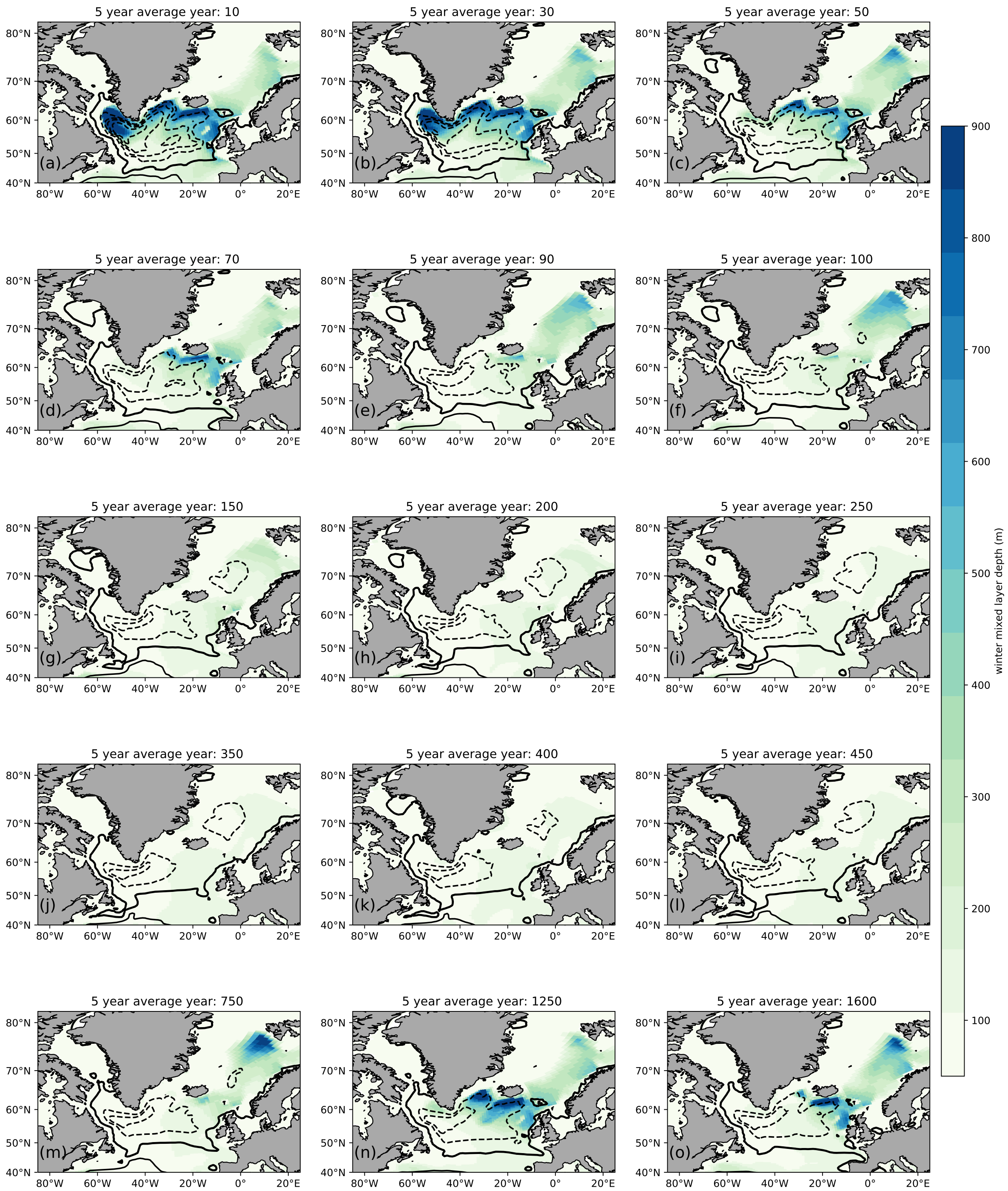

Figure A.7: Evolution of the local maximum winter (January-February-March) mixed layer depth (m). The contour lines show the barotropic streamfunction (Ψ_b in Sv) and the contour interval is 10 Sv. All values are averaged over the last 10 years of the PI simulation.

B

GrIS and Sea level rise

Component	Years	Trend	Years	Trend	Years	Trend	Years	Trend
MB	1-71	-1.108 (0.511)	71-700	0.195 (0.027)	700-1900	-0.510 (0.026)	1900-3000	-0.092 (0.032)
SMB	1-99	-2.965 (0.307)	99-494	-0.016 (0.038)	494-1675	-0.749 (0.024)	1675-3000	-0.104 (0.024)
SLR	1-710	0.470 (0.002)	710-1380	1.000 (0.015)	1380-3000	1.958 (0.002)		

Table B.1: Trends of the GrIS mass balance (MB), surface mass balance (SMB) (Gt yr^{-2}) and GrIS cumulative contribution to sea level rise (SLR) (mm yr^{-1}) from a breakpoint analysis and linear regression. The standard error of the estimated slope is reported in the brackets ().

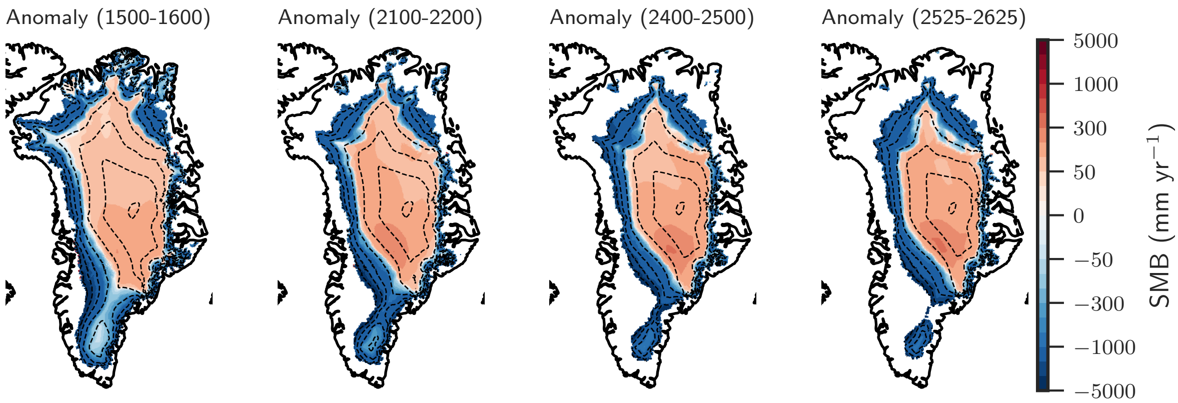

Figure B.1: Evolution of the SMB (mm yr^{-}) for the period between years 1500-2625 given in anomalies with respect to pre-industrial showing the disintegration of the southern dome from the main ice sheet. The accumulation areas are where SMB>0 (red colour) and the ablation areas are where SMB<0 (blue colour). Contour lines every 500 m.

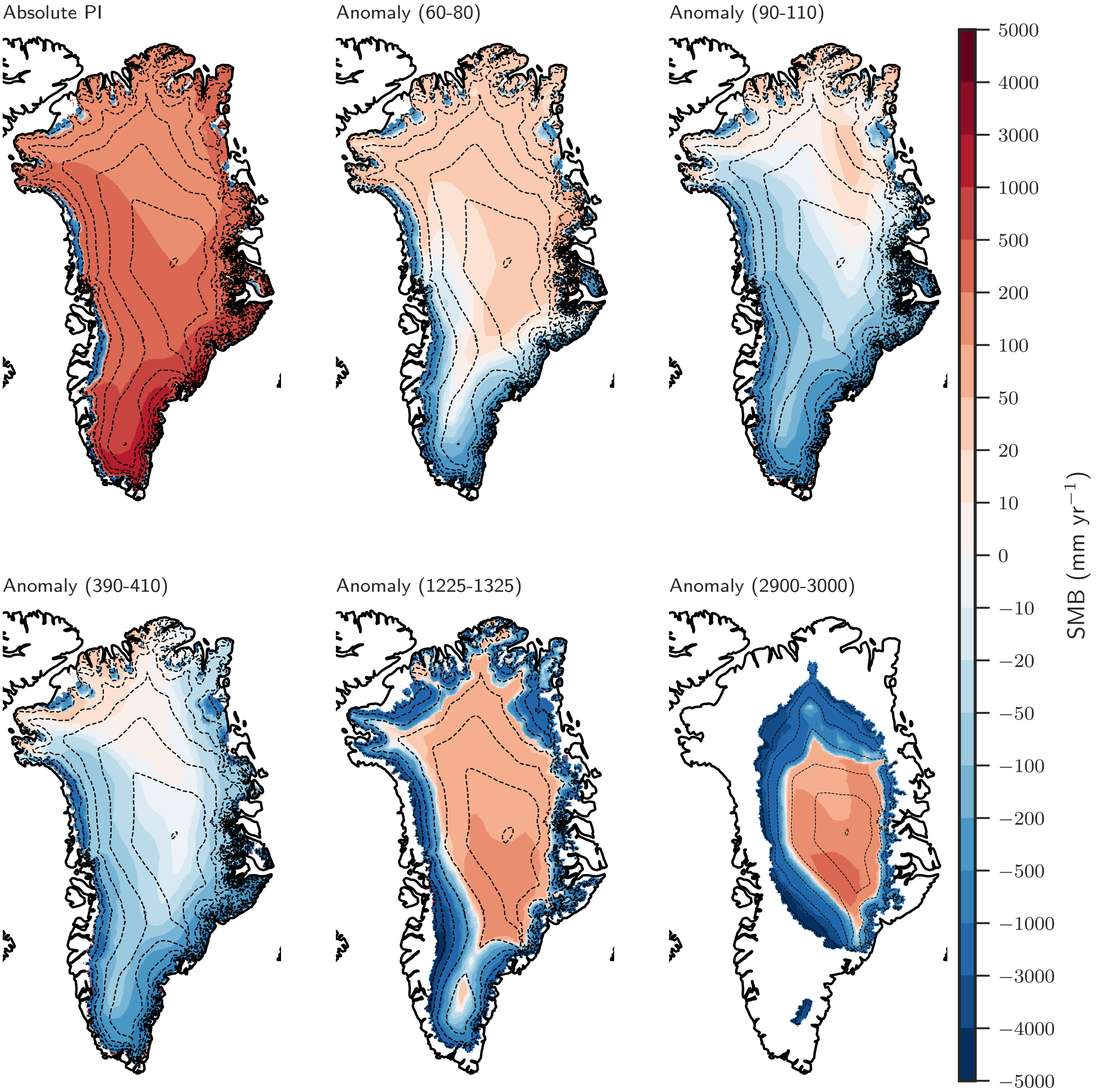

Figure B.2: Evolution of the SMB (mm yr^{-}) with pre-industrial absolute values on the top left and the rest shows anomalies with respect to pre-industrial for the mean between different model years. The accumulation areas are where SMB>0 (red colour) and the ablation areas are where SMB<0 (blue colour). Contour lines every 500 m.

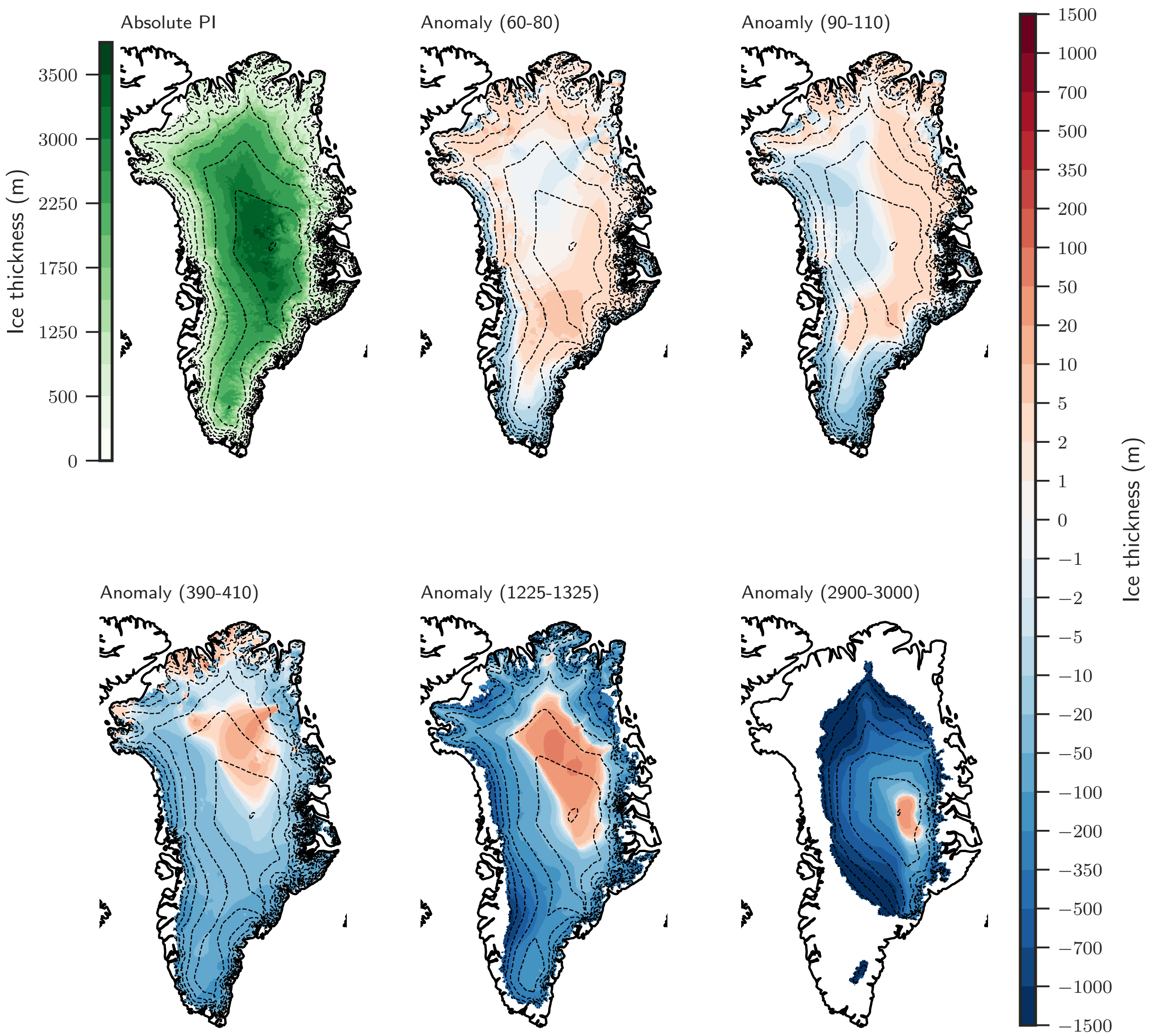

Figure B.3: GrIS ice thickness (m), with pre-industrial absolute values on the top left and the rest shows anomalies with respect to pre-industrial for the mean between different model years. Contour lines every 500 m.

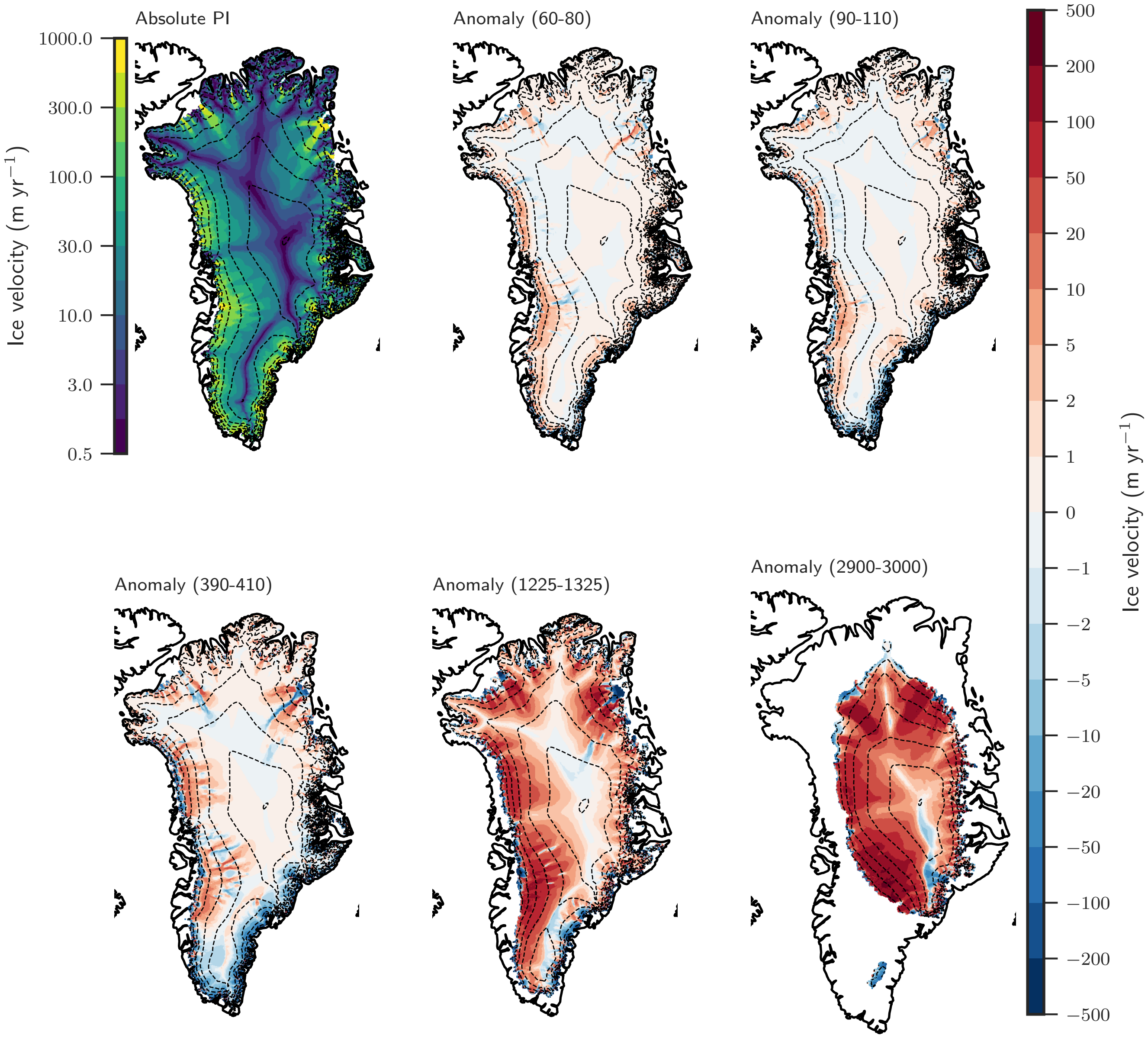

Figure B.4: GrIS ice velocity (m yr^{-1}), with pre-industrial absolute values on the top left and the rest shows anomalies with respect to pre-industrial for the mean between different model years. Contour lines every 500 m.

C

SMB & SEB

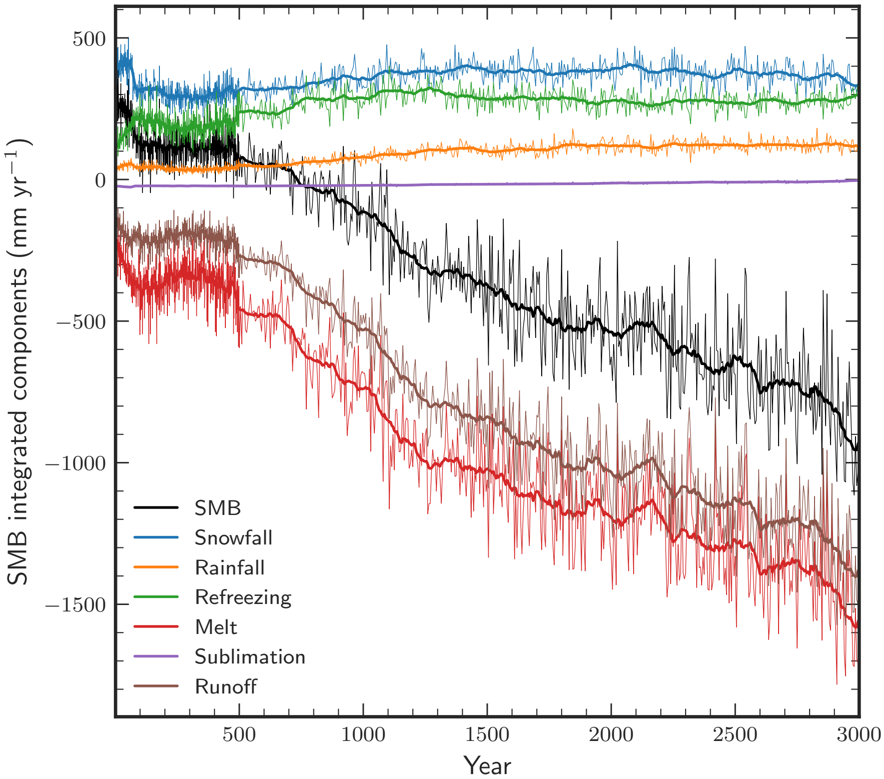

Figure C.1: Annual integrated GrIS SMB components in mm yr^{-1}. The thick lines show the 20-year running means.

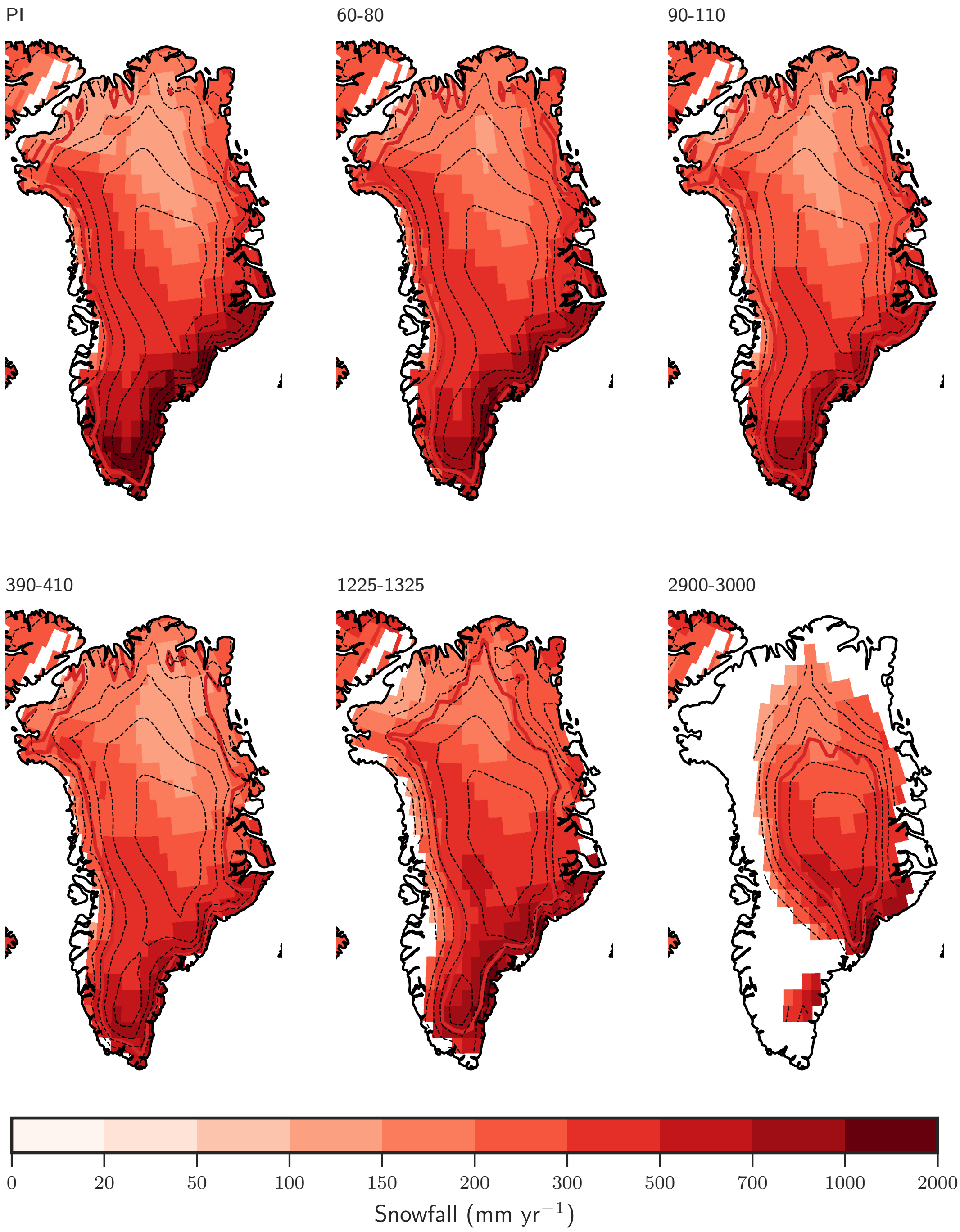

Figure C.2: Evolution of absolute annual amount of snowfall (mm yr^{-1}). The Topmost left shows the absolute of the pre-industrial. The period considered is marked by the respective years. Contour lines for every 500 m elevation. The red contour line denotes the ELA.

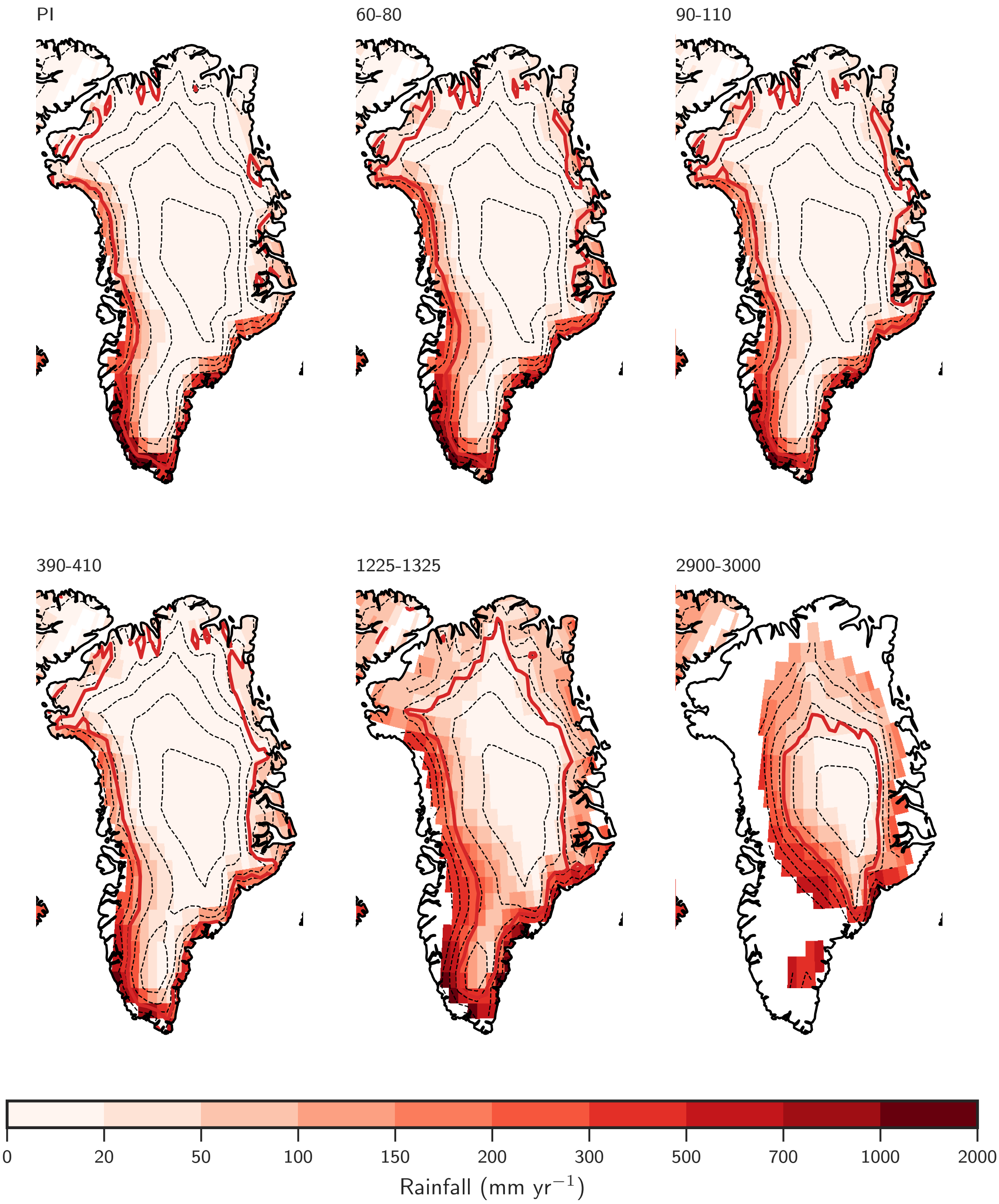

Figure C.3: Evolution of absolute annual amount of rainfall (mm yr^{-1}). The Topmost left shows the absolute of the pre-industrial. The period considered is marked by the respective years. Contour lines for every 500 m elevation. The red contour line denotes the ELA.

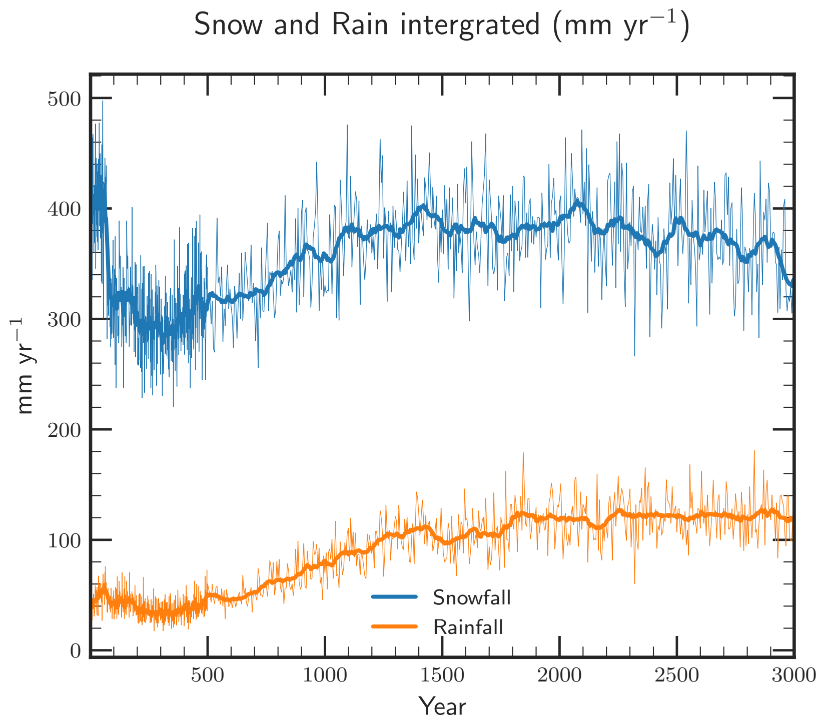

Figure C.4: Integrated annual GrIS time series of snowfall and rainfall in mm yr^{-1}. The thick lines show the 20-year running means.

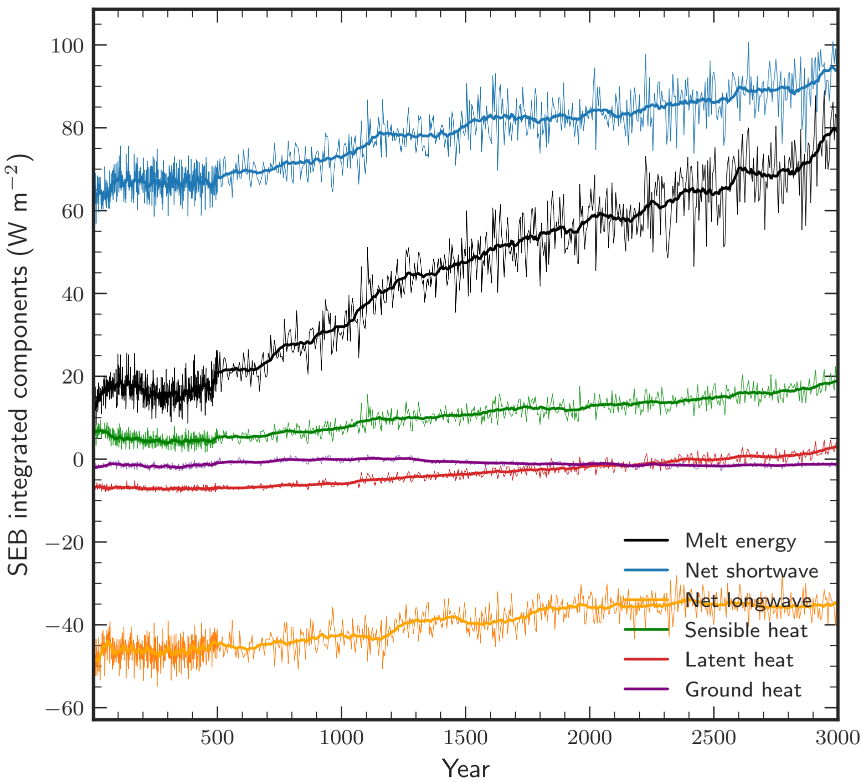

Figure C.6: June-July-August GrIS integrated surface energy balance components (W m^{-2}) with respect to the pre-industrial mean. The thick lines show the 20-year running mean.

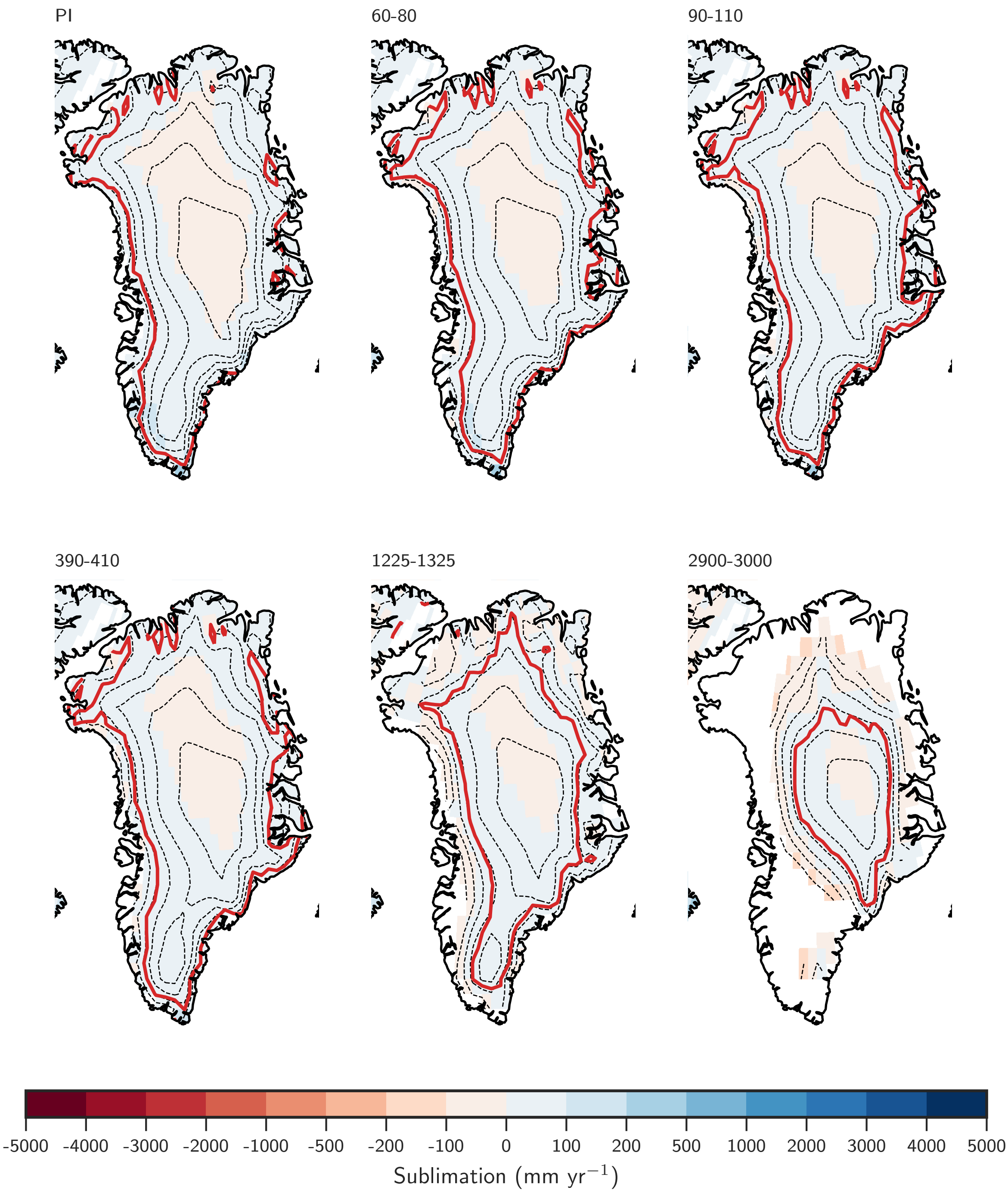

Figure C.5: Evolution of absolute annual amount of sublimation (mm yr^{-1}). The Topmost left shows the absolute of the pre-industrial. The period considered is marked by the respective years. Contour lines for every 500 m elevation. The red contour line denotes the ELA. The red colours indicate mass gain and the blue colours indicate mass loss.

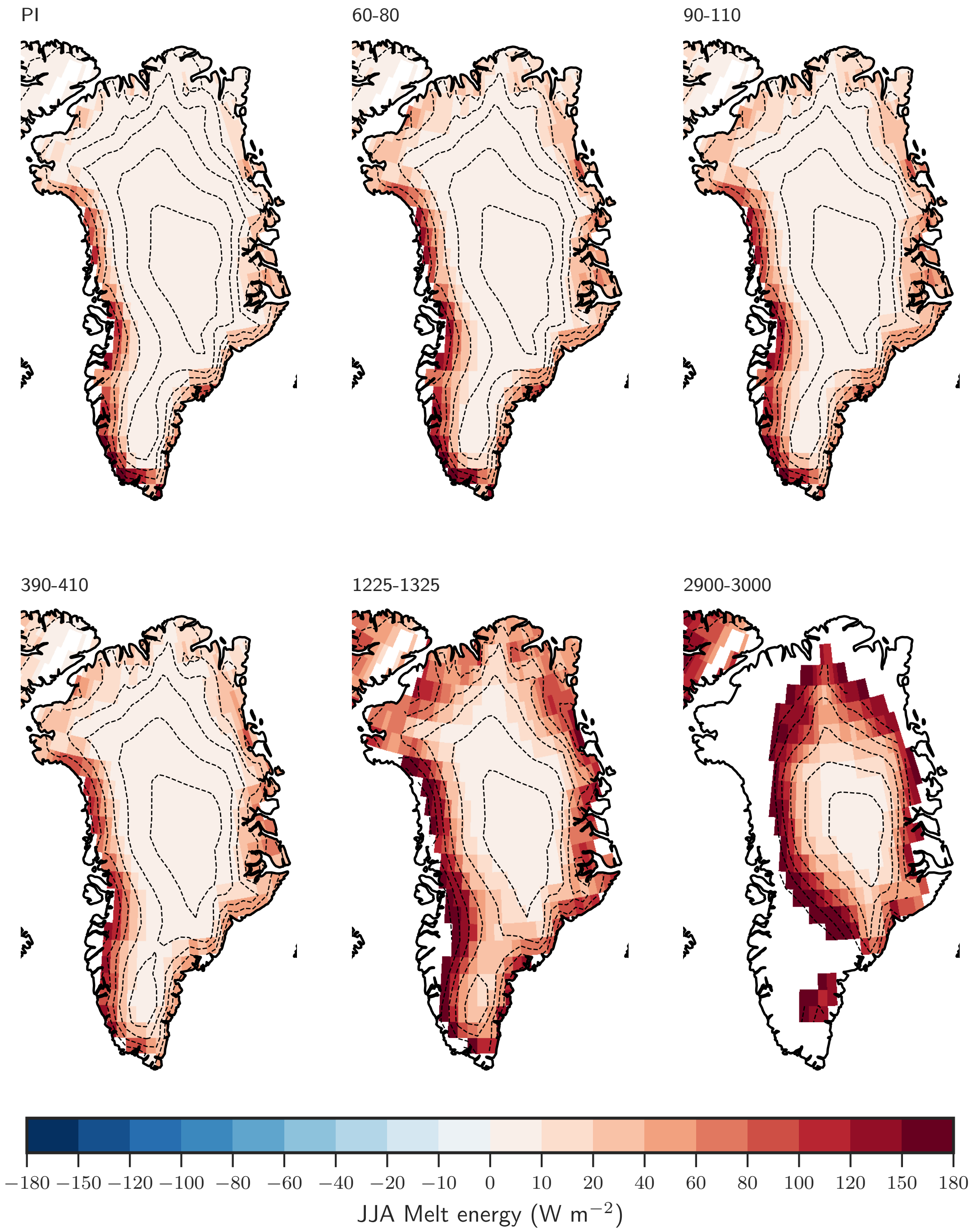

Figure C.7: Evolution of the absolute June-July-August melt energy (W m^{-2}) integrated over GrIS. The Topmost left shows the absolute of the pre-industrial. The period considered is marked by the respective years. Contour lines for every 500 m elevation.

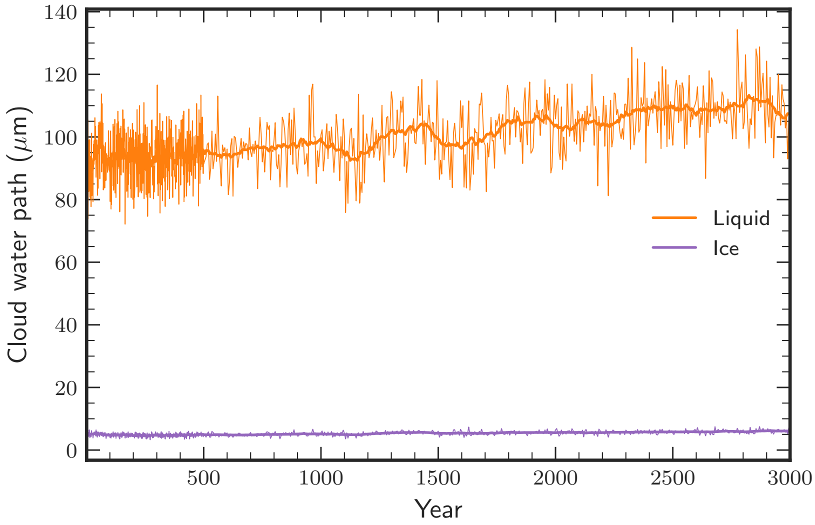

Figure C.8: June-July-August GrIS integrated liquid and ice cloud water path (μm). The thick lines show the 20-year running mean.

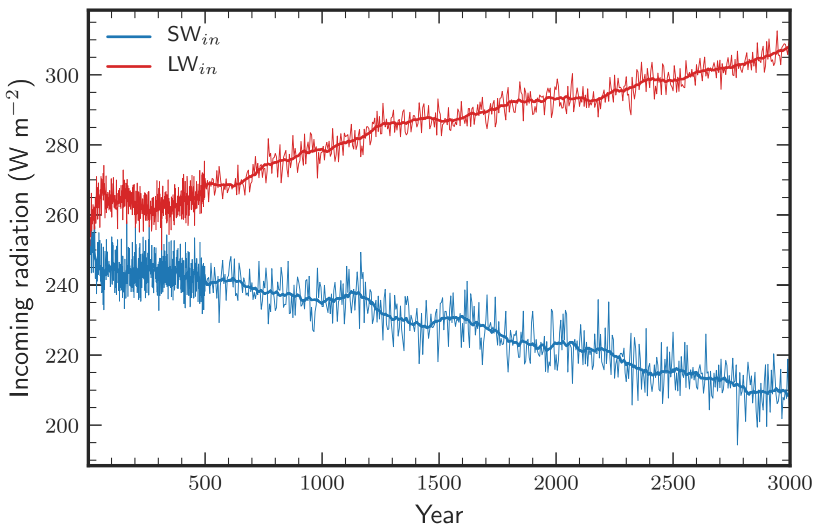

Figure C.9: June-July-August GrIS integrated incoming radiation (W m^{-2}) from SW and LW. The thick lines show the 20-year running mean.

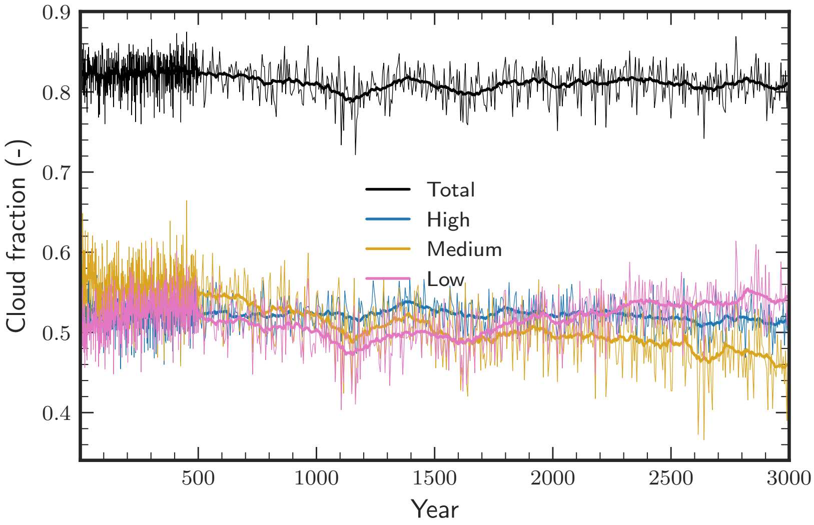

Figure C.10: June-July-August GrIS integrated cloud fraction (-). The thick lines show the 20-year running mean.

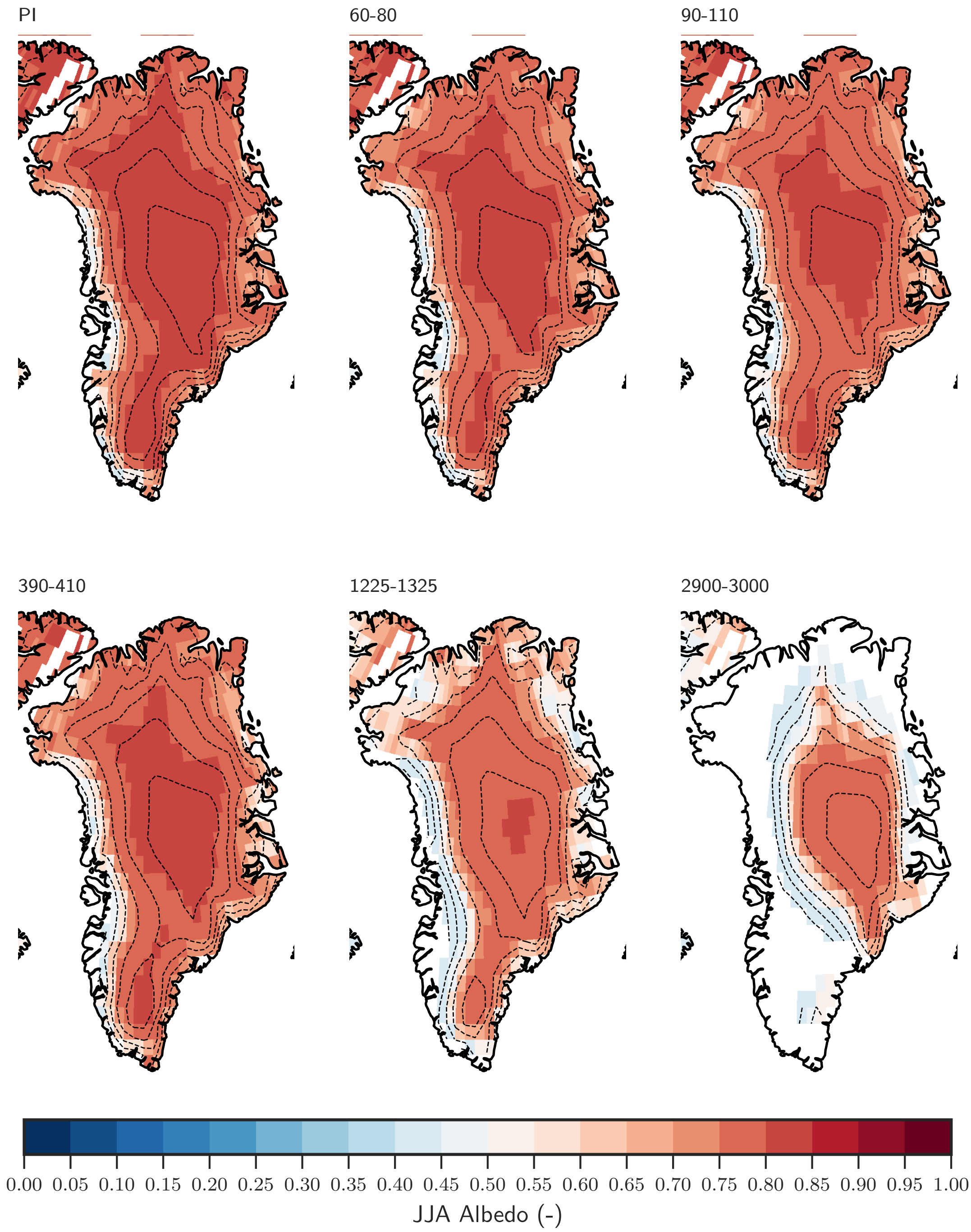

Figure C.11: Evolution of the absolute June-July-August albedo (-) integrated over GrIS. The Topmost left shows the absolute of the pre-industrial. The period considered is marked by the respective years. Contour lines for every 500 m elevation.

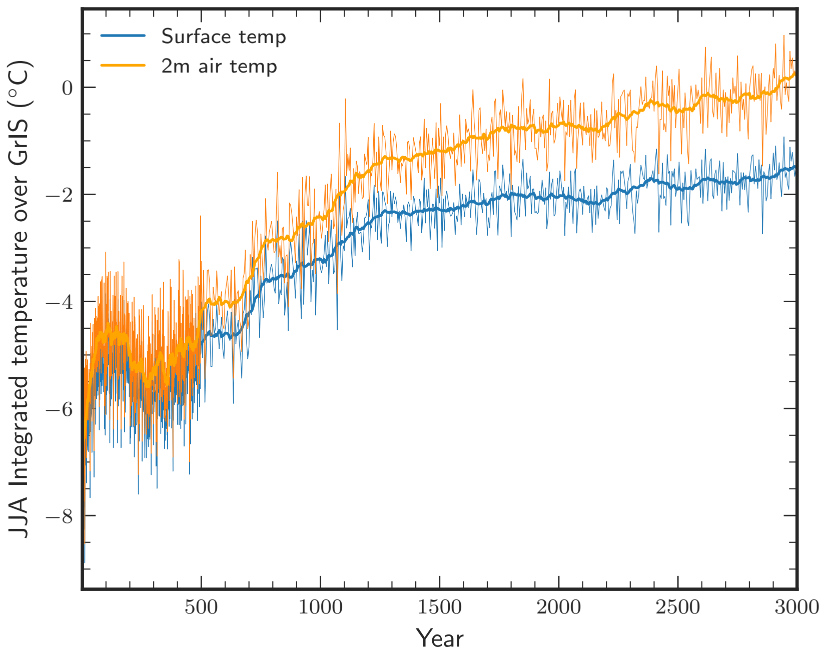

Figure C.12: Evolution of the June-July-August integrated GrIS 2m air temperature and surface temperature ($°C$). The thick lines show the 20-year running mean.

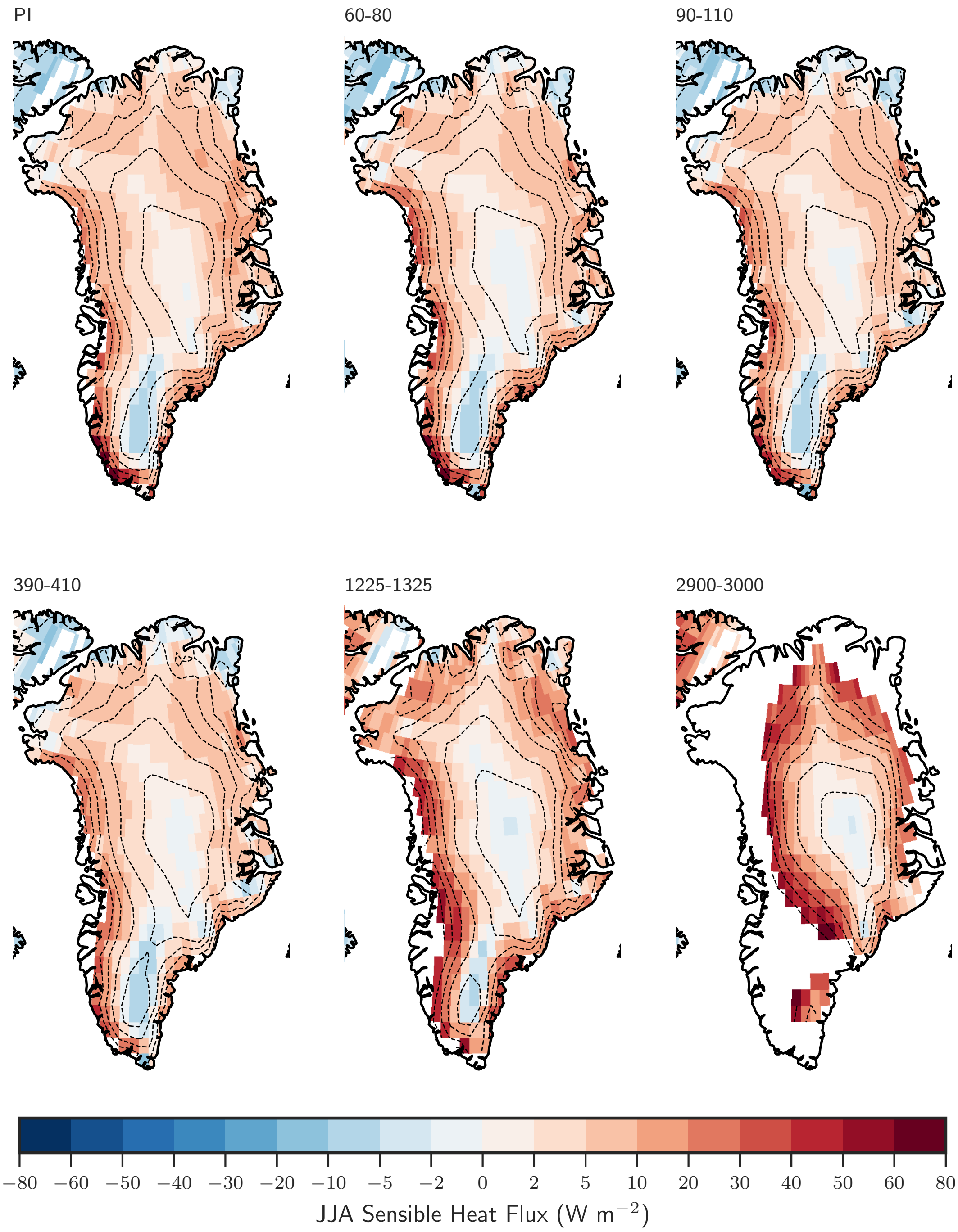

Figure C.13: Evolution of the absolute June-July-August sensible heat flux (SHF) (W m^{-2}) integrated over GrIS. The Topmost left shows the absolute of the pre-industrial. The period considered is marked by the respective years. Contour lines for every 500 m elevation.

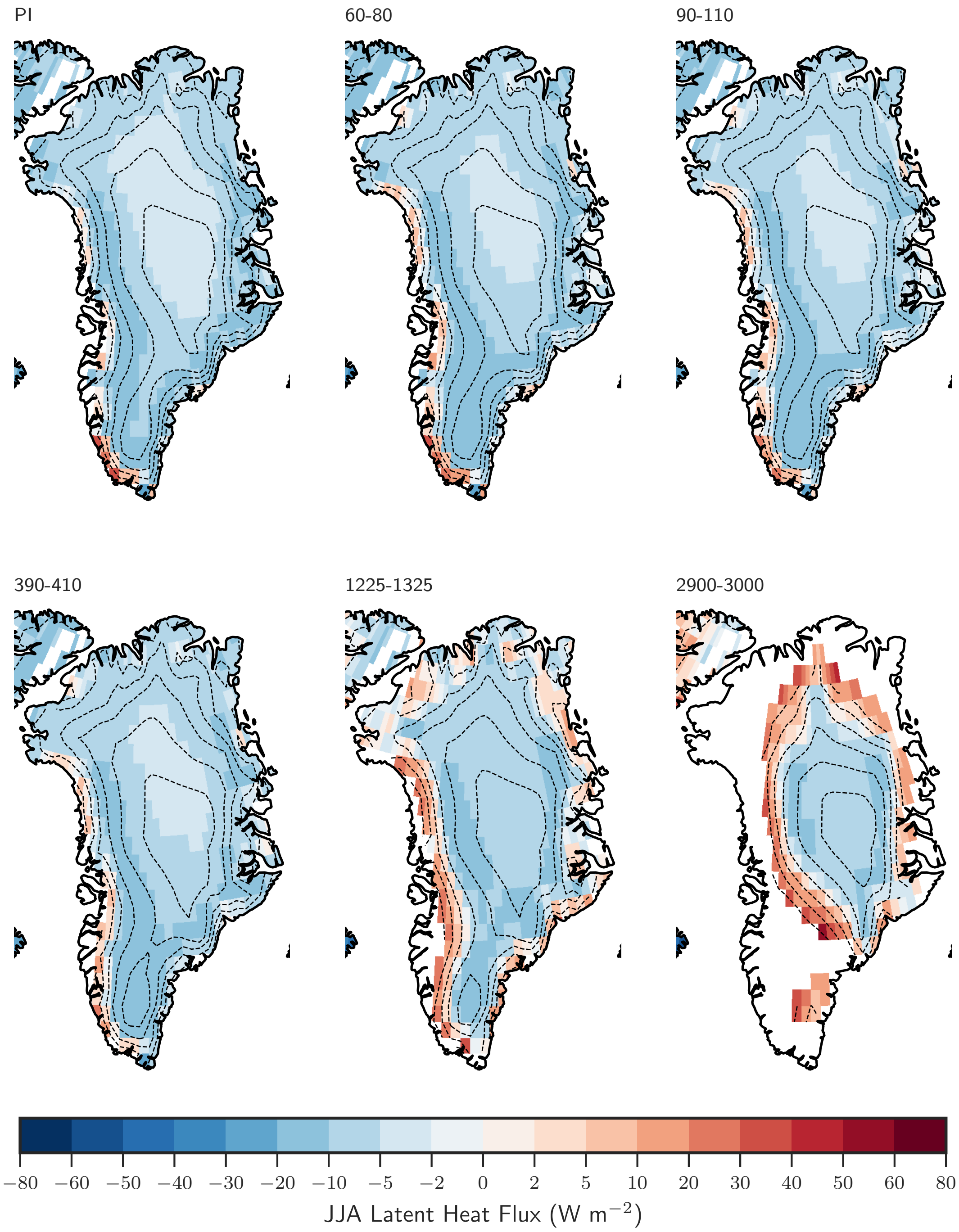

Figure C.14: Evolution of the absolute June-July-August latent heat flux (LHF) (W m^{-2}) integrated over GrIS. The Topmost left shows the absolute of the pre-industrial. The period considered is marked by the respective years. Contour lines for every 500 m elevation.

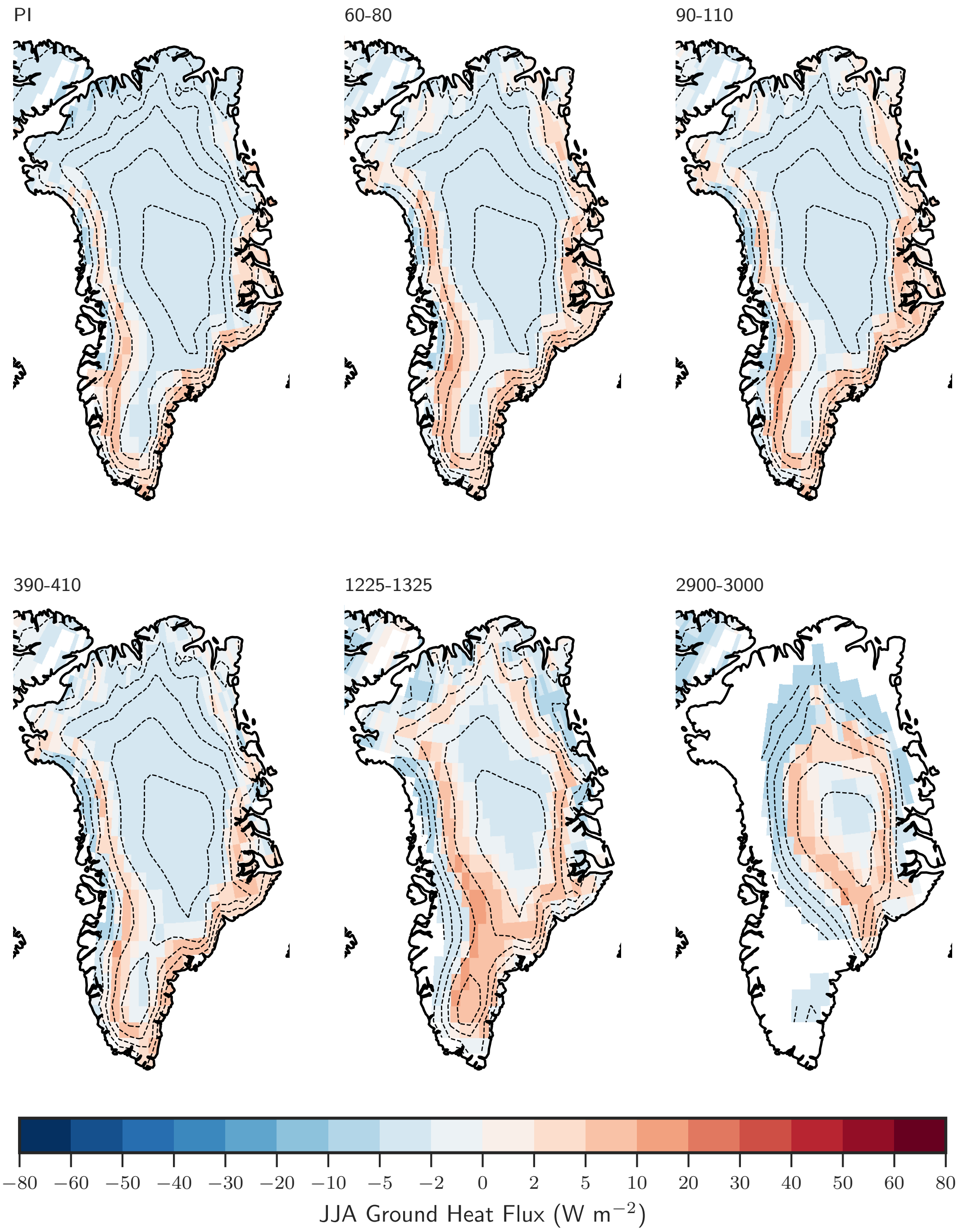

Figure C.15: Evolution of the absolute June-July-August ground heat flux (GHF) (W m^{-2}) integrated over GrIS. The Topmost left shows the absolute of the pre-industrial. The period considered is marked by the respective years. Contour lines for every 500 m elevation.

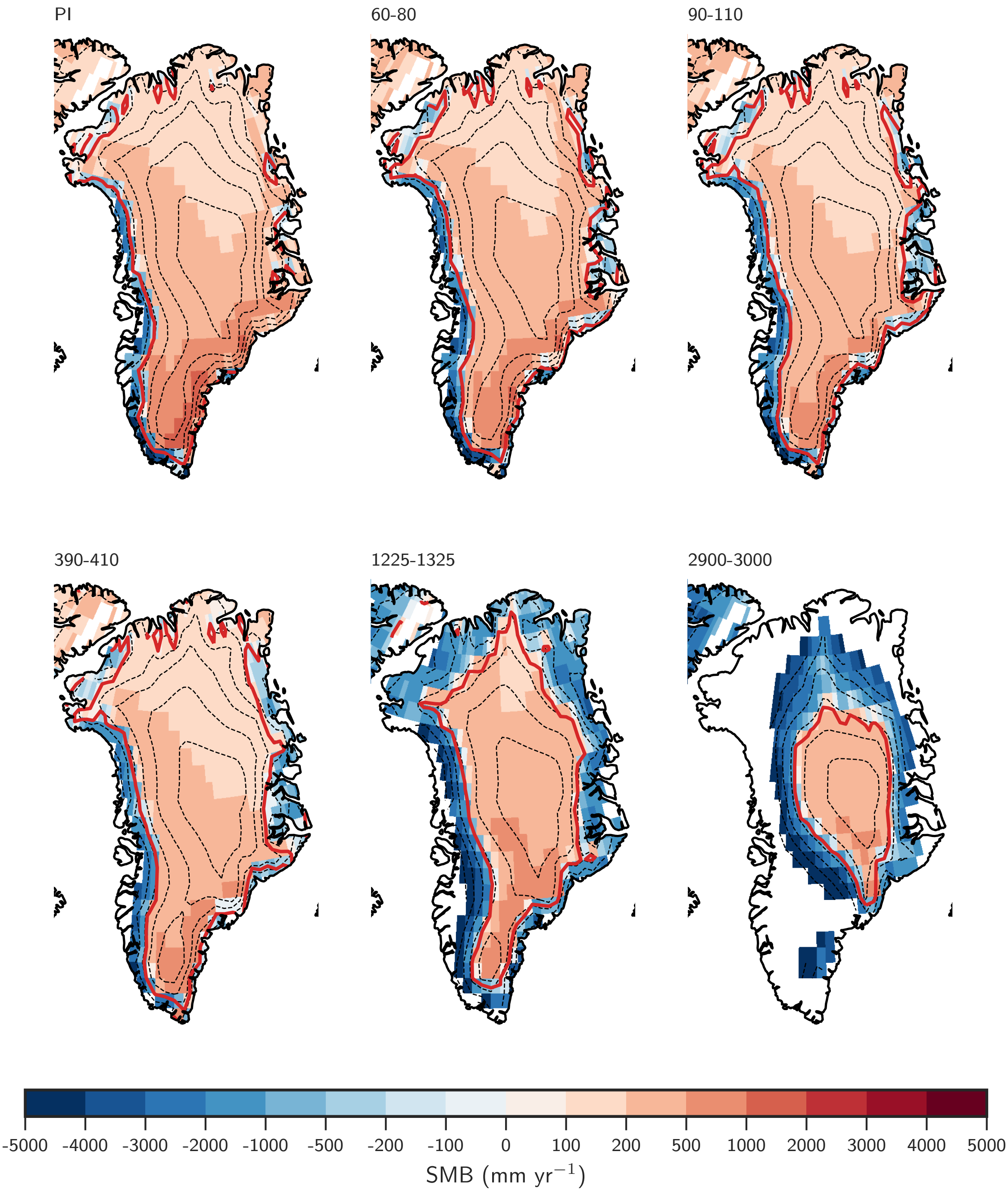

Figure C.16: Evolution of absolute annual surface mass balance (SMB) (mm yr^{-1}). The Topmost left shows the absolute of the pre-industrial. The period considered is marked by the respective years. Contour lines for every 500 m elevation. The red contour line denotes the ELA. The red colours indicate mass gain and the blue colours indicate mass loss.